Physics in Medicine & Biology

TOPICAL REVIEW • OPEN ACCESS

Motion estimation and correction in SPECT, PET and CT

To cite this article: Andre Z Kyme and Roger R Fulton 2021 *Phys. Med. Biol.* **66** 18TR02

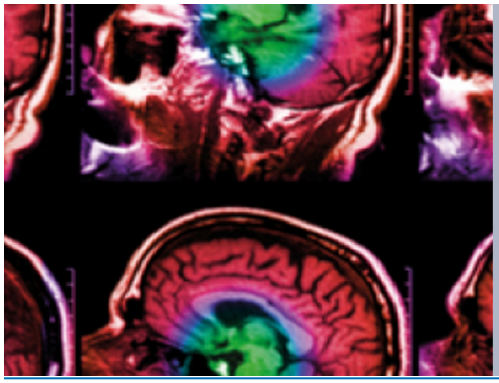

IOP Publishing Phys. Med. Biol. 66 (2021) 18TR02 https://doi.org/10.1088/1361-6560/ac093b

Physics in Medicine & Biology

IPEM Institute of Physics and Engineering in Medicine

OPEN ACCESS

RECEIVED
13 November 2020

REVISED
18 May 2021

ACCEPTED FOR PUBLICATION
8 June 2021

PUBLISHED
15 September 2021

TOPICAL REVIEW

Motion estimation and correction in SPECT, PET and CT

Andre Z Kyme[1,4] **and Roger R Fulton**[2,3,4]

[1] School of Biomedical Engineering, University of Sydney, Sydney, Australia
[2] Sydney School of Health Sciences, University of Sydney, Sydney, Australia
[3] Western Sydney Local Health District, Sydney, Australia
[4] Brain and Mind Centre, University of Sydney, Sydney, Australia

E-mail: andre.kyme@sydney.edu.au

Keywords: motion estimation, motion tracking, motion correction, motion compensation, SPECT, PET and CT

Abstract

Patient motion impacts single photon emission computed tomography (SPECT), positron emission tomography (PET) and x-ray computed tomography (CT) by giving rise to projection data inconsistencies that can manifest as reconstruction artifacts, thereby degrading image quality and compromising accurate image interpretation and quantification. Methods to estimate and correct for patient motion in SPECT, PET and CT have attracted considerable research effort over several decades. The aims of this effort have been two-fold: to estimate relevant motion fields characterizing the various forms of voluntary and involuntary motion; and to apply these motion fields within a modified reconstruction framework to obtain motion-corrected images. The aims of this review are to outline the motion problem in medical imaging and to critically review published methods for estimating and correcting for the relevant motion fields in clinical and preclinical SPECT, PET and CT. Despite many similarities in how motion is handled between these modalities, utility and applications vary based on differences in temporal and spatial resolution. Technical feasibility has been demonstrated in each modality for both rigid and non-rigid motion but clinical feasibility remains an important target. There is considerable scope for further developments in motion estimation and correction, and particularly in data-driven methods that will aid clinical utility. State-of-the-art deep learning methods may have a unique role to play in this context.

1. Introduction

1.1. Aims and scope

The aims of this review are:

i. To outline the motion problem in medical imaging, including the sources of motion and the type and dependencies of motion-induced artifacts (section 2).

ii. To review published methods for estimating motion fields (section 3) and correcting for these motion fields (section 4) in clinical and preclinical SPECT, PET and CT.

iii. To establish some general conclusions regarding the suitability of particular motion estimation and correction methods for the variety of applications and to suggest some opportunities for future development.

We focus on diagnostic applications of SPECT, PET and CT but also mention some examples of motion estimation and correction in surgical and therapeutic applications. Although we do not explicitly address motion estimation and correction for standalone magnetic resonance imaging (MRI), methods developed for hybrid PET/CT and PET/MR are covered and some modality-naive approaches appearing in the MRI literature are touched on. It is also worth noting that many of the concepts described for SPECT, PET and CT are directly

relevant to MRI. For a detailed treatment of motion estimation and correction in standalone MRI, the reader is directed to several excellent MRI-specific surveys (Ozturk *et al* 2003, Axel *et al* 2005, Maclaren *et al* 2013, Godenschweger *et al* 2016).

2. The motion problem in SPECT, PET, and CT

2.1. Sources of motion

We define subject motion as any voluntary or involuntary motion arising from muscular or other physiological movement during the imaging procedure. The sources of motion in humans and animals are largely the same and are summarised in figure 1.

Voluntary motion is typically muscular movement of the head and jaw (Goldstein *et al* 1997, Montgomery *et al* 2006), limbs or whole body (Dinelle *et al* 2006) and can be relatively simple rigid motion (translation and rotation) or more complex motion such as bending and twisting of the spine (Gu *et al* 2010). The causes of voluntary motion include chewing, speaking and swallowing, discomfort, anxiety, restlessness and non-compliance (Birn *et al* 1998, Wheat and Currie 2004a, Dinelle *et al* 2006). Moreover, certain imaging protocols tend to increase the propensity for voluntary movement due to the physical demands on the subject (Wheat and Currie 2004a).

Voluntary head motion in humans tends to be either drifting, abrupt or randomly distributed about a mean position (Fulton 2000, Dinelle *et al* 2006). It is reduced by using various forms of positioning aid and head restraint (Green *et al* 1994, Beyer *et al* 2005), yet displacements of 2–5 mm and rotations of 2°–3° are common and larger magnitudes are expected without restraint or if non-customised supports are used (Ruttimann *et al* 1995, Goldstein *et al* 1997, Lopresti *et al* 1999, Mawlawi *et al* 1999, Beyer *et al* 2005). The head motion reported for cooperative and motivated volunteers likely underestimates values for real patients, especially younger patients and those with disorders impacting their control of movement (Dinelle *et al* 2006). In preclinical studies involving unrestrained and unanaesthetised small animals, voluntary head motion is essentially unbounded and thus motion correction is imperative (Kyme *et al* 2012). Methods to limit the motion of unanaesthetised animals using forcible restraint (Martin *et al* 2002) or paralysis (Peeters *et al* 2001) are possible but can induce a stress response that may confound functional brain measurements (Ohata *et al* 1981).

Involuntary motion includes respiratory-induced thoracic and abdominal motion (Eisner *et al* 1988, Germano *et al* 1993, Nehmeh *et al* 2002, Erdi *et al* 2004, Visvikis *et al* 2006), cardiac motion (Nichols *et al* 2002, Blondel *et al* 2004), peristalsis (Alfidi *et al* 1976), foetal motion (Rousseau *et al* 2006) and movement of the limbs or whole body resulting from reflexes (e.g. sneezing, coughing), sleep and tremor (Dinelle *et al* 2006). Table 1 shows typical respiratory-induced displacements for various tissues and organs in the body. Complicating matters is a hysteresis effect causing organs to traverse slightly different paths during inspiration and expiration. Breath-hold imaging protocols, in which data are acquired at end-inspiration or end-expiration, can avoid diaphragm movement but are limited to scan durations <1 min.

2.2. Types of motion artifacts

Motion-related artifacts in SPECT and PET typically manifest as increased blurring and reduced contrast of organs and lesions, increased noise, mispositioning (ghosting), splitting and deformation of sources of activity, apparent hyper/hypo perfusion defects, and spillover or dispersion of activity (Ivanovic *et al* 2000, Nehmeh *et al* 2002, Wheat and Currie 2004a, Montgomery *et al* 2006, Pretorius and King 2008). In CT, motion also leads to blurring and loss of contrast, along with star, line, streak and band artifacts, anatomical distortion and irregular organ contours, lesion deformation and shift, discontinuities and sampling artifacts (Barrett and Keat 2004, Chen *et al* 2004, Erdi *et al* 2004).

2.3. Dependencies of motion artifacts

The specific nature of motion-induced artifacts has a complex dependency on many factors. Factors related to the actual motion include the type (e.g. rigid/non-rigid, translational/rotational, periodic, drifting, random/abrupt), timing and duration, speed, amplitude and direction of motion (Eisner *et al* 1988, Cooper *et al* 1992, Botvinick *et al* 1993, Germano *et al* 1993, Prigent *et al* 1993, Cullom *et al* 1995, Ivanovic *et al* 2000, McCollough *et al* 2000, Matsumoto *et al* 2001, Wheat and Currie 2004b, Chen *et al* 2004, Naum *et al* 2005, Xu *et al* 2012, Geramifar *et al* 2013). Other factors include the study duration, intrinsic spatial and temporal resolution of the modality, gantry rotation, imaging protocol, lesion size, object position in the field of view (FoV), patient age and condition, and the type of patient support device (Eisner 1992, Ritchie *et al* 1992, McCollough *et al* 2000, Wheat and Currie 2004a, Currie and Wheat 2004, Naum *et al* 2005, Dinelle *et al* 2006, Xu *et al* 2012, Geramifar *et al* 2013). The temporal resolution of a modality is an important determinant of its susceptibility to motion artifacts. The gantry speed of state-of-the-art CT scanners is fast enough (0.3 s/revolution) that the likelihood of

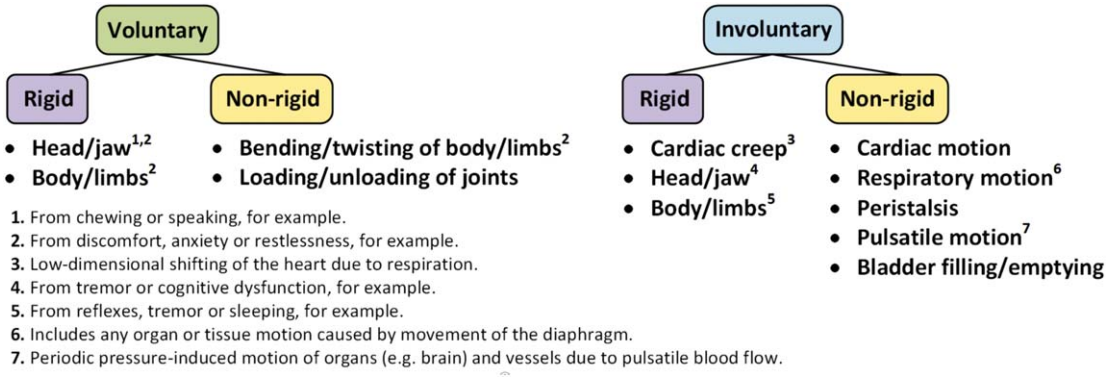

Figure 1. Categorisation of common subject motions during medical imaging procedures.

Table 1. Respiratory-induced motion of tissues, organs and structures in the body.

Tissue/Organ/Structure	Typical motion (mm)[a,b]	References
Lung/Lung tumour	0–22 (10 ± 7)	(Giraud *et al* 2001, Harada *et al* 2002, Allen *et al* 2004)
Heart	4–24 (12.4 ± 6)	(McLeish *et al* 2002)
Liver	10–26 (15 ± 6)	(Clifford *et al* 2002, Brandner *et al* 2006)
Spleen	5–20 (13)	(Brandner *et al* 2006)
Pancreas	13–42 (20 ± 10)	(Feng *et al* 2009)
Kidney	1–25 (14 ± 7)	(Brandner *et al* 2006, Yamashita *et al* 2014)
Diaphragm	9–27 (16 ± 9)	(Wade 1954, Feng *et al* 2009)
Abdominal wall	5–19 (10 ± 4)	(Feng *et al* 2009)

[a] Values shown represent the range (mean ±1 SD).

[b] In general, motion occurs in three dimensions. The values reported here represent maximal displacements along any one of the standard orthogonal directions (lateral, anterior–posterior, cranio-caudal). Maximal displacements are typically cranio-caudal, parallel to the main displacement of the diaphragm.

significant motion during a single frame is reduced. In contrast, cone-beam CT (CBCT), which is common in treatment planning and diagnosis in dentistry, orthopaedics, ENT and radiation therapy, involves slower gantry rotation (20–60 s/revolution) and, therefore, like SPECT and PET, is more susceptible to motion artifacts due to poorer temporal resolution. Although the temporal resolution of PET is poorer than for CT, the full-ring fixed-detector configuration of PET means that data from all projection angles are acquired simultaneously, thus providing an instantaneous 'snap-shot' of motion with complete angular sampling. This is approximated in the sequential CT acquisition by virtue of the very fast gantry rotation. However, for SPECT, the slow and sequential acquisition means that there is no motion 'snap-shot', and one cannot even assume that individual projections are free of motion (Kyme *et al* 2003). In CT, artifacts are usually worse for motion of objects with high or low relative attenuation. In SPECT and PET, the choice of radiotracer can influence the nature of motion artifacts due to varying biodistributions and kinetics. The number of detector heads has also been shown to change the nature of artifacts in SPECT, e.g. Cullom *et al* (1995), Matsumoto *et al* (2001). In summary, although the literature indicates broad agreement on the dependencies of motion artifacts, differences exist regarding the precise nature of these dependencies. In general, the nature, size and extent of artifacts is difficult to predict because of the complex interplay of variables.

2.4. Implications of motion

Although the literature does not offer a straightforward answer regarding when motion artifacts will occur or how they will manifest, it does offer substantial evidence for the clinical significance of such artifacts. Here we list several representative examples.

Head motion impacts visualisation and quantification in all modalities, distorting anatomy, corrupting uptake patterns and masking changes in radioligand binding (Dinelle *et al* 2006, Montgomery *et al* 2006). Head motion is particularly common among paediatric patients who often require sedation to prevent motion (Kaste 2004, Wachtel *et al* 2009). Of the 70 million CT scans performed annually in the United States, about 10% are performed in children (Brenner 2010), and in developing countries about 75% of paediatric CT scans are of the head (Vassileva 2012). The impact of head motion may be exacerbated in CT due to the higher spatial resolution compared to SPECT and PET (Kochunov *et al* 2006). For example, the value of CT brain perfusion

imaging in stroke patients depends on accurate haemodynamic modeling, which can be compromised by the moderate to severe head motion reported in 25% of patients (Fahmi *et al* 2013).

In cardiac studies, approximately 40% of myocardial perfusion SPECT scans may be affected by motion (O'Connor *et al* 1998, Currie and Wheat 2004) with 1/3 of these leading to incorrect diagnoses (Botvinick *et al* 1993, Prigent *et al* 1993, Wheat and Currie 2004b). Up to 66% of dynamic ^{82}Rb cardiac PET studies may be affected by significant motion leading to myocardial blood flow estimates that are in error by up to 500% (Hunter *et al* 2016, Armstrong *et al* 2019). Misclassification of coronary lesions has been reported in 10% of cases (Lassen *et al* 2019).

In tumour assessment studies, patient movement can change PET quantification by up to 35% for a 5 mm tumour and 10% for a 10 mm tumour (McCall *et al* 2010). It is also well known that the apparent enlargement and shape changes of lesions caused by respiratory motion blur can lead to overestimated dose margins in CT-based radiation therapy planning (Nehmeh *et al* 2002, Geramifar *et al* 2013).

When CT-based attenuation correction is performed in SPECT and PET, a potential shift or mismatch between the CT scan and the emission scan is a common problem which induces artifacts that impact quantification. The mismatch arises in part because the scans cannot be performed simultaneously, but also due to the different timescales of imaging; the faster CT scan typically produces a 'snap-shot' of motion whereas SPECT and PET scans contain the effects of motion averaged over a much longer period. This problem occurs in both head and thoracic/abdominal SPECT/CT and PET/CT, and regardless of whether or not breath-hold techniques are used for the CT acquisition (Osman *et al* 2003, Bruyant *et al* 2004, Geramifar *et al* 2013).

In preclinical imaging, the inevitability of motion in awake, unrestrained animals necessitates anaesthesia. However, the potential for anaesthesia to impact the biochemical (e.g. receptor binding) and physiological (e.g. neuro-haemodynamic coupling) processes being studied in the brain using SPECT and PET limits the translational value of the animal model (Momosaki *et al* 2004, Martin *et al* 2006, Cherry 2011).

3. Motion estimation in SPECT, PET and CT

A precondition for all motion correction methods is the estimation of a relevant motion field describing the physical displacement of points comprising the object of interest. In the simplest case, each point undergoes an identical displacement, thereby characterising a rigid translation of the object. In general, each point may undergo a unique displacement resulting in more complex motions such as rigid-body transformations involving rotation of the object, or non-rigid deformation (shape change) of the object. In the literature, motion fields characterising non-rigid motion of an object are sometimes referred to as deformation vector fields (DVFs) or simply as motion vector fields. In this review, we will use the term motion field as a general way of referring to any type of motion, but will preface the term with 'rigid' or 'non-rigid' to distinguish the two cases where this is relevant. Rigid motion fields can be represented compactly via a transformation matrix that operates on all points in the object, thus mapping it to a new location while preserving the relative locations of all points. Non-rigid motion fields, on the other hand, do not in general preserve the relative locations of component points in the object.

A motion field characterises an object's conformation or 'pose' at an instant in time. However, by sampling the motion field repeatedly, one can 'track' the motion of the object over time (e.g. throughout an imaging session). This gives rise to terms such as '4D motion field', which can be thought of as a changing 3D motion field or a time sequence of poses. Estimating the motion field is often an independent step, however it can also be conflated with the correction step in joint estimation/correction methods.

Motion fields can be broadly classified according to whether the motion is rigid or non-rigid. Rigid motion typically pertains to head, brain and dental studies and is characterized by translations and rotations. Non-rigid motion fields mostly pertain to thoracic and abdominal studies in which periodic cardiac and respiratory motion and its effects on the surrounding tissues are most relevant. Non-rigid motion encompasses affine transformations and higher-order DVFs.

Applications in which non-rigid motion fields are particularly relevant include respiratory-gated SPECT and PET, cardiac CT, coronary CT angiography (CCTA), and orthopaedic imaging. Respiratory motion fields are required in SPECT and PET to generate motion-corrected images of the thorax and abdomen and to make accurate quantitative measurements in liver and lung lesions that move periodically with the diaphragm. Cardiac CT is used to derive measures of mechanical function and performance of the heart and therefore relies on accurate estimation of the organ's non-rigid deformation. In CCTA, the non-rigid trajectories of coronary arteries, stents and bypass grafts are tracked during sinus rhythm, requiring high spatial and temporal resolution to resolve the small diameter and fast movement of these structures across temporal frames. Similar approaches are applied to lesions in the liver and lung which undergo periodic displacement due to cardio-pulmonary motion. In orthopaedic imaging, joints and the surrounding tissue may exhibit non-rigid motion under load.

In the remainder of section 3, we begin by defining several important specifications related to motion estimation and then survey various strategies for estimating rigid and non-rigid motion fields in SPECT, PET and CT.

3.1. Specifications encountered in motion estimation

3.1.1. Degrees-of-freedom (DoF)

The number of DoF relates to the complexity of the motion to be modelled. The simplest case is one-dimensional (1D) translational motion, as might be used to model periodic shifts of a lesion due to diaphragmatic motion. In tomography, in-plane motion has 3 DoF, including translation and rotation within the plane perpendicular to the scanner bore axis (the trans-axial plane). Complete rigid-body motion is described by 6 DoF (3 rotations and 3 translations). General affine transformation adds to the rigid-body parameters scaling and shear in each orthogonal axis, giving a total of 12 DoF. Highly non-rigid and deformable motion models may have tens to hundreds of DoFs. The number of DoF will usually determine appropriate representations of the motion (e.g. Euler angles, matrices, quaternions, splines, tensor fields), however this is beyond the scope of this review.

3.1.2. Accuracy and precision

Accuracy is a notoriously vague and varied concept in the literature when applied to motion estimation in medical imaging. This makes comparison of the reported accuracy of different motion estimation methods difficult. We define accuracy simply as the extent to which motion estimates are in agreement with a ground truth or reference value. Precision relates to the variance of a motion measurement and depends on the particular noise (or jitter) sources associated with the measurement and how these sources combine. In practice, precision can be measured as the variance of the noise of the motion estimates.

3.1.3. Sampling rate

Sampling rate refers to how frequently one obtains the raw data required to update the motion field. An example is the frame rate of an optical system used for motion tracking (section 3.2.3). Sampling rate differs from processing rate, which refers to how frequently the motion field is updated. Processing rate is a critical consideration for real-time motion estimation/correction but is less critical when offline processing is possible. Both sampling rate and processing rate requirements will depend on the rate of motion and the temporal and spatial resolution cpability of the imaging modality.

3.1.4. Latency

Latency refers to the delay associated with new motion estimates being available for downstream processing. The rate of availability of newly processed motion estimates is always less than or equal to the sampling rate. 'System' latency is the inverse of the processing rate and is equal to the sum of the measurement latency (the inverse of the sampling rate) and latencies due to data transmission and processing. System latency is relevant when considering the practicality of online motion estimation and correction.

3.1.5. Impact

Impact relates to how a subject is affected by a particular motion estimation method. The impact of external motion tracking methods varies depending upon the physical principles and apparatus involved. In principle, data-driven motion estimation methods have negligible impact on the subject except if additional scans are required that would add extra time or dose.

3.1.6. Constraints

Constraints can be physical or computational and include assumptions or requirements related to the object, lighting, environment ('scene'), working distance, line-of-sight or materials necessary for effective operation of a motion estimation method. Constraints also include assumptions, requirements or limitations related to the scanner (e.g. spatial and temporal resolution) and, in the case of data-driven motion estimation methods, the acquired data (e.g. noise).

3.1.7. Hardware/data requirements

Hardware and data requirements relate to the complexity and relative cost of resources required for motion estimation, and the amount of data generated. These factors have implications for the general practicality of a method.

3.1.8. Scalability

Scalability refers to how easily a motion estimation method can be adapted across object sizes and working volumes. This is important, for example, when considering the utility of motion estimation methods for small animals.

3.2. External motion tracking

An external motion tracking technology is a stand-alone apparatus and associated algorithms enabling the direct or indirect measurement of an object's pose over time. Below we survey external tracking technologies that have been used to estimate motion fields in SPECT, PET and CT.

3.2.1. Mechanical

Mechanical tracking systems involve an articulated mechanical arm to estimate the rigid-body pose of the terminus (end-effector) based on individual joint angles. The range of detectable motion is limited by the kinematics of the joints and any constraints imposed by the workspace. Accuracy is highly dependent on the mechanical stability of the arm and the robustness of the attachment between the mechanical arm and body, an aspect which is challenging in humans and likely to be even more challenging in small animals. Other challenges include the risk of collision between the arm and gantry inside space-constrained, especially narrow bore, scanners (Zhou *et al* 2013), and the time-varying photon attenuation caused by the articulating arm, which is non-trivial to correct for Angelis *et al* (2014). We know of only one implementation of this method in tomographic imaging, to track head motion in SPECT (Fulton 2000). The paucity of examples in the literature probably reflects the impracticality of the approach for motion-corrected imaging applications.

3.2.2. Magnetic

Magnetic tracking systems derive the position and orientation of a sensing coil within a magnetic field based on voltages induced in the coil (Remmell 2006). Using three orthogonal coils allows six DoF pose measurements. Commercial systems are available, mostly using a 'field transmitter' positioned at a fixed distance from the FoV to generate the magnetic field. Although magnetic tracking systems have been used extensively in eye tracking, surgical navigation and motion-adaptive radiotherapy (Birkfellner *et al* 1998b, Balter *et al* 2005), there has been relatively little use in diagnostic imaging. This includes magnetic systems to track head movement in PET (Daube-Witherspoon *et al* 1990, Green *et al* 1994, Mawlawi *et al* 1999) and body movement in cardiac SPECT (Sun *et al* 2001).

The main advantage of magnetic tracking systems compared to other external tracking systems is non-line-of-sight operation. In principle, this makes the approach immune to occlusion and allows tracking of implanted coils. Another advantage is scalability: orthogonal arrays of receiver coils for six DoF measurements can be <1 mm in width. The main drawback of magnetic systems is poor accuracy. The rapid fall-off in dipole field strength with distance results in a measurement error, Δr, given by Nixon *et al* (1998):

$$\Delta r \propto d_{tr}^4, \tag{1}$$

where d_{tr} is the transmitter–receiver distance. Metallic objects can also distort the transmitted field and corrupt measurements due to eddy currents induced in the object. Measurement error associated with this effect is given by Nixon *et al* (1998):

$$\Delta r \propto \frac{d_{tr}^4}{d_{to}^3 d_{ro}^3}, \tag{2}$$

where d_{to} and d_{ro} are the distances from the metallic object to the transmitter and receiver, respectively. Thus, the impact of the metallic object rapidly worsens pose measurements as these distances are reduced. Metallic objects which are ferromagnetic produce additional distortion of the magnetic field due to their high magnetic permeability. Because of these dependencies, it is not uncommon for magnetic systems to exhibit errors of 5–10 mm or greater (up to 100 mm) (Birkfellner *et al* 1998a, Nixon *et al* 1998, Hummel *et al* 2002). Field distortion-related errors due to metallic objects can be reduced to some extent using calibration procedures, however this is only effective if the environment remains static during tracking. Magnetic tracking systems can provide sub-millimetre and sub-degree accuracy for stationary sensing coils within about 30 cm of the transmitter (Hummel *et al* 2002, Schicho *et al* 2005), however accuracy of a few mm or degrees is more realistic for less controlled environmental factors, larger working distances and dynamic measurements (Frantz *et al* 2003). In general, the close proximity of metallic gantry elements and the presence of EM fields associated with high voltage components tend to limit the practicality of magnetic tracking systems in SPECT, PET and CT, especially when high accuracy is a requirement.

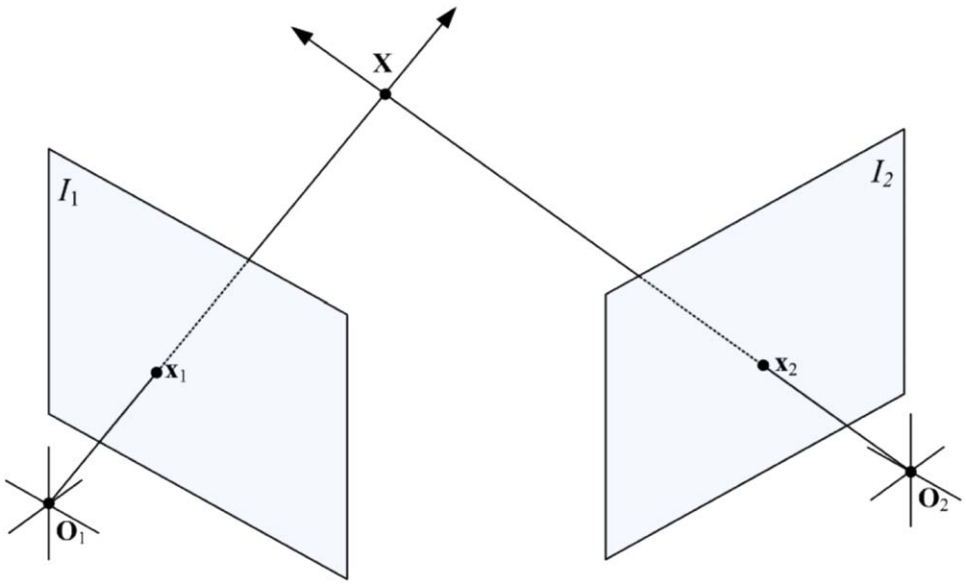

Figure 2. The principle of recovering 3D structure using binocular stereo. If the image of a scene (world) point, **X**, can be identified in two different camera views (I_1 and I_2), and the cameras are spatially calibrated, the 3D location of **X** in a global metric frame can be estimated by back-projecting through the image points, $\mathbf{x}_1$ and $\mathbf{x}_2$, from each view to determine the point of intersection. This process of back-projecting rays to reconstruct 3D points is termed 'triangulation' and is shown here for the ideal case (no noise) where the lines intersect exactly. Note that the distance $\mathbf{O}_1$ to $\mathbf{O}_2$ is referred to as the stereo baseline.

3.2.3. Stereo-vision

Stereo-vision tracking systems usually operate in the visible or near-IR wavelength range and rely on the detection of sparse or dense object features in two or more camera views. Features may be active (powered) markers such as light emitting diodes (LEDs) (Barnes *et al* 2008) or passive areas that reflect light, including native features (Kyme *et al* 2014, 2018) or artificial features such as reflective tape, spheres and patterns (Fulton *et al* 2002). If the two cameras are optically and spatially calibrated, triangulation can be used to estimate the 3D location of features, matched across views, in a real-world metric frame of reference (figure 2) (Hartley and Zisserman 2004). The changing rigid-body pose of an object can then be estimated given at least three such landmarks tracked over time (Horn 1987).

Stereo-vision systems have been by far the most commonly used external tracking approach for head and body motion estimation in SPECT, PET and CT. It is also the main tracking approach to have been applied preclinically: in monkeys (Jin *et al* 2010), mice (Baba *et al* 2013) and rats (Kyme *et al* 2011, 2019).

Several stereo-vision systems are commercially available. The Polaris and Vicra range (Northern Digital Inc., Ontario, Canada) and other similar IR-based binocular systems relying on active or passive markers have been used extensively to track the head (Lopresti *et al* 1999, Fulton *et al* 2002, Bloomfield *et al* 2003, Woo *et al* 2003, Fulton *et al* 2004, Watabe *et al* 2004, Herzog *et al* 2005a, Beyer *et al* 2005, Dinelle *et al* 2006, Montgomery *et al* 2006, Jin *et al* 2010, Keller *et al* 2012) and chest (Beach *et al* 2004, 2007), mostly in PET and SPECT but also in CT (Kim *et al* 2015b). The Vicon (Vicon Motion Systems Ltd, Oxford, UK) is a multi-camera IR system using passive reflective markers. A 5-camera Vicon set-up was used to track arrays of reflective spheres on chest and abdominal belts for respiratory motion estimation (McNamara *et al* 2009, Gu *et al* 2010). The trinocular Optotrak systems (Northern Digital, Ontario, Canada), which use active, pulsed IR markers have been used as benchmark systems due to their extremely high positional accuracy (Barnes *et al* 2008). The mid-focal range Optotrak system was shown to have <10 μm and 50 μm accuracy for in-plane and out-of-plane motion, respectively (precision varied from 0.6 to 30 μm) (Schmidt *et al* 2009) and remains one of the most accurate commercial systems reported in the literature for medical imaging applications. Commercial systems using optical wavelengths are rarer. One such device is the MicronTracker (ClaroNav Inc., Toronto, Ontario, Canada), a short baseline (120 mm) binocular system which detects and tracks checkerboard-like marker patterns printed on paper (Kyme *et al* 2008). To our knowledge, the MicronTracker has only been reported for head tracking of rats in PET (Kyme *et al* 2011, 2012, Spangler-Bickell *et al* 2016).

Numerous research systems have also been reported for stereo-vision motion tracking in SPECT, PET and CT. These include 2-camera IR systems with reflective markers (Weisenberger *et al* 2005, McNamara *et al* 2008); 3-camera IR systems with reflective markers (Schulz *et al* 2011, Baba *et al* 2013) or no markers (Goddard *et al* 2009); 2-camera optical systems using LED markers (Picard and Thompson 1995, Goldstein *et al* 1997), coloured patches

(Gennert *et al* 2004), circular discs (Hu *et al* 2004) or no markers (Ma 2009); and a 4-camera optical system with no markers (Kyme *et al* 2014).

In addition to tracking sparse landmarks on an object, stereo-vision systems are also suitable for generating dense depth maps of surfaces which can in turn be registered across successive frames to estimate motion. This includes a range of consumer-grade depth cameras (known as RGB-D cameras), such as the Intel SR300 and D31X families, which have been applied in medical imaging (Baur *et al* 2013, Lindsay *et al* 2015, Bier *et al* 2018). The second-generation Kinect system (Microsoft Corp., USA) is another consumer-grade depth camera which has been used to track human head and torso motion in PET (Noonan *et al* 2015, Hess *et al* 2016) and respiratory motion in CT (Silverstein and Snyder 2018). The Kinect functions as a time-of-flight camera, providing a pixel-by-pixel depth map of a scene based on the flight time of modulated light emitted by the sensor. This device was adapted for close-range tracking within a clinical PET scanner to provide a potential accuracy of 1 mm and 1 deg for head motion (Noonan *et al* 2015).

Stereo-vision systems have several desirable features for motion tracking applications. Firstly, narrow baseline systems (<1 m) amenable to SPECT, PET and CT gantries can provide positional accuracy of a few tens of microns at working distances of up to several metres (Barnes *et al* 2008, Schmidt *et al* 2009). And, since accuracy scales with working distance, implementing close-range systems is a straightforward way to achieve a performance gain (Qin *et al* 2009, Kyme *et al* 2014). Secondly, stereo-vision systems tend to have good scalability in terms of the number of cameras (Kyme *et al* 2014) and the size of relevant features/markers (Weisenberger *et al* 2005, Kyme *et al* 2008) (for a good example outside of medical imaging, see Migliaccio *et al* (2005)). And, thirdly, the maximum sampling rate is equivalent to the maximum frame rate which, for state-of-the-art CCD and CMOS cameras, readily exceeds 60 Hz for mega-pixel resolution with a global shutter.

The main limitation of stereo-vision systems is line-of-sight operation, leading to tracking drop-out when certain features or regions are occluded (Zhou *et al* 2013, Zhang *et al* 2018). The problem is exacerbated by narrow scanner bores (characteristic of dedicated small animal scanners and MRI), large stereo baseline, and non-planar objects. Use of additional cameras, predictive filtering frameworks (Straw *et al* 2011) and marker-free tracking in which features are not restricted to a particular attachment, e.g. Kyme *et al* (2014), all aid in mitigating the line-of-sight problem. When cameras are located out-of-bore, mirrors can been used to reduce line-of-sight limitations (Andrews-Shigaki *et al* 2011), however in-bore cameras or the use of fibre-optic cables as vision extenders (Slipsager *et al* 2019) are preferable to improve accuracy and reduce the need for out-of-bore setups with high mechanical stability for tracking objects at long range.

Many stereo-vision systems rely on the attachment of specific markers to the subject. Here, robust attachment that prevents decoupling of marker/patient motion is vital for high motion tracking accuracy. For the head, dental molds (Westermann and Hauser 2000), adhesive bandages (Olesen *et al* 2009), headbands (Bhowmik *et al* 2012), glue (Kyme *et al* 2011), modified neoprene caps (Bloomfield *et al* 2003) and goggles (Fulton *et al* 2004, Ooi *et al* 2013) have all been used to attach markers. For the chest, markers have been mounted on blocks or posts (Koshino *et al* 2010) or woven into a wearable garment (Gennert *et al* 2004). In practice, achieving robust attachment without surgery is very difficult and currently no widely accepted method of non-invasive marker attachment exists. In head tracking, there is some evidence that the impact of skin motion on tracking accuracy may be mitigated in part by using a marker with a large area of attachment to the forehead (Spangler-Bickell *et al* 2019). The challenge of marker attachment has motivated the development of stereo-vision systems that rely on native object features rather than physically attached markers. In these systems, features include manually assigned locations such as the eye corners and base of the nose (Gao *et al* 2007), scale-invariant keypoints (Kyme *et al* 2014), and features learned via convolutional neural networks (CNNs) (Blendowski and Heinrich 2019).

3.2.4. Mono-vision

Monocular systems involve a single camera combined with similar computer vision principles and algorithms used for stereo-vision systems. They are well suited to tracking object motion in 2D. The real-time position management system (Varian Medical Systems, Palo Alto, CA), originally developed for monitoring patient motion during radiotherapy, involves video-based position tracking of passive targets. It has been applied in PET to track vertical motion of chest markers to estimate the misalignment between PET and CT scans (Nehmeh *et al* 2004) and to estimate lung lesion motion (Liu *et al* 2011). A similar position tracking system was used for respiratory gating in PET (Nehmeh *et al* 2011). It is also possible to estimate more complex motion (rigid-body and non-rigid deformation) using monocular systems by fitting the 2D image frames to an object or motion model. In computer vision this is referred to as the structure-from-motion (SfM) and non-rigid structure-from-motion (NRSfM) problem. (For an excellent review of SfM and NRSfM, see Ozyesil *et al* (2017).) Examples include a cone-shaped marker with four well-defined holes to track 5 DoF motion (Muraishi *et al* 2004), and a self-encoded marker for rigid-body head tracking (Forman *et al* 2011, Spangler-Bickell *et al* 2019). The latter was reported for MRI but is not modality-specific.

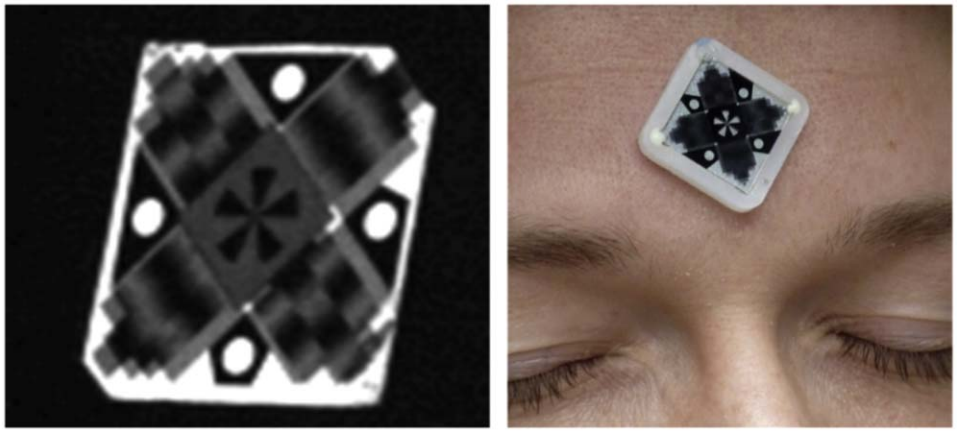

Figure 3. Moiré fringe-based tracking. The miniature marker used for head tracking (left) and attached to the forehead (right). (Maclaren *et al* 2012). Reproduced from Maclaren et al 2012. © 2012 Maclaren *et al* CC BY 4.0.

A key advantage of monocular approaches compared to multi-view stereo approaches is the reduced line-of-sight constraint. In general, however, pose estimates derived from monocular methods typically have poorer overall accuracy compared to stereo. Moreover, the more complex the motion, the more under-constrained the problem is mathematically, leading to increased noise, instability and drift. Pose accuracy from monocular methods is typically a few millimetres or more in the depth direction and achieving sub-millimetre and sub-degree accuracy in other out-of-plane DoF is challenging. However, factors such as increasing the object size, increasing the camera resolution, and reducing the working distance are simple ways to improve accuracy. For example, rotational accuracy $<0.5^{\circ}$ was achieved by Forman, attributable to the large-area marker with large binary features and short working distance of 80 mm (Forman *et al* 2011).

A unique monocular approach with promising accuracy and stability is moiré phase tracking (MPT), a passive marker-based method originally developed for biomechanical studies but which has since been adapted to medical imaging (Weinhandl *et al* 2010). MPT uses a single camera to track a marker consisting of two different gratings on either side of a thin transparent substrate (figure 3). Motion of the marker generates moiré fringes, the phase of which is orientation-dependent and can be used to quantify out-of-plane rotations. The remaining four DoF (3 translations and in-plane rotation) are determined using conventional photogrammetric methods. The method has been implemented with 15 mm $\times$ 15 mm lithographically printed markers at 25 fps (Maclaren *et al* 2012) to provide static tracking accuracy of 0.7 μm ($\pm$1.0 μm) for in-plane translation, 0.07° ($\pm$0.1°) for rotations over an angular range of $>50^{\circ}$, and 100 μm ($\pm$12 μm) for depth. These data represent some of the best figures reported for tracking system performance in medical imaging. Although the method has only been reported for MRI, it is clearly adaptable to other modalities.

3.2.5. Structured light

Structured light systems are conceptually similar to binocular stereo systems, having one camera replaced by a laser or projector to distribute a light pattern onto the object. This approach leverages the fact that projected features are often more easily and reliably detected than native object features. If the projector and camera are spatially calibrated, the depth of recognizable points projected onto the object surface can be determined based on the intersection of the points and the camera line-of-sight, resulting in a dense depth map of the object surface in the form of a point cloud (figure 4). Motion is estimated from frame to frame by registering successive point clouds using a method such as iterative closest points (Bellekens *et al* 2014).

Basic laser profiling, in which a single light ray or plane is swept across the object surface and imaged using a fixed camera, is the simplest form of structured light system. This approach was implemented to track mouse head motion in SPECT using a rapidly rotating mirror to sweep the laser line repeatedly through the working volume (Kerekes *et al* 2003). The main challenge of laser profiling is achieving a suitably high sampling rate to scan fast moving objects and/or a large FoV.

Obtaining a dense depth map from a single image requires projecting multiple light planes simultaneously. This can lead to ambiguity in identifying specific light planes if they are not visually unique (encoded) (Salvi *et al* 2010). Encoding the light planes can be avoided provided there are certain constraints on the camera model or object shape and motion. Examples of un-coded methods include the use of Fourier profilometry to analyse respiratory-induced breast motion (Price *et al* 2009) and phase measurement interferometry (Huang *et al* 1999) to estimate head pose in PET based on surface fitting of the nose, nose bridge and cheek bones (Olesen *et al* 2011). Olesen *et al* used IR

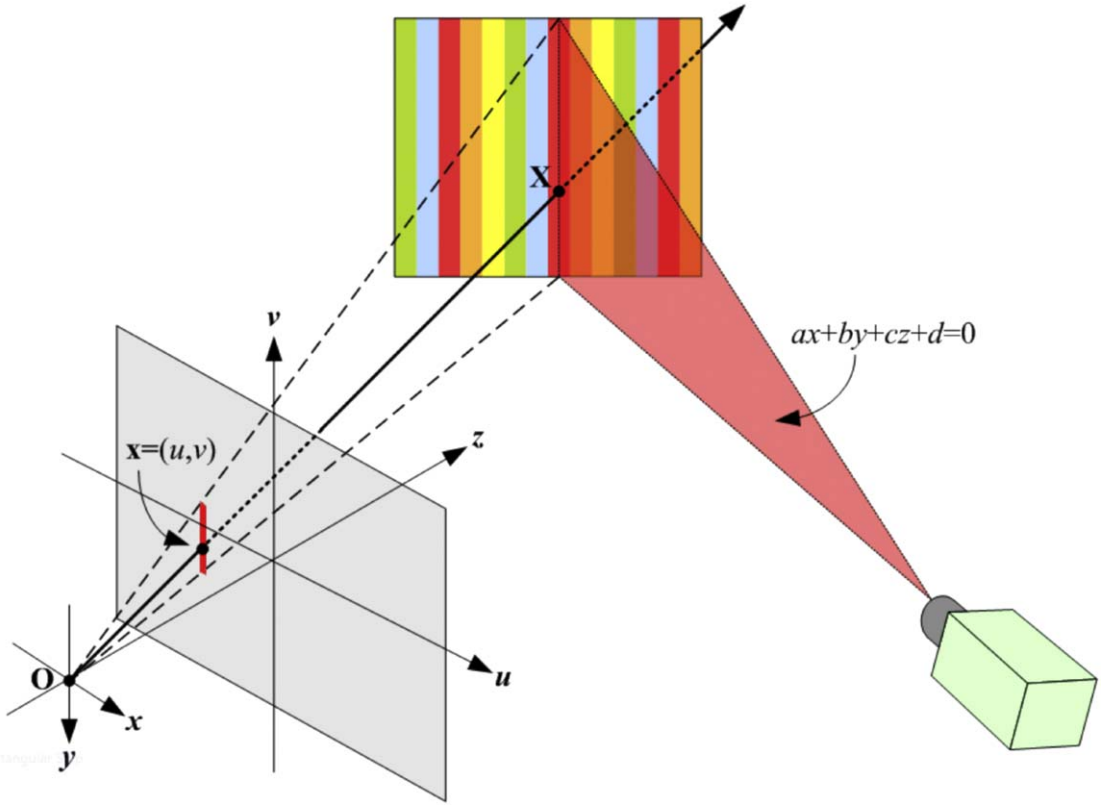

Figure 4. The principle of structured light ranging. A device (e.g. projector) is used to generate patterned illumination on the object surface. The example shown here is a coloured stripe pattern made up of 14 light planes (only the central red light plane is shown for clarity). A camera is used to image the object under the patterned illumination. If the camera and projector are spatially calibrated—i.e. the equation of the red light plane and the equation of any back-projected line through an image point, **x**, is known in a global reference frame (here, the camera frame), the depth (range) of all points along the projected red line in the image can be determined by triangulation.

illumination to reduce the impact of projected light on the subject and, by excluding textured areas such as eyebrows, achieved an accuracy of 0.25 mm and 0.1° for typical head motion (Olesen *et al* 2011, 2013). A MRI-compatible version, in which the in-bore optics are located at the end of long optical fibres originating from out-of-bore hardware (projector, camera and electronics), has also been reported for use in combined PET/MR (Slipsager *et al* 2019).

For rapidly moving objects or objects undergoing large pose changes, pattern encoding strategies are usually necessary to compute unambiguous depth maps from a single image. Spatially encoded light patterns exist which enable single-shot depth maps at high frame rate with sub-mm depth range accuracy at working distances <1 m (Forster 2006).

Structured light has been used to track head motion during PET imaging of awake rats, however the performance was limited by occlusions, non-rigid deformation of the head and prohibitive computation time for a sub-millimetre resolution mesh. In our experience, structured light also performs rather poorly on rodents, presumably because the high local contrast of the fur distorts the light pattern (Kyme 2012).

Overall, structured light methods have several desirable properties for tracking in medical imaging: (i) relatively inexpensive hardware; (ii) potential depth accuracy of 0.1–0.2 mm at working distances <1 m; (iii) high sampling rates; and (iv) the ability to estimate high DoF motion fields by fitting surface mesh models to rich depth map data (Wilm *et al* 2011). The limitations of using structured light include the requirement that surfaces clearly reflect the structured pattern and have large topological changes to ensure robust surface-surface registration. The computational demands of a structured light approach are also greater than for sparse point cloud tracking, however as is the case for commercially available depth cameras, customized and optimized hardware makes real-time tracking rates feasible (Slipsager *et al* 2019).

3.2.6. Inertial sensors

Inertial tracking systems typically combine object-mounted linear accelerometers and angular-rate gyroscopes to determine the position and orientation of an object in a navigation reference frame (Woodman 2007). Position is derived by double integration of the outputs of orthogonally-arranged accelerometers and

orientation is obtained, with respect to the reference frame, by integrating the outputs of orthogonally-arranged gyroscopes. This design is the basis of a 6 DoF inertial measurement unit (IMU). With the advent of chip-sized, low-cost accelerometers and gyroscopes based on micro-electro-mechanical-systems technology (Shaeffer 2013), IMU use has expanded from more traditional aerospace applications to human and animal motion tracking, e.g. Roetenberg *et al* (2007), Ribeiro *et al* (2009), Cuesta-Vargas *et al* (2010). However, there has been very limited use of inertial sensors for motion tracking in nuclear medicine and CT. The few reports include 3 and 6-axis mechanical gating of cardiac and respiratory motion for SPECT and PET (Jafari Tadi *et al* 2014, 2017) and monitoring of knee motion in standing patients imaged using C-arm CT (Maier *et al* 2018).

Inertial systems have important benefits for tracking: they function at long range since both accelerometers and gyroscopes are self-contained; there is no line-of-sight limitation as with optical systems; and they allow high sampling rates with low latency. The main challenge with these systems is compensating for drift in the gyroscope and accelerometer measurements caused by bias and bias instability, noise and calibration residuals. Even minute drifts in gyroscope output can lead to large errors in orientation within a short time, and positional error from the double integration of accelerometer measurements increases quadratically in time for a given fixed bias of the device (Woodman 2007). One way to correct for drift and thus improve the accuracy and stability of an IMU is to use additional sensors to periodically re-reference the gyroscope/accelerometer measurements. However, even without additional sensors, additional hardware is required to power IMUs and wirelessly transmit signals. Thus, for medical imaging the benefits of IMU-based motion tracking are probably outweighed by poor accuracy (several mm/degrees) of current consumer-grade miniature devices and the impracticality of attaching fully self-contained inertial systems to the body.

3.2.7. Other external motion tracking approaches

Several modality-naive optical methods which do not fall neatly into the above classification (sections 3.2.3–3.2.5) have been reported. Commercially available bend-sensitive fibre-optic tape was used to measure head position and orientation in MRI brain scans (Herbst *et al* 2011). Head rotation about two orthogonal axes was estimated using an optical lever in which a single laser beam was deflected onto a distant wall from a mirror rigidly attached to a dental bite (Ruttimann *et al* 1995). And non-optical approaches include ultrasound-based motion tracking in PET (Schwaab *et al* 2015) and radar-based estimation of respiratory motion in 4D CT (Pfanner *et al* 2013).

Many other external motion tracking methods exist based either on optical principles (e.g. depth-from-focus/defocus (Schechner and Kiryati 2000)) and non-optical principles (e.g. time-of-flight positioning using ultra-wideband or microwave technology (Zhang *et al* 2006)). However, to our knowledge, these methods have not been applied for motion estimation in SPECT, PET or CT.

3.3. Dual-modality approaches

The pairing of PET and SPECT with CT into dedicated dual modality scanners has been standard for well over a decade (Buck *et al* 2008, Townsend 2008) and, more recently, pairing with MRI either in a fully integrated system or via a PET/SPECT insert has rapidly expanded. The CT or MRI component of dual-modality PET and SPECT systems present a lot of options for estimating the motion fields needed for motion correction. In the majority of reports these are the respiratory and/or cardiac motion fields in thoracic studies.

Using CT, respiratory and cardiac motion fields can be derived from specific 'snap-shots', such as end-expiration and end-inspiration, or from 4D gated CT data by registering consecutive frames (Qiao *et al* 2006). In either case, since the CT and SPECT/PET acquisitions are not simultaneous, the derived motion field will, in general, differ from the motion field during the SPECT/PET acquisition, and thus adaptation of the motion field to the specific study will be necessary. This can be performed based on simultaneously acquired respiratory belt or ECG data (Bettinardi *et al* 2013). Many variations of the CT-derived motion field paradigm exist and the reader is referred to some good reviews (Pepin *et al* 2014, Guerra *et al* 2017).

Similarly to CT, MRI snapshots of an organ's periodic motion can be used to generate interpolated cardiac and respiratory motion fields (Reyes *et al* 2007, Balfour *et al* 2015, Küstner *et al* 2017). Numerous other methods also exist for deriving respiratory and cardiac motion fields from MRI, including navigator sequences, self-gating, tagged MRI and wireless MR markers (Tsoumpas *et al* 2010, Catana *et al* 2011, Guerin *et al* 2011, Chun and Fessler 2012, Ullisch *et al* 2012, Würslin *et al* 2013, Huang *et al* 2014b, Fayad *et al* 2016). Several authors have derived PET respiratory motion fields from simultaneously measured MR data using non-rigid image registration, e.g. Tsoumpas *et al* (2010). Alternatively, a respiratory motion model based upon a short-duration simultaneous PET/MR acquisition can be used to establish the correspondence between 3D motion fields and a surrogate signal in order to predict motion during a PET scan from the surrogate signal alone. One such surrogate signal used successfully to reconstruct motion-compensated PET images is a respiratory signal extracted using PCA from the raw PET data (Manber *et al* 2016). Myocardial wall motion has been derived using tagged-MR (Petibon *et al* 2013) and combined with respiratory motion derived from dedicated MRI sequences

to generate a complete cardio-respiratory motion field (Ouyang *et al* 2013). The reader is referred to several surveys for a discussion of these and other approaches (Catana 2015, Fürst *et al* 2015, Gillman *et al* 2017).

Advantages of pairing SPECT and PET with CT versus MRI for motion estimation include the mature nature of SPECT/CT and PET/CT technology, cheaper cost, and the prevalence of CT in diagnostic work-ups. The chief drawback is the added dose from CT which, for 4D acquisitions, is significant. On the other hand, the advantages of pairing SPECT and PET with MRI are the potential for truly simultaneous acquisition, superior soft tissue contrast, and the wealth of options for motion estimation due to the flexibility of MRI sequences and the mature history of MRI-based motion estimation research (Ozturk *et al* 2003, Axel *et al* 2005, Maclaren *et al* 2013, Godenschweger *et al* 2016).

3.4. Fiducial-based approaches

Fiducial markers are features that share the same intrinsic contrast mechanism as the imaging modality and which are either inserted into the subject or attached to the surface. They include radioactive point or line sources for PET and SPECT (Miranda *et al* 2017) and radio-opaque markers such as steel beads for CT (Schäfer *et al* 2004). Fiducials are easily isolated in the raw or reconstructed data and may be exploited for motion estimation. A single fiducial enables the estimation of 1D motion, and three fiducials are sufficient to estimate full rigid-body motion (3 rotations, 3 translations) using the same principles as stereo-vision (section 3.2.3). Fiducials can be tracked either in the sinogram (projection) space (Noo *et al* 2000, Schäfer *et al* 2004, Li *et al* 2006, Becker *et al* 2010, Bhowmik *et al* 2012, Choi *et al* 2014, Miranda *et al* 2017) or image space (Germano *et al* 1993, Ivanovic *et al* 2000, Naum *et al* 2005, Nazarparvar *et al* 2012, Chu *et al* 2018) and can be especially useful for estimating motion in low-count data.

Fiducial markers attached to the head have been used in PET and CT to track rigid-body head motion of humans (Naum *et al* 2005, Bhowmik *et al* 2012) and unanaesthetised rats and mice (Miranda *et al* 2017, 2019a, 2019b). The latter involved localising the fiducial centroids in consecutive 33 ms frames of the raw PET list mode data, equivalent to a tracking rate of 30Hz. Fiducials have also been used to estimate 4D respiratory motion fields (Schäfer *et al* 2004, Li *et al* 2006), tumour motion (Becker *et al* 2010), and joint motion in orthopaedics (Choi *et al* 2014).

The main benefits of using fiducials for motion estimation are the ease of identification of the fiducial signal in the raw or reconstructed data and the fact that they share the same coordinate frame as the raw data, thus circumventing the need for a cross-calibration. Drawbacks of fiducial-based approaches include the additional time required to prepare fiducial markers, the risk of fiducial motion becoming decoupled from subject motion if attachment of the fiducial markers is not robust, and the limitations in accurately localising fiducials markers imposed by the scanner (e.g. intrinsic spatial and temporal resolution, sensitivity and noise). Additional dose and scatter from radioactive fiducials in PET and SPECT is usually only minor and thus not a notable drawback.

3.5. Fully data-driven motion estimation

Data-driven motion estimation is where motion fields are derived from the acquired imaging data alone without the need for any external hardware (e.g. motion tracking systems) (Kesner *et al* 2014). However, in the following survey of data-driven methods, we relax this definition slightly to include gating-based approaches that rely on respiratory and/or ECG monitoring devices (Bettinardi *et al* 2013).

3.5.1. SPECT and PET

Registration of the reconstructed image frames from dynamic acquisitions, gated acquisitions or acquisitions framed based on a motion threshold is a very common and useful data-driven method to estimate relatively discrete (inter-frame) motion (Picard and Thompson 1997, Mawlawi *et al* 2001, Naum *et al* 2005, Costes *et al* 2009, Su 2011, Woo *et al* 2011). Here, motion estimation is implicit in the image registration process. Rigid registration of frames has been applied successfully in organs such as the brain, heart and liver in both humans and animals and supports sub-millimetre and sub-degree accuracy. The feasibility of this approach in brain PET using frames as short as 1s was recently demonstrated (Spangler-Bickell *et al* 2021). Non-rigid registration has also been applied to obtain cardiac and respiratory motion fields using a variety of motion models including affine (Klein *et al* 2001b, Yu *et al* 2006), B-spline (Thorndyke *et al* 2006, Bai and Brady 2009b) and higher-dimensional fields from optical flow (Klein *et al* 1997, Dawood *et al* 2008). In all cases, data-driven alignment of reconstructed frames is limited by image statistics and possible redistribution of the radiotracer (Andersson 1998). In low-count frames, registration convergence and accuracy can be improved by noise regularisation (Bai and Brady 2009b) and incorporating additional constraints from priors and spatio-temporal cost functions (Klein *et al* 2001a), physical models (Barnett *et al* 2011) and joint estimation of motion and other parameters (Jiao *et al* 2012).

A variety of centre-of-mass (CoM) based techniques have been reported for data-driven motion estimation in SPECT and PET. Early methods in SPECT used CoM tracking in sinogram space to estimate simple

translational shifting of the heart caused by respiratory motion (Geckle *et al* 1988, Bruyant *et al* 2002). Data-driven respiratory gating of axial motion based on the CoM of back-projected events in 500 ms frames was used for myocardial perfusion SPECT (Ko *et al* 2015). In PET, the CoM of raw PET list mode data within successive temporal bins can be used for data-driven gating or to estimate low-dimensional motion of lesions in cardio-thoracic studies (Klein *et al* 2001b, Bundschuh *et al* 2007). CoM methods can be applied in conjunction with an appropriate threshold for auto-framing of PET list mode data, with subsequent frame-to-frame registration to estimate rigid or non-rigid motion fields. An example of this approach is the estimation of bulk body motion based on the CoM of PET count rates in 200 ms time bins (Lassen *et al* 2019). A variation of the approach exploits the additional information available in ToF PET data by computing the centre of distribution based on the central ToF bin for every PET event within short time intervals to estimate 3D respiratory motion fields for internal organs (Ren *et al* 2017), bulk body motion (Lu *et al* 2019) and brain motion (Lu *et al* 2020). Although not strictly data-driven, measurements from a respiratory belt were correlated with organ CoM to derive a high temporal resolution internal-to-external motion model for respiratory motion in PET (Liu *et al* 2011). This approach was subsequently extended to non-rigid motion fields (Cha *et al* 2018).

Other sinogram-based approaches for data-driven estimation of simple 1D and 2D motion in SPECT and PET involve comparing adjacent projections based on peak fitting of cross-correlation profiles (Eisner *et al* 1987), optical flow (Noumeir *et al* 1996), and phase-only matched filtering (Chen *et al* 1993). A more sophisticated approach fits dynamic PET sinogram data to temporal basis functions to estimate respiratory and cardiac motion fields (Ahmed *et al* 2015). In SPECT, rigid-body motion of the brain and heart has been estimated by minimising the error between measured projections and projections generated from the motion-corrupted reconstruction under rigid transformation (Arata *et al* 1996, Lee and Barber 1998, Matsumoto *et al* 2001, Hutton *et al* 2002, Kyme *et al* 2003, Bai *et al* 2009, Mukherjee *et al* 2013). Overall, the approach is well suited to motion that approximates step-wise movement between projections but less well suited to continuous motion. To our knowledge, a similar concept has not been applied in PET. Rigid-body motion may also be computed using the CoM and inertia of at least three simultaneously acquired projection angles via a principle-axes method (Feng and King 2013). In theory, this approach is applicable to 3-headed SPECT systems and PET.

Neural networks are yet another possible approach for data-driven motion estimation in SPECT and PET. Early work included traditional neural networks applied to cardiac motion estimation (Beach *et al* 2007), however the state-of-the-art is to use many-layer (i.e. 'deep') CNNs. To date, we are only aware of supervised CNNs being applied for non-rigid registration of 4D gated frames for respiratory motion correction in PET (Clough *et al* 2018, Li *et al* 2020). With insufficient training data it appears that CNN-based methods struggle to out-perform more traditional approaches based on manifold learning (Clough *et al* 2018). Developing methods to address this particular challenge is, therefore, an important area of research. CNN and other deep learning-based methods are extremely new and there is much to learn about their feasibility, usefulness and limitations for motion-related tasks—especially motion estimation—with noisy SPECT and PET data.

3.5.2. CT

For rigid motion typical of head and dental CT studies, data-driven motion estimation methods can be either projection-based or image-based. Authors have tended to preference working directly with the projection data both for efficiency (avoiding the need to reconstruct) and the fact that motion-related artifacts are generally more localized in the projection data compared to the reconstructed image (where smearing of motion-induced artifacts can make motion estimation more difficult) (Mooser *et al* 2013).

In projection-based approaches, translational and rotational motion vectors have been estimated from projection moments (Pauchard *et al* 2011) and cross-correlation of adjacent projections (Wang and Vannier 1995, Eldib *et al* 2018) or opposing projections (Gu *et al* 2017). Projections can also be represented as a linear sum of nearest-neighbours generated by forward projecting the motion-corrupted reconstruction under many rigid-body transformations. The resulting weights of the linear sum are then used to iteratively update a rigid-body estimate in either fan-beam or cone-beam geometry (Chen *et al* 2018).

Projection-based methods may rely additionally on mathematically formulated data consistency conditions describing redundancies in the sinogram domain. The best known of these are the Helgason-Ludwig consistency conditions (HLCC), originally described for parallel-beam geometry. Extensions of the HLCC have been derived for fan-beam geometry and used to estimate translational and rigid in-plane motion (Yu *et al* 2006, Leng *et al* 2007, Yu and Wang 2007, Clackdoyle and Desbat 2015). The HLCC were further extended to 3D cone-beam geometry but the formulation was not applicable to circular orbits (Clackdoyle and Desbat 2013). Akin to the HLCC, the Fourier consistency conditions are defined in the Fourier domain of the sinogram and have been applied to fan-beam geometry to estimate detector shifts (Berger *et al* 2014) and to cone-beam geometry to iteratively correct for 3D translational motion (Berger *et al* 2017).

Image-based approaches for rigid motion estimation typically involve rigid registration of multiple CT volumes. This is used when multiple fast 3D frames are acquired, as in CT brain perfusion studies for stroke.

Each frame can be registered to one of the individual frames or to another reference image such as a non-contrast CT (Fahmi *et al* 2014). Such methods do not, however, compensate for motion occurring during each individual frame.

For non-rigid motion, data-driven motion estimation in CT is typically performed using one of three approaches: image-based registration of gated data, 3D–2D registration, or iterative minimisation of an image-based motion metric. By far the most common of these is the gating approach to compute periodic motion fields (Guerrero *et al* 2004, Ehrhardt *et al* 2007, Yang *et al* 2008, Schirra *et al* 2009, Tang *et al* 2012, Li *et al* 2013). In cardiac CT, for example, the heart is commonly scanned during a breath-hold (to avoid respiratory motion) at increments of 10% of the cardiac cycle, providing a 4D dataset. Similarly, a 4D dataset is obtained in thoracic and abdominal CT by scanning at increments of 10%–20% of the respiratory cycle (Sonke *et al* 2005). In each case, gating can be performed either retrospectively or prospectively, usually based on a surrogate such as the ECG or the signal from a respiratory belt. Estimation of global motion fields from respiratory-gated CT is usually performed by non-rigid registration of the temporal CT frames. In cardiac CT, where the goal is to obtain parameters of cardiac function, relevant structures are first segmented from the individual gates (e.g. using active shape models) and then tracked across gates (e.g. using optical flow). A similar approach is used to track and segment lung nodules and other structures that move due to cardio-pulmonary motion (Cha *et al* 2018). Variations of this general approach to estimate motion fields from 4D gated data have also been reported based on partial-angle reconstructions (Kim *et al* 2015a, 2018) and short scan images (Rohkohl *et al* 2013).

Bias in motion field estimation can arise in several ways using gating-based approaches. Ignoring the temporal consistency of the data is one source of bias that is typically handled by performing isotropic smoothing to regularise 4D motion fields across 4D data sets (Montagnat and Delingette 2005, Metz *et al* 2011). For non-smooth motion (e.g. sliding motion at the surface of the chest wall and abdominal wall), direction-dependent regularisation is preferable (Fu *et al* 2018). Bias is further reduced if all gated frames are registered to an unbiased group-wise mean instead of one specific frame (e.g. end-expiration or end-inspiration) (Metz *et al* 2011). In principle, double-gating provides 5D (3D + respiratory gate + cardiac gate) data sets from which cardio-pulmonary motion fields may be estimated via gate-gate registration. This is robust for normal CT, which is fast enough (~0.3 s/revolution) for individual gates to have sufficient angular sampling and be free of artifacts. However, for CBCT, the individual gates may contain only 2% of the total data (e.g. if 20% respiratory and 10% cardiac temporal framing is used) due to the slower gantry rotation (~10–40 s), and the resulting streak artifacts from undersampled projection angles will strongly bias the estimation of motion fields based on gate-gate registration. One approach to mitigate this problem is to register the original gated frames (with motion + sampling artifacts) to a simulated motion-free gated data set containing only sampling artifacts (Brehm *et al* 2015).

3D–2D registration approaches estimate and compensate for motion by registering the measured projection images to those generated from a known reference volume or initial reconstruction that is iteratively updated (Zeng *et al* 2005, Hansis *et al* 2008, Berger *et al* 2016, Ouadah *et al* 2016). This has been applied in all forms of CT, including registration of a reference gate and individual respiratory-gated CBCT frames to determine non-rigid motion fields (Dang *et al* 2015); registration of a motion-free reconstruction of the tibia and femur with 2D projection images of the bones under load (Berger *et al* 2016); and registration of a 3D arterial tree model and 2D projection images to estimate motion in CBCT angiography (Blondel *et al* 2004, Klugmann *et al* 2018).

The third main approach for data-driven estimation of non-rigid motion characterises the motion via a motion artifact metric defined in image space. Motion correction is then performed by iterative minimisation of this metric. These methods usually impose various assumptions about the object and seek to optimize quantities such as entropy or positivity measures for the 3D reconstruction (Kyriakou *et al* 2008, Katsevich *et al* 2011, Rohkohl *et al* 2013). Although conceptually appealing, achieving robust estimation (and correction) using these methods has proven difficult in practice.

Recently, CNNs have been applied directly or indirectly to data-driven motion estimation in CT. This includes CNN-derived 3D keypoints to drive a downstream non-rigid registration of respiratory-gated CT frames (Blendowski and Heinrich 2019); CNN-based image registration (Foote *et al* 2019, Lei *et al* 2019); CNN-based detection and classification of motion artifacts in CCTA (Sprem *et al* 2017, Elss *et al* 2018, Lossau *et al* 2019a); and CNN-based cardiac motion estimation directly (Lossau *et al* 2019b). The latter exhibited poor rotational accuracy of several tens of degrees, which may be explained in part by the small training set. It is likely that for robust performance in ambitious CNN-based tasks like direct motion estimation, large training sets will be essential. Unfortunately, large training sets are not readily available with ground truth for different CT applications. This presents an important area for future development so that the full potential of CNNs can be exploited. In summary, the feasibility and rationale of specific implementations of CNN-based approaches for data-driven motion estimation is yet to be clearly demonstrated, but the time is ripe for a thorough development of such methods .

3.6. Summary and outlook

Clearly many different techniques exist for motion estimation in SPECT, PET and CT. This diversity reflects both the diversity of applications and the absence of a 'silver bullet' solution. In table 2 we attempt a comparison of the different approaches surveyed in this review. Where possible an absolute comparison is shown (e.g. sampling rate) but in all cases a relative comparison is expressed using colour-coding: green for the best performance, orange for intermediate performance, and red for the worst performance. Combinations of colours indicate where variation in performance is expected.

Stereo-vision has clearly been the most widely used external tracking method for motion estimation in motion-corrected imaging, but mostly limited to research studies. Stereo implementations have benefited from the extensive development of methods and algorithms from fields outside of medical imaging, including computer vision, photogrammetry and robotics. However, the prevalence of this approach mainly reflects good performance and flexibility across the range of relevant specifications (section 3.1 and table 2). More recently there has been a notable trend towards marker-free stereo tracking based on multi-view camera systems, structured light systems and depth cameras (Olesen *et al* 2011, Kyme *et al* 2014, Noonan *et al* 2015). Marker-free systems attempt to mitigate an important practical limitation of vision-based systems, namely the attachment of markers to the subject and the associated risk of decoupling of marker-subject motion. The trend also reflects the importance of simplifying implementations for practical deployment and thereby encouraging more widespread uptake of vision-based systems for motion-corrected imaging in research and clinical applications (Kyme *et al* 2018).

With the exception of rigid-body motion (e.g. of the head, jaw and limbs) where, in general, external tracking may provide a robust direct surrogate for internal motion, external motion estimation methods all require an implicit or explicit model mapping external-to-internal motion. This is particularly challenging in the abdomen and thorax. In these cases, data-driven methods have obvious appeal. For this reason, and also because of their practical convenience (i.e. no other hardware or equipment required, with the exception perhaps of a gating device such as ECG or respiratory belt), data-driven motion estimation methods have consistently featured in the literature. Data-driven methods do, however, vary in performance due to both theoretical factors and data limitations (e.g. noise). Nevertheless, we expect to see a continued effort towards improving the robustness of data-driven methods for all forms of motion in different applications of SPECT, PET and CT.

The rise of deep learning techniques, in particular CNN-based models applied to imaging data sets, also presents a new opportunity for data-driven motion estimation in SPECT, PET and CT. To date only a handful of studies exist which involve CNNs being applied to motion-related tasks in SPECT, PET and CT. An obvious opportunity is to apply CNN-based registration methods to gated SPECT, PET and CT data to estimate non-rigid cardio-pulmonary motion fields (Clough *et al* 2018). However, numerous other approaches involving CNNs are possible. CNNs have shown excellent promise in providing image-based correction of other sources of artifacts in PET, such as attenuation and scatter (Yang *et al* 2018, Shiri *et al* 2019), thus it seems natural to explore their potential for motion estimation and correction. Many open questions exist, including: the extent to which the manifestation of motion can be learned, especially as the number of DoF increases; whether motion can indeed be learned directly or whether CNNs better serve as one step in a larger pipeline; which input is optimal: raw data, projection (sinogram) data or image data; and how such models can be extensively trained given the paucity of labelled data and in the absence of ground truth. We see these and other questions as very productive avenues of future research.

Having considered approaches for motion estimation, we now turn to how the derived motion fields are used to correct for motion in SPECT, PET and CT.

4. Motion correction methods in SPECT, PET and CT

4.1. Introduction

Conventional image reconstruction methods for SPECT, PET and CT rely on the assumption that the subject remains stationary during data acquisition. If this assumption is violated the reconstructed images suffer from motion artifacts that typically manifest as distortions and blurring and which lead to a loss of quantitative accuracy. This section reviews methods of motion correction, which are techniques to reduce or eliminate such artifacts. Nearly all of these methods are closely associated with methods of motion estimation since they require knowledge of the subject's motion during the scan to apply a correction. A possible exception to this would be the future development of neural network-based approaches trained to remove motion artifacts from reconstructed images without *a priori* knowledge of the motion.

The motivation for motion correction largely depends on the imaging application: clinically it is used primarily to obtain images free of motion artifacts for improved diagnosis and patient management; in research it allows observations to be based upon more accurate image data; in preclinical imaging, correction for

Table 2. Comparision of motion estimation technologies for SPECT, PET and CT. Technologies are compared across several specifications using a relative colour scale: green (best performance), orange (intermediate performance) and red (worst performance). A combination of colours is used where variation in performance is expected. In some cases the technologies are compared in an absolute sense, indicated by a specific value[(a)].

MOTION ESTIMATION METHOD		SPECIFICATION							
		DoF	Accuracy[(b)]	Sampling rate (Hz)[(c)]	Latency (ms)[(d)]	Impact	Constraints	Hardware & data	Scalability
EXTERNAL									
Mechanical		6	0	>100	<10	Attachment of mechanical arm; inertia of mechanical arm.	Collisions with gantry; photon attenuation!; rigid attachment.	Low bandwidth for high data rate.	Bulky mechanical arm.
Magnetic		6	+	>50	<10	Attachment of sensors and wireless hardware; tethered sensors also possible.	Nearby metallic objects; EM interference; tethering necessary if not wireless.	Low bandwidth for high data rate.	Sensors + hardware for wireless transmission unless tethering is used.
Stereo-vision (sparse)		6+	-	>30	≥10	Impact is reduced if marker-free (i.e. native features used).	Multi-camera line-of-sight.	Multi-camera data stream.	Miniature cameras available; accuracy scales with working distance / sensor resolution.
Stereo-vision (dense)		6+	-	>30	≥10	Typically marker-free.	Multi-camera line-of-sight.	High bandwidth required.	Consumer-grade depth cameras too bulky for miniature applications.
Mono-vision		6+	0	>30	≥10	Attachment of marker.	Single camera line-of-sight.	Single camera data stream.	Miniature cameras available; accuracy scales with working distance / sensor resolution.
Moire grating		6	-	>50	40	Attachment of marker.	Single camera line-of-sight.	Single camera data stream.	Limit on practical marker size for robust measurement.
Structured light		6+	-	>10	≥50	No impact if IR illumination.	Surface properties and topology.	Projector, camera; large data stream.	Improved by using optical fibre coupling of projected light and/or camera.
Inertial sensors		6	+	>100	<10	Attachment of sensors, power and wireless hardware; tethered sensors also possible.	Self-contained; non line-of-sight; tethering necessary if not wireless.	Low bandwidth for high data rate.	Sensors + power + hardware for wireless transmission unless tethering is used.
FIDUCIAL-BASED		6+	(e)	(f)	Variable	Attachment / implantation.	Firm attachment; limited number of fiducials.	Working with native raw data.	Limited only by the intrinsic resolution of the scanner.
DUAL MODALITY									
SPECT/PET	CT	6+	+	~3 (g)		Additional dose from CT	Motion and energy mismatch between SPECT/PET and CT.	Dual-modality scanners are standard	Clinical and preclinical systems available.
SPECT/PET	MR	6+	+	(h)		No additional dose; potential anxiety from claustrophobia.	Many MR sequence options during PET acquisition.	Cost is significantly greater compared to SPECT/CT and PET/CT.	Clinical and preclinical systems available.
DATA-DRIVEN									
Projection-based	SPECT/PET	1-6+				Data-driven.	Number of SPECT heads; increased noise; intra-frame motion.	Data-driven.	
	CT	1-6+				Data-driven.	Rate of acquisition (CT v CBCT).	Data-driven.	
Consistency condition-based	SPECT/PET	1-6				Data-driven.	Mathematical / geometric; increased noise.	Data-driven.	
	CT	1-6				Data-driven.	Mathematical / geometric.	Data-driven.	
3D-2D registration	SPECT/PET	6+				Data-driven.	Reference scan required; intra-frame motion; increased noise.	Data-driven.	
	CT	6+				Data-driven.	Reference scan required.	Data-driven.	
Image-based	SPECT/PET	6+				Data-driven.	Intra-frame motion; increased noise.	Data-driven.	
	CT	6+				Data-driven.	Rate of acquisition (CT v CBCT).	Data-driven.	
CNN-based		?	?	?	?	Data-driven.	Sourcing sufficient (labelled) training data is likely to have a significant impact on performance.	Specialised hardware required for model training.	

(a) Since many different implementations are possible, absolute values represent our best estimate of performance across a range of research and commercial implementations.
(b) For accuracy, '+' refers to worse than 1 mm / 1 deg; '0' refers to approximately 1 mm / 1 deg; and '–' refers to sub-millimetre / sub-degree.
(c) Measurement sampling rate, as defined in Section 3.1.3.
(d) Processing latency, as defined in Section 3.1.4.
(e) Better than the reconstructed spatial resolution of the scanner due to sub-pixel estimation of fiducial locations.
(f) Variable. Depends on the temporal resolution of the imaging modality: SPECT (worst) < PET < CT (best).
(g) ~3 rotations/s for state-of-the-art CT; corresponds approximately to a 20% respiratory gating window (5 bins) between end-expiration and end-inspiration.
(h) Variable. Depends on the MRI sequence used.

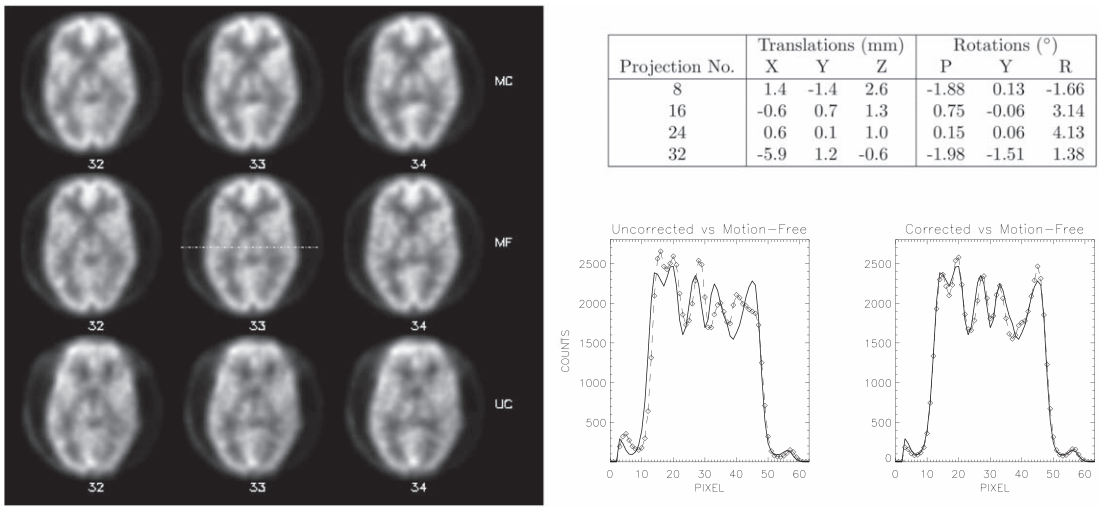

Projection No.	Translations (mm) X	Y	Z	Rotations (°) P	Y	R
8	1.4	-1.4	2.6	-1.88	0.13	-1.66
16	-0.6	0.7	1.3	0.75	-0.06	3.14
24	0.6	0.1	1.0	0.15	0.06	4.13
32	-5.9	1.2	-0.6	-1.98	-1.51	1.38

Figure 5. Motion correction of a rigidly moving Hoffman brain phantom acquired on a Trionix Triad SPECT scanner. Left: Reconstructed slices of the moving phantom without motion correction (lower row), with the phantom stationary (middle row), and moving phantom with motion correction (upper row). Right: Step motions applied to the phantom during acquisition (top), and comparison of horizontal profiles through the middle of the image with and without motion correction versus motion-free reference (bottom) (Fulton *et al* 1999). Reproduced with permission from Fulton 2000.

respiratory and cardiac motion may be beneficial for anaesthetised animals, but correction for head motion is usually unnecessary as it can be well controlled using a head holder. Head motion correction is, however, necessary when imaging awake and unrestrained animals.

In classifying motion correction approaches we distinguish between methods addressing rigid motion and non-rigid motion. Rigid motion, such as motion of the head, is relatively easy to measure accurately using the motion of surface points as a surrogate (see section 3). However, it is much more challenging to obtain accurate estimates of non-rigid internal motion in the abdomen and thorax from external observations. Therefore, correction for non-rigid motion is generally less robust unless accurate knowledge of the internal motion is available—e.g. from gated frames or from the MR data in simultaneous PET/MR imaging.

4.2. Correction for rigid motion

Although correction methods for rigid motion can in principle be applied to any body part that moves rigidly, they have been applied primarily to the brain and heart.

4.2.1. SPECT

Early works on rigid motion correction in brain SPECT had the disadvantage that they required projection data at certain angles affected by motion to be discarded, or were unable to correct for motion in all six DoF (Eisner *et al* 1987, Li *et al* 1995a, 1995b, Pellot-Barakat *et al* 1998). Correcting for motion in all DoF can, however, be achieved by reconstructing from a 'virtual' detector trajectory that is obtained by perturbing the actual trajectory by the inverse of the head motion at each projection angle (Fulton *et al* 1994, 1999) (figure 5). While able to correct for view-to-view motion, this method cannot address motion during the acquisition of individual projection views unless the projection data are acquired in list mode (McNamara *et al* 2008). Reconstructing from a modified (virtual) detector trajectory restores projection consistency but cannot compensate for situations in which the patient's head motion, in combination with the detector motion, results in incomplete data (Orlov 1975, Tuy 1983).

The feasibility of obtaining motion information from the projection images themselves, termed data-driven motion estimation, rather than using a motion tracking system, and reconstructing with the virtual projection method, has also been investigated (Hutton *et al* 2000, 2002, Kyme *et al* 2003, Feng *et al* 2006). Whereas these works treated motion estimation and motion correction as separate problems to be performed in succession, the motion estimation and correction steps can be combined into a single optimization problem, in which the 6 DoF motion and the motion corrected image are successively updated in a 2-step iterative fashion (Schumacher *et al* 2009).

Rigid motion correction methods have also been developed for SPECT cardiac imaging. The heart tends to shift in the superior–inferior direction as respiration slows following the exercise phase of a stress/rest imaging protocol. Correction may be applied by shifting the projection data to compensate, with motion modelled as a rigid translation, e.g. Mester *et al* (1991), Botvinick *et al* (1993), Eisner *et al* (1993), Germano *et al* (1993),

Britten *et al* (1998), Lee and Barber (1998), Mitra *et al* (2012). The accuracy of this approach is limited by the fact that cardiac motion is non-rigid (Rahmim *et al* 2007). The heart rotates and changes shape during contraction, as well as being affected by respiratory motion, for which no rigid motion correction method can fully compensate (Pretorius *et al* 2016). Several automated or semi-automated correction algorithms for upward creep have been reported, e.g. Matsumoto *et al* (2001), Uchiyama *et al* (2005), Mitra *et al* (2011), Kangasmaa and Sohlberg (2014). Motion correction may also be combined with strategies for mitigating cardiac motion, including the use of pharmacological vasodilation for exercise (Anagnostopoulos *et al* 1995) or patient support devices (Cooper and McCandless 1995).

In contrast to conventional Anger camera-based SPECT systems, the introduction of dedicated cardiac SPECT cameras characterised by stationary solid state cadmium–zinc–telluride detector modules allows a different approach to the correction of upward creep in myocardial imaging (Redgate *et al* 2016, Wu and Liu 2019). On these systems pinhole images are acquired by all detectors simultaneously, so that shifts in the x, y and z directions can be estimated from changes in position of the images on the detectors and knowledge of the detector inclinations. Alternatively, motion can be estimated by segmenting the emission data into a series of short frames, reconstructing the frames, and estimating the motion from the reconstructed frames (Van Dijk *et al* 2016, 2018). With either approach corrections can be applied for translations along all 3 coordinate axes.

Correction of intra-frame motion requires a SPECT scanner with list mode capability, enabling a time-specific correction for rigid motion to be applied to each event prior to reconstruction (Bruyant *et al* 2002, Ma *et al* 2005).

In preclinical brain SPECT, motion correction has been successfully applied to fully conscious unrestrained mice inside a 'burrow' within the scanner (Weisenberger *et al* 2005, Baba *et al* 2013), using list mode reconstruction and data from a synchronised optical motion tracking system.

4.2.2. PET

Much more has been published on rigid motion correction methods for PET than SPECT because of the more widespread use of PET in neuroimaging and neuroscience. The multiple acquisition frame (MAF) motion correction method is applicable to PET scans acquired as a series of dynamic (temporal) frames (Picard and Thompson 1997). The separately reconstructed frames are registered in 3D to one of the frames chosen as a reference. The six DoF transformations to register each frame with the reference frame can be obtained using either an automated 3D image registration algorithm, or from an optical motion tracking system calibrated to the PET coordinate frame (section 3.2.3). When image registration is used to obtain the transformations, their accuracy depends on the individual images having sufficient counts and being free of artifacts caused by intra-frame motion. For accurate attenuation and scatter correction it is necessary to transform the attenuation data to match the pose of the emission data prior to the reconstruction of each frame (Fulton *et al* 2002). To counteract intra-frame motion a new frame may be commenced whenever motion reaches a preset threshold. However, there is a practical limit here as correction for continuous head motion would entail the reconstruction and registration of an unwieldy number of low-count frames. The efficacy of the MAF method has been demonstrated in PET research applications, for example parametric imaging (Tellmann *et al* 2004, Herzog *et al* 2005b).

With cooperative healthy subjects intra-frame motion is often negligible. However, a more sophisticated approach is needed when intra-frame motion is sufficient to cause artifacts. Intra-frame motion can be corrected by acquiring the data in list mode and adjusting the position and orientation of the lines-of-response (LoR) of individual coincidence events in response to changing head pose (Daube-Witherspoon *et al* 1990, Menke *et al* 1996). Motion relative to an arbitrarily chosen reference pose at any time during the scan is expressed as a six DoF spatial transformation. The inverse of this transformation is applied to the 3D coordinates of the detectors in coincidence to obtain a motion-corrected LoR, which is recorded in a 3D sinogram. Reconstruction of this motion-corrected sinogram provides the motion-corrected image. The transformations can be performed either post-acquisition (Bloomfield *et al* 2003, Fulton *et al* 2003, Woo *et al* 2003, Bühler *et al* 2004, Fulton *et al* 2004, Watabe *et al* 2004), or on-the-fly during acquisition by performing the geometrical transformations in hardware (Jones 2002).

In contrast to the MAF method where the same motion-corrective transformation is applied to all events in a frame, event-by-event methods apply the transformation to the much smaller number of events in a list mode time bin (typically 1 ms in duration). In the presence of rapid motion this enhances the ability of the motion correction algorithm to apply the true transformation to each event. The full potential of this 1 kHz update rate has not yet been realised due to the relatively low sampling frequency of optical motion tracking systems (30–120 Hz).

While potentially more accurate than the MAF method, the sinogram-based LoR rebinning method has the disadvantage that some events cannot be recorded in the motion-corrected sinogram after spatial transformation because the obliqueness of the transformed LoR exceeds the maximum allowed ring difference or because the LoR moves entirely out of the transaxial FoV (Akhtar *et al* 2013). The extent of the count loss

depends on the magnitude, direction and duration of pose changes relative to the reference pose during the scan. Thus, it can be mitigated in part by a shrewd choice of reference pose, but even then the count losses and their impact on quantitative accuracy can be substantial. In awake animal studies the losses can exceed 80% of all coincidence events.

An alternative to histogram-based LoR rebinning that avoids count losses is to pass the transformed coordinates of the detectors involved in each coincidence event directly to a list mode expectation maximisation (LM-EM) reconstruction algorithm (Qi and Huesman 2002, Reader *et al* 2002, Carson *et al* 2004, Johnson *et al* 2004, Rahmim *et al* 2004). This approach removes the constraint that transformed LoRs must intersect with a detector pair and allows all transformed events to contribute to the motion-corrected image. There is also an improvement in accuracy since the transformed LoR coordinates may be used directly in reconstruction instead of assuming, as is done in histogram-based LoR rebinning, that each photon of the transformed coincidence pair interacted with the centre of the nearest physical detector.

In all of these LoR transformation methods, normalisation requires special attention since the normalisation coefficient of the LoR to which the event is assigned after transformation is likely to differ from that of the LoR on which it was detected. If the transformed events are histogrammed into a sinogram, LoRs associated with detector pairs with different normalisation coefficients will be recorded in the same sinogram bin, causing errors when conventional normalisation is applied during reconstruction (Fulton *et al* 2003, Bühler *et al* 2004). It has been shown that these methods can produce artifacts unless the different numbers of LoRs contributing to sinogram bins as a result of data compression strategies (axial and angular mashing) are properly accounted for (Zhou *et al* 2009). As an alternative to pre-normalisation, post-normalisation methods can be applied if a motion-averaged normalisation array is constructed (Thielemans *et al* 2004, 2008). However, this can be very demanding computationally, especially for scanners with large numbers of LoRs and when the motion is frequent, and requires the emission data to be precorrected for attenuation. A faster alternative is to calculate, using a GPU, a time-weighted motion compensated sensitivity matrix in image space. This is applicable to both histogram-based and LM-EM LoR transformation methods and is done by considering the trajectory of each object voxel as it moves within the FoV, averaging the values of all the conventional sensitivity matrix voxels visited along the way, weighted for the time spent in each location (Rahmim *et al* 2004, 2008, Bashar *et al* 2013). Some typical approaches to scatter correction in conjunction with motion-corrected reconstruction are described in Carson *et al* (2004), Thielemans (2005), Rahmim *et al* (2008).

Deconvolution approaches have also been explored as a means of correcting for head motion in brain PET. If the motion is known (e.g. from optical motion tracking) an iterative ML-EM deconvolution scheme can be used to estimate the true activity distribution (image) from the motion-corrupted image (Faber *et al* 2009, Raghunath *et al* 2009). Here, deconvolution is used to find the estimate of the true image which, when the known motion is applied to it, gives a best match to the motion-blurred image.

Variations of the above motion correction methods have been adapted successfully to brain PET imaging in animals, including rats (Zhou *et al* 2008, Spangler-Bickell *et al* 2016, Miranda *et al* 2017, Angelis *et al* 2019, Kyme *et al* 2019) and non-human primates (Watabe *et al* 2002, Jin *et al* 2014). Here the primary objective of motion correction is to enable the brain of an animal to be imaged while awake, avoiding the need for anaesthesia which is known to affect measured parameters of neurological function such as blood flow and receptor binding. In some implementations, the animal's brain is imaged while the animal is moving freely within an enclosure in the PET FoV (Angelis *et al* 2019, Kyme *et al* 2019).

The introduction of integrated PET/MR systems capable of simultaneous PET and MR imaging has provided new ways to correct PET studies based on motion derived from MRI (section 3.3). In one of the first demonstrations of this approach, 3D translational and rotational head motion estimates were obtained in human volunteer studies from echo planar imaging and cloverleaf navigator sequences every 3 s and 20 ms, respectively, then applied offline for motion correction of the PET data with LoR rebinning (Catana *et al* 2011). Correction accuracy was limited by signal contamination from non-rigid motion of the neck. Good results have also been obtained using wireless coils (Huang *et al* 2014b) (figure 6), an optical camera attached to the head coil (Spangler-Bickell *et al* 2019), and 3D image registration (Reilhac *et al* 2018) to provide 6 DoF motion information for list mode reconstruction in simultaneous PET/MR. The application of 3D image registration to PET frames as short as 1s has been shown to provide 6 DoF motion estimates of sufficient accuracy for motion correction of brain PET scans with list mode reconstruction in PET/CT and PET/MR (Spangler-Bickell *et al* 2021).

Methods for direct parametric reconstruction of dynamic brain PET data, with motion correction, have also been reported. Rather than reconstructing a series of dynamic frames, these methods incorporate the kinetic model into the reconstruction algorithm to directly fit the model to each voxel time-activity curve. To correct for motion, the motion may be estimated by an optical motion tracking system and undone using LoR transformation (Germino *et al* 2017) or, alternatively, estimated along with kinetic parameters from the raw

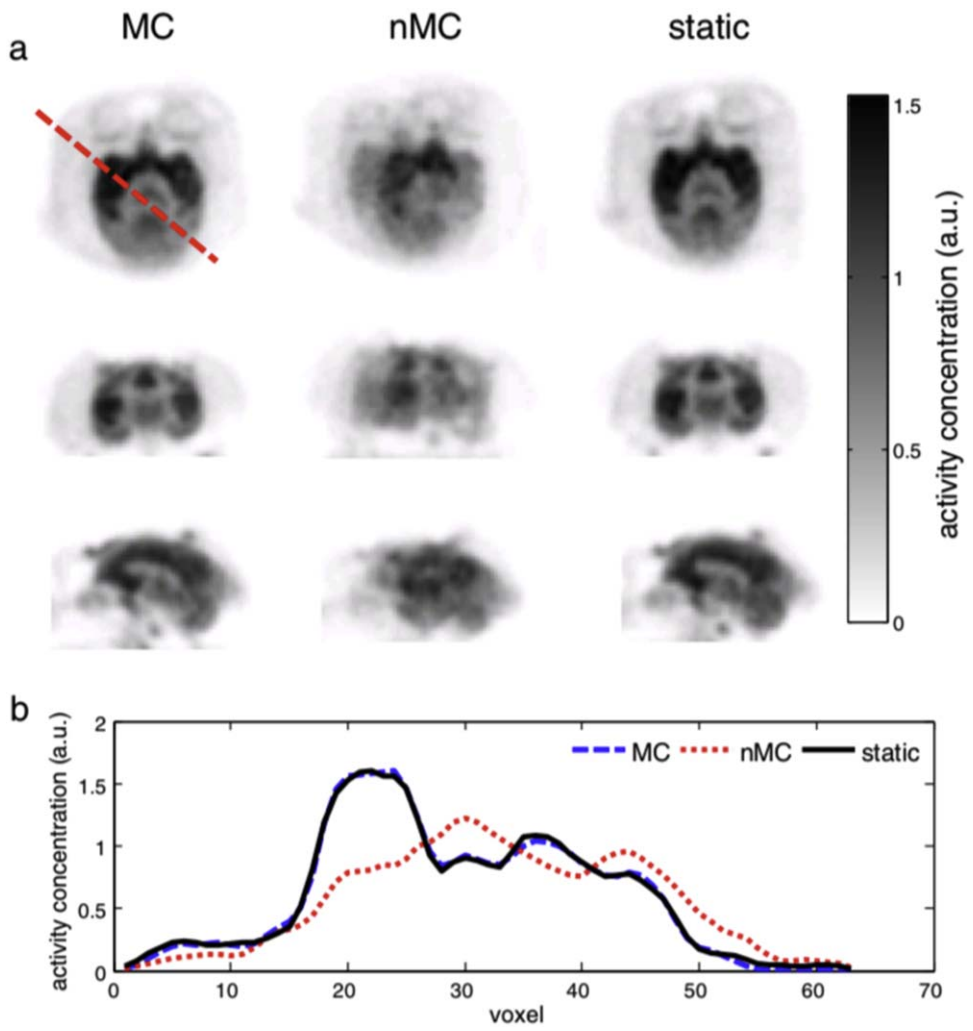

Figure 6. A PET brain scan of an anaesthetised monkey acquired on an integrated PET/MR scanner, in which 6 DoF head motion was estimated by tracking miniature wireless coils on the head with a dedicated MR sequence. (a) Motion-corrected images (left column), uncorrected images (middle column) and motion-free images (right column). (b) Comparison of motion-corrected, uncorrected and motion-free images profiles along the direction shown in (a). Adapted from Huang *et al* 2014. Copyright © 2014 Elsevier Inc. All rights reserved.

PET data in a joint estimation problem where the kinetic and motion parameters of the likelihood function are alternately updated (Jiao *et al* 2017).

4.2.3. CT

The majority of publications on motion correction methods for CT imaging address non-rigid motion in cardiac and other forms of thoracic CT imaging (see section 4.3.3). Relatively little has been published on the less challenging, but nevertheless non-trivial, problem of correcting for the motion of bodies that move rigidly, such as the head.

Early rigid motion correction methods for CT were limited to in-plane motion. Correction for in-plane translation of the object during helical CT acquisition was achieved by applying compensatory shifts to the projection data prior to interpolation into parallel projection views and reconstruction (Wang and Vannier 1995), and other similar approaches (Schäfer *et al* 2004, Yu *et al* 2006, Zafar *et al* 2007, Pauchard and Boyd 2008). In-plane (i.e. transaxial) rotation can be corrected similarly since it causes an apparent shift of the object in the tangential direction that can be undone by shifting the projection data in the opposite direction (Fahrig and Holdsworth 2000, Yu and Wang 2007, Zafar 2011). Rotations about axes other than the CT scanner rotation axis have effects on the projection data that cannot be compensated merely by shifting or rotating detected rays in-plane.

A more general approach, analogous to the 'virtual' detector trajectory method for SPECT described in section 4.2.1, is to reconstruct the motion-corrected image from a virtual source/detector trajectory obtained by perturbing the true trajectory to account for object motion at each view. This method can be applied to any

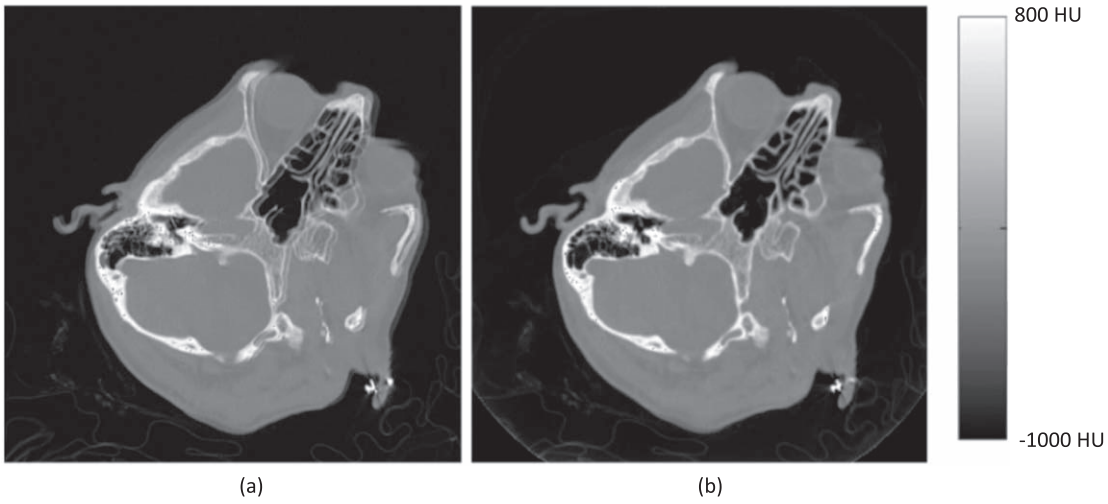

Figure 7. Motion correction applied to the helical CT scan of a patient with possible head trauma, acquired on a Siemens Force scanner (pitch 0.55, rotation time 1.0 s, 4200 projection views per rotation). (a) A slice with the vendor's standard reconstruction algorithm, showing ghost artifacts due to head motion. (b) The same slice reconstructed with motion correction using an iterative algorithm that jointly estimates head motion and the motion-corrected image (Sun *et al* 2016). John Wiley & Sons. © 2016 American Association of Physicists in Medicine.

6 DoF motion. The potential of this approach in CT appears to have been first explored by Bodensteiner *et al* (2007) who used it in an iterative procedure to identify and compensate for small perturbations of gantry motion and object motion in mobile C-Arm CT. It was subsequently applied to compensate for 'nodding' motion of a head phantom in slowly-rotating CBCT using a FBP reconstruction algorithm (Jacobson and Stayman 2008). A related technique, termed '3D re-registration motion correction', was applied to simulations of 3 DoF motion (2 rotations and one translation) using a modified FDK algorithm (Feldkamp *et al* 1984, Wells *et al* 2011).

Kim and co-workers applied the virtual trajectory approach to helical CT using motion information from an optical motion tracking system to modify the effective trajectory of the source and detector during reconstruction (Kim *et al* 2013, 2015b). In contrast to its application in SPECT where correction for intra-projection motion was problematic, intra-projection motion is negligible in helical CT since projections are acquired within very short time intervals (typically <1 ms).

The feasibility of compensating for rigid head motion in helical CT scans using a data-driven approach has also been demonstrated (figure 7) (Sun *et al* 2015, 2016). This method involves the same motion-corrected reconstruction approach as Kim *et al* (2015b) but view-to-view rigid head motion is estimated by attempting to identify, at each projection angle, the best 2D–3D registration of the current image estimate and the measured projection data. Each time the motion estimate is updated it is used to update the motion-corrected image. Estimates of the motion and the motion-corrected image are successively updated in an iterative process. Similar methods have been reported by other groups: Bruder *et al* (2016) explored one data-based (L2-norm) and two image-based (image entropy and total variation) cost functions to estimate motion from projections, rather than a linearization approximation (Sun *et al* 2015, 2016); and a locally linear embedding scheme was shown to improve motion estimation and motion correction accuracy on simulated clinical CT data and real micro-CT data (Chen *et al* 2018).

The use of iterative reconstruction algorithms in conjunction with a virtual source/detector trajectory to obtain motion-corrected images can result in reconstruction times orders of magnitude longer than conventional analytical reconstruction algorithms used in clinical CT. Recently, the analytical reconstruction algorithms FBP and FDK have been successfully applied to a virtual source/detector trajectory to provide motion-corrected helical CT images in much shorter times (Bruder *et al* 2016, Jang *et al* 2018, Nuyts and Fulton 2020). These methods have the potential to be easily integrated into clinical imaging protocols as they can be applied retrospectively to raw CT datasets with no *a priori* knowledge of the motion.

As mentioned in the context of SPECT motion correction (section 4.2.1), the combination of detector and object motion in CT imaging may result in a virtual trajectory that provides insufficient data for exact reconstruction. The potential for this problem to arise in clinical CT head imaging has been investigated in simulated CT scans with a range of realistic head motion patterns obtained from volunteers using optical motion tracking (Kim *et al* 2016). Residual data-insufficiency artifacts in the motion-corrected images were only observed when the head motion was 'severe', i.e. when subjects moved their head rapidly in multiple directions. To identify regions of an image in which motion artifact-free reconstruction is not assured, one may use a local

Table 3. Sample rigid motion correction methods.

Modality	Method	Example
SPECT (brain)	Projection selection	(Pellot-Barakat *et al* 1998)
	Virtual trajectory	With motion tracking (Fulton *et al* 1999) Data-driven (Kyme *et al* 2003) Joint estimation (Schumacher *et al* 2009)
SPECT (heart)	Projection shift	Upward creep (Mitra *et al* 2011)
	Event-by-event	(Ma *et al* 2005) Preclinical (Baba *et al* 2013)
	Dedicated scanners	(Wu and Liu 2019)
PET (brain)	Multiple acquisition frames	(Picard and Thompson 1997, Fulton *et al* 2002)
	Event-by-event	LoR rebinning (Bloomfield *et al* 2003) List mode reconstruction (Rahmim *et al* 2004) Preclinical (Spangler-Bickell *et al* 2016) Simultaneous PET/MR (Spangler-Bickell *et al* 2021) Direct parametric reconstruction (Germino *et al* 2017)
	Deconvolution	With known motion (Faber *et al* 2009)
CT (head)	In-plane correction	Projection shift (Schäfer *et al* 2004)
	Virtual trajectory	Optical tracking (Kim *et al* 2015b) Data-driven (Sun *et al* 2016)

measure quantifying the degree to which Tuy's completeness condition is violated in each voxel (Tuy 1983, Sun *et al* 2014). A summary of rigid motion correction methods is provided in table 3.

4.3. Non-rigid motion

Whereas rigid objects preserve their shape as they move, non-rigid motion of an object involves relative motion between the particles comprising it, and thus a change of shape or 'deformation'. The magnitude and nature of the deformation varies at different points within the object. A brief review of approaches to compensate for non-rigid motion in SPECT, PET and CT follows. It is worth noting that, as for rigid motion, most of these approaches rely on accurate information about the motion of the object during the scan (see section 3.2).

4.3.1. SPECT

In thoracic and abdominal SPECT imaging, respiratory motion often results in serious artifacts due to the motion of the diaphragm, liver, lungs, thoracic cage and abdominal organs. One of the first attempts to correct for respiratory motion by modelling it as deformable motion was to approximate in-plane thoracic motion as a combination of time-varying magnification and displacement in 1D (Crawford *et al* 1996) or 2D (Lu and Mackie 2002). Motion information was extracted from the SPECT sinogram by examining the sinusoidal traces of prominent features. The projection data were then rescaled and interpolated to compensate for motion effects prior to reconstruction. In practice, the traces of distinct native features were difficult to identify. This led to attempts to elucidate internal respiratory motion by tracking reflective spheres attached to the chest and using a neural network to decompose the motion data into rigid and non-rigid components (the latter representing respiratory motion) (Beach *et al* 2007, Mitra *et al* 2007).

A common approach to compensating for respiratory motion in SPECT, PET and CT is the use of respiratory gating. Synchronising the acquisition of a fixed number of sequential image 'frames' with the respiratory cycle results in a set of N images, each depicting the body at a different phase of the cycle, over a time interval N times shorter than the full cycle. This limits the amount of motion affecting each image at the expense of increasing the noise in each image. The trade-off is more significant in SPECT and PET where projection images are inherently noisy. In myocardial SPECT imaging respiratory artifacts are significantly reduced provided that the amplitude of respiratory-induced heart motion during a gating time period is <1 cm (Segars and Tsui 2002). Kovalski *et al* combined respiratory gating with list-mode acquisition, detecting the shifts between bins and rebinning the data into projections to compensate for these shifts (Kovalski *et al* 2007). Motion correction of respiratory-gated SPECT images of the lung has also been reported. End-exhalation and

end-inspiration respiratory gated 99^m-Tc-MAA lung perfusion images may be non-rigidly registered and added together to obtain a less noisy image (Ue *et al* 2006, 2007).

Cardiac-gated SPECT acquisition, synchronized with the cardiac cycle via an ECG signal, produces a set of images of the myocardium at different phases of the cardiac cycle, each with reduced motion artifacts (but increased noise) compared to the ungated image. The gated images allow one to model and correct for the physical deformation of the heart during the cardiac cycle in order to create a motion-corrected summary image with a SNR similar to that of the ungated image. Various approaches have been developed to identify cardiac motion, including tracking anatomical points within the heart through the series of gated images to create a vector field of displacements (Laading *et al* 1999), and incorporating a temporal regularization into the reconstruction process using a temporal prior (Yang and Gravier 2004, Gravier *et al* 2007). Optical flow methods have also been used extensively to estimate frame-to-frame heart deformations in cardiac-gated imaging. A content-adaptive mesh model tomographic reconstruction framework based on a deformable non-uniform sampling grid (Brankov *et al* 2004) has shown good performance for motion-corrected cardiac-gated myocardial SPECT imaging (Marin *et al* 2010). For a good summary of these approaches see (Gilland *et al* 2008).

Further improvement in SPECT myocardial perfusion image quality has been reported with simultaneous respiratory and cardiac gating (Bitarafan *et al* 2008, Kovalski *et al* 2009, Chan *et al* 2014, Qi *et al* 2017).

4.3.2. PET

In PET lung imaging, the ability of respiratory gating to reduce respiratory motion artifacts has been well demonstrated (Nehmeh *et al* 2002, Rahmim *et al* 2007, Guerra *et al* 2012). Deformable registration methods that combine the gated images into a single composite image have been developed using, for example, a 12-parameter affine motion model (Klein *et al* 2001a), optical flow (Dawood *et al* 2005, 2008, Huang *et al* 2014a) and polynomial warping (Woo *et al* 2005). Jacobson *et al* proposed a motion correction method for ungated data that incorporates parameters describing the deformable motion into a statistical projection model. Joint maximum likelihood estimation of both deformation parameters and the image parameters allowed for more accurate motion estimation than frame-based reconstruction followed by image registration, however it did not improve the accuracy of lesion uptake measurements (Jacobson and Fessler 2004). Similar approaches have been reported by Blume *et al* (2010), Kalantari *et al* (2016). These methods model the time-varying relationship between the motion and projection data with respect to a single motion-free image. By optimizing an objective function, the image and motion may be jointly estimated in PET/CT (Bousse *et al* 2016), and in PET/MRI with motion-adjusted attenuation information derived from the MRI scan (Bousse *et al* 2017). Several CT and MRI-based methods can be used to estimate the required non-rigid motion fields (see section 3.3).

Motion correction methods using frame-based image reconstruction followed by deformable image registration of respiratory-gated PET data suffer from errors due to the difficulty of accurately estimating non-rigid motion from frames containing high levels of noise. There is good evidence that improved registration accuracy, and better computational efficiency, can be achieved using deep neural networks. For example, unsupervised non-rigid image registration was incorporated into PET image reconstruction (Li *et al* 2020). Unsupervised approaches have excellent practical utility since model training does not require ground truth.

Respiratory motion can also reduce the accuracy of operator-drawn ROIs and the resulting time-activity curves, for example in dynamic $^{13}NH_3$-ammonia PET myocardial blood flow studies. Accuracy can be improved by aligning the measured data to template images of blood pool and myocardium typifying the tracer distribution at different stages of uptake (Turkington *et al* 1997). This method provides accurate 3D image registration, even in early frames with low counts. In PET/CT, mismatch between PET and CT images (due to the PET image being acquired relatively slowly over multiple respiratory cycles compared to the 'snapshot' CT) can lead to significant error in estimating regional cardiac uptake, as had previously been shown at the borders between lung and soft tissue in oncologic PET/CT (Le Meunier *et al* 2006). Respiratory gating mitigates this effect (Livieratos *et al* 2006, Wells *et al* 2010, Ren *et al* 2017, 2019).

In PET, as in other imaging modalities, contractile motion of the heart itself can be mitigated using cardiac gating (Rahmim *et al* 2007). There have been several efforts to recover a single composite motion-corrected cardiac image from all acquired events, including using deformable image registration (Klein *et al* 1997, Klein 1999) or the optical flow constraint (Gilland *et al* 2008) to align the cardiac gated images.

Cardiac motion effects can also be mitigated using motion data derived from simultaneous PET/MR. Once non-rigid myocardial wall motion fields are obtained (using, for example, tagged MRI), this information may be incorporated, together with a position-dependent point spread function, into the reconstruction system matrix to obtain an image with correction for both motion blurring and the partial volume effect (Petibon *et al* 2013). Both cardiac and respiratory motion estimates can be combined into a single non-rigid motion vector field for incorporation into a motion-corrected reconstruction with time-dependent MR-derived attenuation correction (Ouyang *et al* 2014). Variations of this approach are described in Robson *et al* (2018) and Kolbitsch *et al* (2019).

Several groups have investigated dual-gating approaches, in which respiratory and cardiac gating are performed simultaneously, and estimates of both non-rigid respiratory motion and non-rigid cardiac motion are used to apply motion correction (Lamare *et al* 2014, Feng *et al* 2016, Klen *et al* 2016, Feng *et al* 2018). Motion correction may be applied after (AR), during (DR), or before (BR) reconstruction (Feng *et al* 2016). In AR methods, motion correction is applied to gated images via non-rigid registration, whereas DR methods incorporate the motion information in the reconstruction algorithm, and BR methods apply the correction in the projection domain. A mass-preserving image registration algorithm was applied to dual-gated cardiac PET data to estimate and apply AR correction for both respiratory and cardiac motion (Gigengack *et al* 2012). However, changes in the attenuation distribution due to motion were not considered in this work, limiting quantitative accuracy. An inter-comparison of AR, DR and BR respiratory motion and cardiac motion methods, using Monte-Carlo simulated dual-gated data and attenuation maps transformed according to the estimated respiratory motion, was conducted by Feng *et al* (2016). Optimal motion correction accuracy over a range of noise levels was obtained with DR motion correction. In a comparison of four different AR methods with simulated data, separate estimation of respiratory and cardiac motion, with modeling of respiratory motion before cardiac motion estimation, provided the most accurate estimation of respiratory and cardiac motion (Feng *et al* 2018).

Deconvolution-based motion correction methods rely on the estimation of a suitable de-blurring motion kernel (El Naqa *et al* 2006, Thomas *et al* 2019) which, in dual-modality systems, can be estimated from CT or MRI-derived motion fields. It is, however, also feasible to derive the motion PSF directly from ungated SPECT and PET reconstructions corrupted by respiratory motion (Xu *et al* 2011), albeit with limited practicality for small lesions.

For quantitatively accurate correction of both rigid and non-rigid motion in PET, it is important to correct not only for motion/deformation of the radioactivity distribution within the patient but also accompanying changes in the attenuation distribution (Pevsner *et al* 2005, Khurshid *et al* 2006, McQuaid and Hutton 2008, Bai and Brady 2011). In PET/CT, gating of both the CT and PET scan can provide well-matched images, but this entails a high radiation dose from the gated CT scan (Ponisch *et al* 2008). An alternative approach is to construct registered CT attenuation images for each PET frame by applying spatial transformations to a single CT scan. In an example of this approach, Radon consistency conditions were used to transform a single CT image into alignment with the respiratory-gated PET frames prior to attenuation correction, then the inverse transformations were applied to align the gated PET images into a single image (Alessio *et al* 2007).

4.3.3. CT

Non-rigid motion of internal organs, as a result of respiration, cardiac contraction and gastrointestinal motion, also causes image artifacts in abdominal and thoracic CT imaging. This affects the use of slow-rotating CBCT for tumour delineation as part of radiotherapy treatment planning and the use of modern multi-slice helical CT scanners in diagnostic procedures (Moorrees and Bezak 2012).

When imaging is fast, as with helical CT, respiratory motion may sometimes be avoided by breath-hold imaging provided the patient is able to comply. However, this is rarely the case in CBCT where the acquisition of a full set of projection data typically takes minutes. Some of the earliest work in this area was to model cardiac and respiratory motion as entirely in-plane, evaluating at every pixel to derive a motion map (Ritchie *et al* 1996). Motion artifacts were shown to be reduced in clinical scans by pixel-specific backprojection, i.e. by performing the backprojection in a frame of reference that moves with the object. The main shortcoming of this method was its inability to correct for out-of-plane motion.

In slow-rotating CBCT, a commonly used approach is respiratory gating, e.g. Sonke *et al* (2005), Hinkle *et al* (2012), Moorrees and Bezak (2012). This reduces the severity of motion artifacts since the amount of motion affecting each gated image is less than the motion during the entire respiratory cycle. However, it has the drawback of requiring the acquisition of a larger number of total projections, increasing the patient radiation dose. To counteract this, a limited subset of projections is typically acquired for the reconstruction of each phase, at the expense of image quality. Alternatively, the motion can be taken into account during image reconstruction (Rit *et al* 2009a, 2009b). In such approaches, 3D deformable motion fields due to respiration are obtained by analysis of a 4D treatment planning CT performed separately from the 3D CBCT scan and assumed to share the same respiratory motion characteristics. The motion-corrected image is then obtained using a reconstruction algorithm incorporating this motion. A similar approach has been used in C-arm imaging (Schäfer *et al* 2012).

An iterative image-based correction for respiratory motion artifacts in CBCT has also been reported (Schretter *et al* 2009). Motion artifacts are first extracted in projection space (as differences between the acquired projections and corresponding forward projections of the image reconstructed in the previous iteration step), then reconstructed in image space and subtracted from the original reconstructed image.

Wang *et al* showed that joint estimation of 3D non-rigid motion fields and the motion-compensated image in 4D CBCT could improve estimates of the reconstructed image and motion trajectory as compared to

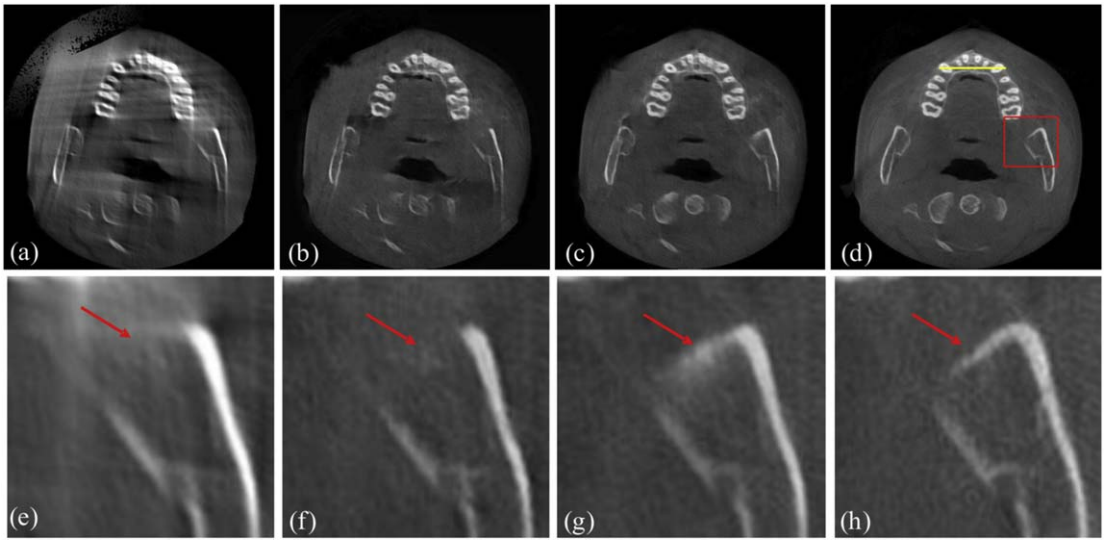

Figure 8. Motion artifact reduction in dental CT using a deep learning approach. A generative adversarial network with Wasserstein distance and mean squared error loss (m-WGAN) was trained to remove motion artifacts from real dental CT images. (a) Input image with motion artifact; (b) image obtained with standard GAN; (c) result obtained with the proposed m-WGAN; (d) labelled image. Panels (e)–(h) show zoomed portions of panels (a)–(d), bounded by the box shown in in (d). Reproduced with permission from (Jiang *et al* 2019) © (2019) COPYRIGHT Society of Photo-Optical Instrumentation Engineers (SPIE).

conventional sequential 4D-CBCT reconstruction and motion estimation in image-guided radiation therapy (Wang and Gu 2013). Following a subsequent finding that motion estimation was less accurate in the lung due to the relative absence of high-contrast structures, the same group used a CNN to fine-tune DVFs derived from joint estimation (Huang *et al* 2020).

CT volume imaging of the heart became feasible in the early 2000s with the introduction of 16-slice CT scanners with shorter rotation times of about 0.4 s, and the use of ECG-gated acquisition (Kachelriess and Kalender 1998, Kachelriess *et al* 2000). ECG-gated projection data can be reconstructed into separate frames, from which motion fields are calculated, e.g. using non-rigid registration, to characterize the motion at multiple points in the cardiac cycle. A final motion-compensated reconstruction takes the motion into account. This can significantly improve the diagnostic value of x-ray CT angiography by correcting for the motion of the coronary arteries (Isola *et al* 2012). The general approach can be applied iteratively with alternating updates of the motion field and motion-corrected image (Tang *et al* 2012). To avoid the high radiation dose of gated CT, motion correction can also be based on motion fields estimated by deformable registration of partial angle reconstructions (Kim *et al* 2015a). A point matching approach has also been used to improve the visualisation of coronary arteries without ECG gating (Bhagalia *et al* 2012).

There is growing interest in AI-based methods to replace or supplement more traditional algorithms for non-rigid motion estimation and correction, e.g. Huang *et al* (2020). A generative adversarial network (GAN) using the Wasserstein distance and mean squared error loss (m-WGAN) was trained to suppress motion artifacts in dental CT images (Jiang *et al* 2019) (figure 8). A deep learning approach has also been applied to the detection of motion artifacts in noninvasive CT coronary angiography (Elss *et al* 2018). Here, to avoid the unnecessary computation of applying a motion correction algorithm to datasets without motion artifacts, a CNN was trained to classify 2D coronary cross-sectional images as either motion-free or motion-perturbed. Training data were generated by applying artificial motion vector fields to nine high-quality ECG-triggered clinical cases. However, as recognised by the authors, it remains unclear how this method would perform on real clinical data acquired with a variety of scanner types and imaging protocols. Thus this work is still at quite a preliminary stage. Table 4 provides a summary of non-rigid motion correction methods.

4.4. Summary and outlook

The development of effective and practical methods to correct for rigid and non-rigid motion in medical and preclinical imaging with SPECT, PET, CT and the hybrid modalities PET/CT and PET/MR is an area of active research.

For the estimation and correction of rigid head motion, demonstrably effective and technically feasible methods now exist for all of these modalities. In PET, both human and preclinical, combining optical motion tracking, LoR transformation and list mode reconstruction provides an effective solution which is in routine use at several leading research centres. In PET/MR, the potential to motion-correct PET data using head motion

Table 4. Sample non-rigid motion correction methods.

Modality (motion)	Method	Example
SPECT (respiratory)	Sinogram correction	(Lu and Mackie 2002)
	Respiratory gating	(Segars and Tsui 2002) Deformable registration (Ue *et al* 2006)
SPECT (cardiac)	ECG gating	(Gilland *et al* 2008)
	Dual gating	(Qi *et al* 2017)
PET (respiratory)	Respiratory gating	(Guerra *et al* 2012) Deformable registration (Huang *et al* 2014a) Joint estimation (Bousse *et al* 2016) Deep learning (Li *et al* 2020)
	Ungated	Joint estimation (Jacobson and Fessler 2004)
	PET/MR	MR-based motion estimation (Ouyang *et al* 2014)
	Deconvolution	(El Naqa *et al* 2006, Xu *et al* 2011)
PET (cardiac)	ECG gating	(Rahmim *et al* 2007) Deformable registration (Gilland *et al* 2008)
	Dual gating	(Feng *et al* 2018)
	PET/MR	Cardiac (Petibon *et al* 2013) Cardiac and respiration (Kolbitsch *et al* 2019)
CT (respiratory)	Respiratory gating	In-plane (Ritchie *et al* 1996) CBCT (Moorrees and Bezak 2012) Algebraic (Rit *et al* 2009b)
	Joint estimation	(Wang and Gu 2013)
CT (cardiac)	ECG gating	Reconstruction-based (Isola *et al* 2012)
	Ungated	Point matching (Bhagalia *et al* 2012) Partial angle reconstruction (Kim *et al* 2015a)
	Deep learning	(Huang *et al* 2020)

data estimated from simultaneously-acquired MR sequences, instead of optical tracking, has also been demonstrated. The feasibility of correcting for head motion in SPECT has also been clearly demonstrated in human and preclinical imaging, using optically-derived motion estimates within the reconstruction. In CT, recent developments have demonstrated the feasibility of jointly estimating head motion and the motion-corrected image with a data-driven approach.

Despite technical feasibility having been established in the research environment, this has not been successfully translated into clinical feasibility since few rigid motion correction solutions are available commercially. A likely explanation for this is the issue of practicality (Kyme *et al* 2018). If head motion is continuous, high-frequency motion sampling is required. Until recently, this has only been achievable in PET and SPECT with external tracking approaches such as optical tracking. However, optical motion tracking has its own limitations, including the fact that it usually requires the attachment of markers and the setting up and calibration of a motion tracking system, all of which increases the complexity of the scanning procedure. In PET, recent work showing that 6 DoF motion estimation at 1 Hz is feasible in PET using a data-driven approach is a promising development (Spangler-Bickell *et al* 2021). In CT, data-driven motion estimation approaches can provide useful motion estimates at still higher frequencies due to the much lower noise in the rapidly-sampled projection data. Effective data-driven correction for head motion has been demonstrated using 6 DoF motion estimated jointly with the motion-corrected image from raw CT projection data in multi-slice helical CT. The practicality of this approach was limited until recently by the extensive computation required to perform motion-corrected ML-EM reconstruction, which made the method too slow for clinical use. However, recent efforts to use analytical reconstruction algorithms such as FBP and FDK are bringing reconstruction times closer

to clinically acceptable timeframes (Bruder *et al* 2016, Jang *et al* 2018, Nuyts and Fulton 2020). With further acceleration motion correction could become a clinically feasible option in head CT in the future.

Methods to estimate the rigid motion of the head with optical tracking systems are subject to several sources of error. The accuracy depends on the intrinsic accuracy of the system and the accuracy of the rigid transformation relating the coordinate systems of the tracker and scanner (usually determined via a calibration procedure, e.g. Fulton *et al* (2002)). Tracking accuracy may also be limited by the rigidity of marker attachment to the head, the frequency with which motion updates are obtained relative to the velocity of motion, and, in data-driven motion estimation, the noise level in the projection data from which the motion is estimated. Because of these potential sources of error, methods to assess the accuracy of motion correction are of interest, e.g. Keller *et al* (2012), Schleyer *et al* (2015). Robotic testing platforms which allow phantoms to be manipulated using highly reproducible and accurate motion trajectories play an important part in the performance evaluation of motion tracking and correction methods (Kyme *et al* 2014, 2020). Interested readers are referred to several studies comparing the accuracy of different motion correction methods in PET head imaging, e.g. Montgomery *et al* (2006), Rahmim *et al* (2008), Jin *et al* (2009, 2014).

Residual motion blur in motion-corrected images due to sources of motion tracking error can be reduced using deconvolution methods. Miranda *et al* report improved spatial resolution in PET imaging of unrestrained rats using a deconvolution algorithm with a spatially variant kernel that is dependent on the observed head motion (Miranda *et al* 2014). Angelis *et al* directly measured the motion-dependent kernel during the PET acquisition by attaching a small point source to the rat's head (Angelis *et al* 2018).

In general, it appears that additional complexity and long reconstruction times have been the major barriers to commercially available rigid motion correction methods for all the imaging modalities considered here and thus to their more widespread clinical use. Productive research areas in the future could include the development of more automated, yet reliable and accurate, optical motion tracking methods, including extensions of recent efforts to develop markerless optical motion tracking solutions, and more computationally-efficient motion-corrected reconstruction methods.

Correcting for non-rigid motion (e.g. respiratory or cardiac motion) is a more challenging problem than rigid motion correction, mainly because of the difficulty of accurately estimating the motion and deformation of internal structures. Nevertheless, it has attracted considerable interest from researchers due to its major potential clinical impact. Non-rigid respiratory and cardiac motion artifacts can be reduced using gating techniques which produce separate images at predefined intervals during the respiratory or cardiac cycle. Each gated image is affected to a much lesser extent by motion than a composite, ungated image, but more affected by noise. Gating does not require motion to be estimated directly, but 3D non-rigid motion fields can be estimated from the gated images, e.g. using non-rigid registration, and input to a reconstruction algorithm to produce a single reconstructed image based on all of the data. The degree of success depends largely on the spatial and temporal accuracy with which the deformation can be estimated from the noisy gated images. Despite its limitations, in PET for example, simultaneous cardiac and respiratory gating has been shown to enable estimates of both motion types and their incorporation into the reconstruction process to produce a motion corrected image that provides clinical benefits.

It is interesting to consider that current endeavours to improve PET coincidence timing resolution for time-of-flight may eventually enable the annihilation site to be localized with sub-pixel accuracy. In this case it may be possible to apply event-by-event corrections for rigid and non-rigid motion with much greater precision than at present (Meikle *et al* 2021).

In emission tomography, whether the aim is to correct for rigid motion or non-rigid motion, it is vital to account for motion of both the emission and attenuation distributions. Accounting for motion of the emission distribution during reconstruction while treating the attenuation distribution as static will result in artifacts and quantitative errors.

Although little has been published so far on state-of-the-art machine learning methods in this field, it is clear that such methods could aid, or eventually replace, existing motion estimation and motion correction methods. The attraction of machine learning methods, and specifically deep neural networks, in the context of motion correction is threefold: (i) the potential for a network to comprehensively model the underlying physics—compared to the limited physics captured within explicit analytical models; (ii) the potential to substitute specific components of a traditional motion correction pipeline with a neural network-based module that provides better performance; and (iii) the potential for neural networks to enable highly accurate and practical fully data-driven correction—ideally, exclusively in the image domain—a long-term but elusive goal for practitioners in SPECT, PET and CT. There is much scope for further work in this area.

5. Conclusion

In this review we have described the clinical importance of subject motion in SPECT, PET and CT and critically surveyed methods to estimate and correct for this motion. Despite many similarities in how motion is handled in these modalities, utility and applications vary based on differences in temporal and spatial resolution. Technical feasibility has been demonstrated in each modality for both rigid and non-rigid motion, but clinical feasibility remains an elusive target. There is considerable scope for further developments in motion estimation and correction. Deep neural network-based methods may have a unique role to play in this context.

Acknowledgments

The authors wish to thank the anonymous reviewers for their helpful comments and suggestions.

ORCID iDs

Andre Z Kyme https://orcid.org/0000-0003-3297-5390
Roger R Fulton https://orcid.org/0000-0003-2536-2190

References

Ahmed M A A, Xiao P and Xie Q 2015 New approach for simultaneous respiratory and cardiac motion correction in cardiac PET (NAMC-CPET) *Phys. Med. Biol.* **60** 7779–804

Akhtar M, Kyme A, Zhou V, Fulton R and Meikle S 2013 An investigation of the challenges in reconstructing PET images of a freely moving animal *Australas. Phys. Eng. Sci. Med.* **36** 405–15

Alessio A, Kohlmyer S and Kinahan P 2007 Consistency driven respiratory phase alignment and motion compensation in PET/CT *2007 IEEE Nuclear Science Symp. Conf. Record (Honolulu, HI, 26 October–3 November 2007)* (Picastaway, NJ: IEEE) pp 3115–9

Alfidi R, MacIntyre W and Haaga J 1976 The effects of biological motion on CT resolution *Am. J. Roentgenol.* **127** 11–5

Allen A, Siracuse K and Hayman J 2004 Evaluation of the influence of breathing on the movement and modeling of lung tumors *Int. J. Radiat. Oncol. Biol. Phys.* **58** 1251–7

Anagnostopoulos C, Pennell D, Laney R and Underwood S R 1995 Avoidance of upward creep artifact during Tl-201 myocardial perfusion tomography using adenosine infusion: a case report *Clin. Nucl. Med.* **20** 685–7

Andersson J L R 1998 How to obtain high-accuracy image registration: application to movement correction of dynamic positron emission tomography data *Eur. J. Nucl. Med.* **25** 575–86

Andrews-Shigaki B C, Armstrong B S, Zaitsev M and Ernst T 2011 Prospective motion correction for magnetic resonance spectroscopy using single camera retro-grate reflector optical tracking *J. Magn. Reson. Imaging* **33** 498–504

Angelis G, Gillam J E, Kyme A Z, Fulton R R and Meikle S R 2018 Image-based modelling of residual blurring in motion corrected small animal PET imaging using motion dependent point spread functions *Biomed. Phys. Eng. Express* **4** 035032

Angelis G I, Gillam J E, Ryder W J, Fulton R R and Meikle S R 2019 Direct estimation of voxel-wise neurotransmitter response maps from dynamic PET data *IEEE Trans. Med. Imaging* **38** 1371–83

Angelis G I, Kyme A Z, Ryder W J, Fulton R R and Meikle S R 2014 Attenuation correction for freely moving small animal brain PET studies based on a virtual scanner geometry *Phys. Med. Biol.* **59** 5651–66

Arata L K, Pretorius P H and King M A 1996 Correction of organ motion in SPECT using reprojection data *IEEE Nuclear Science Symp. and Medical Imaging Conf. Record* vol 3 *(San Francisco, CA, 21–28 October 1995)* (Picastaway, NJ: IEEE) pp 1456–60

Armstrong I S, Memmott M J, Saint K J, Saillant A, Hayden C and Arumugam P 2019 Assessment of motion correction in dynamic rubidium-82 cardiac PET with and without frame-by-frame adjustment of attenuation maps for calculation of myocardial blood flow *J. Nucl. Cardiol.* 1–13

Axel L, Montillo A and Kim D 2005 Tagged magnetic resonance imaging of the heart: a survey *Med. Image Anal.* **9** 376–93

Baba J S *et al* 2013 Molecular imaging of conscious, unrestrained mice with awake SPECT *J. Nucl. Med.* **54** 969–76

Bai C, Maddahi J, Kindem J, Conwell R, Gurley M and Old R 2009 Development and evaluation of a new fully automatic motion detection and correction technique in cardiac SPECT imaging *J. Nucl. Cardiol.* **16** 580–9

Bai W J and Brady M 2009b Regularized B-spline deformable registration for respiratory motion correction in PET images *Phys. Med. Biol.* **54** 2719–36

Bai W J and Brady M 2011 Motion correction and attenuation correction for respiratory gated PET images *IEEE Trans. Med. Imaging* **30** 351–65

Balfour D R, Marsden P K, Polycarpou I, Kolbitsch C and King A P 2015 Respiratory motion correction of PET using MR-constrained PET-PET registration *Biomed. Eng. Online* **14** 85

Balter J M, Wright J N, Newell L J, Friemel B, Dimmer S, Cheng Y, Wong J, Vertatschitsch E and Mate T P 2005 Accuracy of a wireless localization system for radiotherapy *Int. J. Radiat. Oncol. Biol. Phys.* **61** 933–7

Barnes P J, Baldock C, Meikle S R and Fulton R R 2008 Benchmarking of a motion sensing system for medical imaging and radiotherapy *Phys. Med. Biol.* **53** 5845–57

Barnett R, Meikle S and Fulton R 2011 Deformable image registration by regarding respiratory motion as 1D wave propagation in an elastic medium *IEEE Nuclear Science Symp. and Medical Imaging Conf. (NSS/MIC) (Valencia, Spain, 23–29 October 2011)* (Picastaway, NJ: IEEE) pp 2956–63

Barrett J F and Keat N 2004 Artifacts in CT: recognition and avoidance *Radiographics* **24** 1679–91

Bashar R, Ryder W J, Angelis G I, Meikle S R and Fulton R R 2013 GPU-accelerated motion compensated OSEM list-mode PET reconstruction using a time-averaged sensitivity matrix *2013 IEEE Nuclear Science Symp. and Medical Imaging Conf. (2013 NSS/MIC) (Seoul, 27 October–2 November 2013)* (Picastaway, NJ: IEEE) pp 1–4

Bauer S, Seitel A, Hofmann H, Blum T, Wasza J, Balda M, Meinzer H, Navab N, Hornegger J and Maier-Hein L 2013 Real-time range imaging in health care: a survey *Time-of-Flight and Depth Imaging. Sensors, Algorithms, and Applications* (*Lecture Notes in Computer Science* 8200) (Wadern, Germany: Springer) pp 228–54

Beach R D, Depold H, Boening G, Bruyant P P, Feng B, Gifford H C, Gennert M A, Nadella S and King M A 2007 An adaptive approach to decomposing patient-motion tracking data acquired during cardiac SPECT imaging *IEEE Trans. Nucl. Sci.* **54** 130–9

Beach R D, Pretorius H P, Boening G, Bruyant P, Feng B, Fulton R R, Gennert M A, Nadella S and King M A 2004 Feasibility of stereo-infrared tracking to monitor patient motion during cardiac SPECT imaging *IEEE Trans. Nucl. Sci.* **51** 2693–8

Becker N, Smith W, Quirk S and Kay I 2010 Using cone-beam CT projection images to estimate the average and complete trajectory of a fiducial marker moving with respiration *Phys. Med. Biol.* **55** 7439–52

Bellekens B, Spruyt V and Weyn M 2014 A survey of rigid 3D pointcloud registration algorithms *Proc. 4th Int. Conf. on Ambient Computing, Applications, Services and Technologies* pp 8–13

Berger M, Maier A, Xia Y, Hornegger J and Fahrig R 2014 Motion compensated fan-beam CT by enforcing Fourier properties of the sinogram *3rd Int. Conf. on Image Formation in X-ray Computed Tomography* ed F Noo pp 329–32

Berger M, Muller K, Aichert A, Unberath M, Thies J, Choi J, Fahrig R and Maier A 2016 Marker-free motion correction in weight-bearing cone-beam CT of the knee joint *Med. Phys.* **43** 1235–48

Berger M, Xia Y, Aichinger W, Mentl K, Unberath M, Aichert A, Riess C, Hornegger J, Fahrig R and Maier A 2017 Motion compensation for cone-beam CT using Fourier consistency conditions *Phys. Med. Biol.* **62** 7181–215

Bettinardi V, De Bernardi E, Presotto L and Gilardi M C 2013 Motion-tracking hardware and advanced applications in PET and PET/CT *PET Clin.* **8** 11–28

Beyer T, Tellmann L, Nickel I and Pietrzyk U 2005 On the use of positioning aids to reduce misregistration in the head and neck in whole-body PET/CT studies *J. Nucl. Med.* **46** 596–602

Bhagalia R, Pack J D, Miller J V and Iatrou M 2012 Nonrigid registration-based coronary artery motion correction for cardiac computed tomography *Med. Phys.* **39** 4245–54

Bhowmik U, Zafar Iqbal M and Adhami T 2012 Mitigating motion artifacts in FDK based 3D cone-beam brain imaging system using markers *Open Eng.* **2** 369–82

Bier B, Ravikumar N, Unberath M, Levenston M, Gold G, Fahrig R and Maier A 2018 Range imaging for motion compensation in C-arm cone-beam CT of knees under weight-bearing conditions *J. Imaging* **4** 13

Birkfellner W, Watzinger F, Wanschitz F, Enislidis G, Kollmann C, Rafolt D and Nowotny R 1998a Systematic distortions in magnetic position digitizers *Med. Phys.* **25** 2242–8

Birkfellner W, Watzinger F, Wanschitz F, Ewers R and Bergmann H 1998b Calibration of tracking systems in a surgical environment *IEEE Trans. Med. Imaging* **17** 737–42

Birn R, Bandettini P, Cox R, Jesmanowicz A and Shaker R 1998 Magnetic field changes in the human brain due to swallowing or speaking *Magn. Reson. Med.* **40** 55–60

Bitarafan A *et al* 2008 Respiratory motion detection and correction in ECG-gated SPECT: a new approach *Korean J. Radiol.* **9** 490–7

Blendowski M and Heinrich M P 2019 Combining MRF-based deformable registration and deep binary 3D-CNN descriptors for large lung motion estimation in COPD patients *Int. J. Comput. Assist. Radiol. Surg.* **14** 43–52

Blondel C, Vaillant R, Malandain G and Ayache N 2004 3D tomographic reconstruction of coronary arteries using a precomputed 4D motion field *Phys. Med. Biol.* **49** 2197–208

Bloomfield P M, Spinks T J, Reed J, Schnorr L, Westrip A M, Livieratos L, Fulton R and Jones T 2003 The design and implementation of a motion correction scheme for neurological PET *Phys. Med. Biol.* **48** 959–78

Blume M, Martinez-Moller A, Keil A, Navab N and Rafecas M 2010 Joint reconstruction of image and motion in gated positron emission tomography *IEEE Trans. Med. Imaging* **29** 1892–906

Bodensteiner C, Darolti C, Schumacher H, Matthaus L and Schweikard A 2007 Motion and positional error correction for cone beam 3D-reconstruction with mobile C-arms *Medical Image Computing and Computer-Assisted Intervention – MICCAI 2007* ed N Ayache, S Ourselin and A Maeder vol 4791 (Berlin: Springer) pp 177–85

Botvinick E H, Zhu Y Y, Oconnell W J and Dae M W 1993 A quantitative assessment of patient motion and its effect on myocardial perfusion SPECT images *J. Nucl. Med.* **34** 303–10

Bousse A, Manber R, Holman B F, Atkinson D, Arridge S, Ourselin S, Hutton B F and Thielemans K 2017 Evaluation of a direct motion estimation/correction method in respiratory-gated PET/MRI with motion-adjusted attenuation *Med. Phys.* **44** 2379–90

Bousse A, Bertolli O, Atkinson D, Arridge S, Ourselin S, Hutton B and Thielemans K 2016 Maximum-likelihood joint image reconstruction/motion estimation in attenuation-corrected respiratory gated PET/CT using a single attenuation map *IEEE Trans. Medical Imaging* **35** 217–28

Brandner E, Wu A and Chen H 2006 Abdominal organ motion measured using 4D CT *Int. J. Radiat. Oncol. Biol. Phys.* **65** 554–60

Brankov J G, Yang Y and Wernick M N 2004 Tomographic image reconstruction based on a content-adaptive mesh model *IEEE Trans. Med. Imaging* **23** 202–12

Brehm M, Sawall S, Maier J, Sauppe S and Kachelrie M 2015 Cardiorespiratory motion-compensated micro-CT image reconstruction using an artifact model-based motion estimation *Med. Phys.* **42** 1948–58

Brenner D 2010 Slowing the increase in the population dose resulting from CT scans *Radiat. Res.* **174** 809–15

Britten A J, Jamali F, Gane J N and Joseph A E A 1998 Motion detection and correction using multi-rotation 180 degrees single-photon emission tomography for thallium myocardial imaging *Eur. J. Nucl. Med.* **25** 1524–30

Bruder H, Rohkohl C, Stierstorfer K and Flohr T 2016 Compensation of skull motion and breathing motion in CT using data-based and image-based metrics, respectively *Proc. SPIE* **9783** 9783E-1

Bruyant P P, Feng B, Pretorius P H and King M A 2004 Impact of respiratory motion compensation in cardiac SPECT when attenuation maps are not motion-compensated *2003 IEEE Nuclear Science Symp., Conf. Record* vol 1-5 *(Portland, OR, 19–25 October 2003)* (Picastaway, NJ: IEEE) pp 2941–5

Bruyant P P, King M A and Pretorius P H 2002 Correction of the respiratory motion of the heart by tracking of the center of mass of thresholded projections: a simulation study using the dynamic MCAT phantom *IEEE Trans. Nucl. Sci.* **49** 2159–66

Buck A *et al* 2008 SPECT/CT *J. Nucl. Med.* **49** 1305–19

Bühler P, Just U, Will E, Kotzerke J and van den Hoff J 2004 An accurate method for correction of head movement in PET *IEEE Trans. Med. Imaging* **23** 1176–85

Bundschuh R, Martinez-Moeller A, Essler M, Martinez M, Nekolla S and Ziegler S 2007 Postacquisition detection of tumor motion in the lung and upper abdomen using list-mode PET data: a feasibility study *J. Nucl. Med.* **48** 758–63

Carson R E, Barker W C, Liow J S and Johnson C A 2004 Design of a motion-compensation OSEM list-mode algorithm for resolution-recovery reconstruction for the HRRT *2003 IEEE Nuclear Science Symp., Conf. Record* vol 1-5, pp 3281–5
Catana C 2015 Motion correction options in PET/MRI *Semin. Nucl. Med.* **45** 212–23
Catana C, Benner T, van der Kouwe A, Byars L, Hamm M, Chonde D B, Michel C J, El Fakhri G, Schmand M and Sorensen G 2011 MRI-assisted PET motion correction for neurologic studies in an integrated MR-PET scanner *J. Nucl. Med.* **52** 154–61
Cha J, Farhangi M M, Dunlap N and Amini A A 2018 Segmentation and tracking of lung nodules via graph-cuts incorporating shape prior and motion from 4D CT *Med. Phys.* **45** 297–306
Chan C, Harris M, Le M, Biondi J, Grobshtein Y, Liu Y H, Sinusas A J and Liu C 2014 End-expiration respiratory gating for a high-resolution stationary cardiac SPECT system *Phys. Med. Biol.* **59** 6267–87
Chen G, Kung J and Beaudette K 2004 Artifacts in computed tomography scanning of moving objects *Semin. Radiat. Oncol.* **14** 19–26
Chen M Y, He P, Feng P, Liu B D, Yang Q S, Wei B and Wang G 2018 General rigid motion correction for computed tomography imaging based on locally linear embedding *Opt. Eng.* **57** 023102
Chen Q, Franken P, Defrise M, Jonckheer M and Deconinck F 1993 Detection and correction of patient motion in SPECT imaging *J. Nucl. Med. Technol.* **21** 198–205
Cherry S R 2011 Functional whole-brain imaging in behaving rodents *Nat. Methods* **8** 301–3
Choi J H, Maier A, Keil A, Pal S, McWalter E, Beaupre G, Gold G and Fahrig R 2014 Fiducial marker-based correction for involuntary motion in weight-bearing C-arm CT scanning of knees: II. Experiment. Fiducial marker-based correction for involuntary motion *Med. Phys.* **41** 61902
Chu L L, Knebel R J, Shay A D, Santos J, Badawi R D, Gandara D R and Knollmann F D 2018 CT perfusion imaging of lung cancer: Benefit of motion correction for blood flow estimates *Eur. Radiol.* **28** 5069–75
Chun S Y and Fessler J A 2012 Spatial resolution properties of motion-compensated tomographic image reconstruction methods *IEEE Trans. Med. Imaging* **31** 1413–25
Clackdoyle R and Desbat L 2013 Full data consistency conditions for cone-beam projections with sources on a plane *Phys. Med. Biol.* **58** 8437
Clackdoyle R and Desbat L 2015 Data consistency conditions for truncated fanbeam and parallel projections *Med. Phys.* **42** 831–45
Clifford M, Banovac F, Levy E and Cleary K 2002 Assessment of hepatic motion secondary to respiration for computer assisted interventions *Comput. Aided Surg.* **7** 291–9
Clough J R, Balfour D R, Prieto C, Reader A J, Marsden P K and King A P 2018 Evaluation of strategies for PET motion correction - manifold learning vs. deep learning *Understanding and Interpreting Machine Learning in Medical Image Computing Applications* (*Lecture Notes in Computer Science (including subseries Lecture Notes in Artificial Intelligence and Lecture Notes in Bioinformatics)* 11038) (Switzerland: LNCS Springer) pp 61–9
Cooper J A and McCandless B K 1995 Preventing patient motion during tomographic myocardial perfusion imaging *J. Nucl. Med.* **36** 2001–5
Cooper J A, Neumann P H and Mccandless B K 1992 Effect of patient motion on tomographic myocardial perfusion imaging *J. Nucl. Med.* **33** 1566–71
Costes N, Dagher A, Larcher K, Evans A C, Collins D L and Reilhac A 2009 Motion correction of multi-frame PET data in neuroreceptor mapping: Simulation based validation *Neuroimage* **47** 1496–505
Crawford C R, King K F, Ritchie C J and Godwin J D 1996 Respiratory compensation in projection imaging using a magnification and displacement model *IEEE Trans. Med. Imaging* **15** 327–32
Cuesta-Vargas A I, Galán-Mercant A and Williams J M 2010 The use of inertial sensors system for human motion analysis *Phys. Therapy Rev.* **15** 462–73
Cullom S, Folks R, Vansant J and Nowak D 1995 The differences in motion artifacts for single and dual 90-degree detector cardiac SPECT *J. Nucl. Med* **36** 168P
Currie G M and Wheat J M 2004 The impact of acquisition protocol on the incidence of patient motion in Tc-99m based myocardial perfusion SPECT *Nucl. Med. Commun.* **25** 1191–5
Dang J, Gu X, Pan T and Wang J 2015 A pilot evaluation of a 4-dimensional cone-beam computed tomographic scheme based on simultaneous motion estimation and image reconstruction *Int. J. Radiat. Oncol. Biol. Phys.* **91** 410–8
Daube-Witherspoon M E, Yan Y, Green M V, Carson R and Kempner K M 1990 Correction for motion distortion in PET by dynamic monitoring of patient position *J. Nucl. Med.* **31** 816
Dawood M, Büther F, Jiang X and Schäfers K 2008 Respiratory motion correction in 3-D PET data with advanced optical flow algorithms *IEEE Trans. Med. Imaging* **27** 1164–75
Dawood M, Jiang X, Lang N, Schober O and Schäfers K P 2005 Lung motion correction of respiratory gated 3D PET-CT images *Eur. J. Nucl. Med. Mol. Imaging* **32** S95–95
Dinelle K, Blinder S, Cheng J C, Lidstone S, Buckley K, Ruth T J and Sossi V 2006 Investigation of subject motion encountered during a typical positron emission tomography scan *2006 IEEE Nuclear Science Symp. Conf. Record* vol 1-6, pp 3283–7
Ehrhardt J, Werner R, Saring D, Frenzel T, Lu W, Low D and Handels H 2007 An optical flow based method for improved reconstruction of 4D CT data sets acquired during free breathing *Med. Phys.* **34** 711–21
Eisner R 1992 Sensitivity of SPECT thallium-201 myocardial perfusion imaging to patient motion *J. Nucl. Med.* **33** 1571–3
Eisner R L, Aaron A M, Worthy M R, Boyers A S, Leon A R, Fajman W A and Patterson R E 1993 Apparent change in cardiac geometry during single-photon emission tomography Tl-201 acquisition—a complex phenomenon *Eur. J. Nucl. Med.* **20** 324–9
Eisner R L, Noever T, Nowak D, Carlson W, Dunn D, Oates J, Cloninger K, Liberman H A and Patterson R E 1987 Use of cross-correlation function to detect patient motion during SPECT imaging *J. Nucl. Med.* **28** 97–101
Eisner R *et al* 1988 Quantitative-analysis of the tomographic Tl-201 myocardial bullseye display - critical role of correcting for patient motion *J. Nucl. Med.* **29** 91–7
El Naqa I, Low D A, Bradley J D, Vicic M and Deasy J O 2006 Deblurring of breathing motion artifacts in thoracic PET images by deconvolution methods *Med. Phys.* **33** 3587–600
Eldib M E, Hegazy M A A, Cho M H, Cho M H and Lee S Y 2018 A motion artifact reduction method for dental CT based on subpixel-resolution image registration of projection data *Comput. Biol. Med.* **103** 232–43
Elss T, Nickisch H, Wissel T, Schmitt H, Vembar M, Morlock M and Grass M 2018 Deep-learning-based CT motion artifact recognition in coronary arteries *Proc. SPIE* **vol 10574** 1057416
Erdi Y, Nehmeh S, Pan T, Pevsner A, Rosenzweig K, Mageras G, Yorke E, Schoder H, Hsiao W and Squire O 2004 The CT motion quantitation of lung lesions and its impact on PET-measured SUVs *J. Nucl. Med.* **45** 1287–92
Faber T L, Raghunath N, Tudorascu D and Votaw J R 2009 Motion correction of PET brain images through deconvolution: I. Theoretical development and analysis in software simulations *Phys. Med. Biol.* **54** 797–811

Fahmi F, Beenen L, Streekstra G, Janssen N, de Jong H, Riorda A, Roos Y, Majoie C, Van Bavel E and Marquering H 2013 Head movement during CT brain perfusion acquisition of patients with suspected acute ischemic stroke *Eur. J. Radiol.* **82** 2334–41
Fahmi F, Marquering H, Borst J, Streekstra G, Beenen L, Niesten J, Velthuis B, Majoie C and van Bavel E 2014 3D movement correction of CT brain perfusion image data of patients with acute ischemic stroke *Neuroradiology* **56** 445–52
Fahrig R and Holdsworth D W 2000 Three-dimensional computed tomographic reconstruction using a C-arm mounted XRII: Image-based correction of gantry motion nonidealities *Med. Phys.* **27** 30–8
Fayad H, Lamare F, Merlin T and Visvikis D 2016 Motion correction using anatomical information in PET/CT and PET/MR hybrid imaging *Q. J. Nucl. Med. Mol. Imaging* **60** 12–24
Feldkamp L A, Davis L C and Kress J W 1984 Practical cone-beam algorithm *J. Opt. Soc. Am.* A **1** 612–9
Feng B, Gifford H C, Beach R D, Boening G, Gennert M A and King M A 2006 Use of three-dimensional gaussian interpolation in the projector/backprojector pair of iterative reconstruction for compensation of known rigid-body motion in SPECT *IEEE Trans. Med. Imaging* **25** 838–44
Feng B and King M A 2013 Estimation of 6-degree-of-freedom (6-DOF) rigid-body patient motion from projection data by the principal-axes method in iterative reconstruction *IEEE Trans. Nucl. Sci.* **60** 1658–63
Feng T, Wang J Z, Fung G and Tsui B 2016 Non-rigid dual respiratory and cardiac motion correction methods after, during, and before image reconstruction for 4D cardiac PET *Phys. Med. Biol.* **61** 151–68
Feng T, Wang J Z and Tsui B M W 2018 Dual respiratory and cardiac motion estimation in PET imaging: methods design and quantitative evaluation *Med. Phys.* **45** 1481–90
Feng Y Q, Liu X W, Ma J H, Lu Z T and Chen W F 2009 Affine motion compensation with improved reconstruction in PROPELLER MRI *EMBC: 2009 Annual Int. Conf. of the IEEE Engineering in Medicine and Biology Society* vol 1-20, pp 2680–3
Foote M D, Zimmerman B E, Sawant A and Joshi S C 2019 Real-time 2D-3D deformable registration with deep learning and application to lung radiotherapy targeting *Information Processing in Medical Imaging* (Cham: Springer International Publishing) pp 265–76
Forman C, Aksoy M, Hornegger J and Bammer R 2011 Self-encoded marker for optical prospective head motion correction in MRI *Med. Image Anal.* **15** 708–19
Forster F 2006 A high-resolution and high accuracy real-time 3D sensor based on structured light *3rd Int. Symp. on Data Processing, Visualization, and Transmission* pp 208–15
Frantz D D, Wiles A D, Leis S E and Kirsch S R 2003 Accuracy assessment protocols for electromagnetic tracking systems *Phys. Med. Biol.* **48** 2241–51
Fu Y, Liu S, Li H H, Li H and Yang D 2018 An adaptive motion regularization technique to support sliding motion in deformable image registration *Med. Phys.* **45** 735–47
Fulton R 2000 Correction for patient head movement in emission tomography *PhD Thesis* University of Technology Sydney
Fulton R, Nickel I, Tellmann L, Meikle S, Pietrzyk U and Herzog H 2003 Event-by-event motion compensation in 3D PET *2003 IEEE Nuclear Science Symp. Conf. Record* vol 5 *(Portland, OR, 19–25 October 2003)* (Picastaway, NJ: IEEE) pp 3286–9
Fulton R, Tellman L, Pietrzyk U, Winz O, Stangier I, Nickel I, Schmid A, Meikle S and Herzog H 2004 Accuracy of motion correction methods for PET brain imaging *IEEE Nuclear Science Symp. and Medical Imaging Conf. Record* pp 4226–30
Fulton R R, Eberl S, Meikle S R, Hutton B F and Braun M 1999 A practical 3D tomographic method for correcting patient head motion in clinical SPECT *IEEE Trans. Nucl. Sci.* **46** 667–72
Fulton R R, Hutton B F, Braun M, Ardekani B and Larkin R 1994 Use of 3D reconstruction to correct for patient motion in SPECT *Phys. Med. Biol.* **39** 563–74
Fulton R R, Meikle S R, Eberl S, Pfeiffer J, Constable C J and Fulham M J 2002 Correction for head movements in positron emission tomography using an optical motion-tracking system *IEEE Trans. Nucl. Sci.* **49** 116–23
Fürst S, Grimm R, Hong I, Souvatzoglou M, Casey M E, Schwaiger M, Nekolla S G and Ziegler S I 2015 Motion correction strategies for integrated PET/MR *J. Nucl. Med.* **56** 261–9
Gao X W, Anishenko S, Shaposhnikov D, Podlachikova L, Batty S and Clark J 2007 High-precision detection of facial landmarks to estimate head motions based on vision models *J. Comput. Sci.* **3** 528–32
Geckle W J, Frank T L, Links J M and Becker L C 1988 Correction for patient and organ movement in SPECT—application to exercise Tl-201 cardiac imaging *J. Nucl. Med.* **29** 441–50
Gennert M A, Ho J K, Quina A C, Wang J H, Bruyant P P and King M A 2004 Feasibility of tracking patient respiration during cardiac SPECT imaging using stereo optical cameras *IEEE Nuclear Science Symp., Conf. Record* vol 1–5, pp 3170–2
Geramifar P, Zafarghandi M, Ghafarian P, Rahmim A and Ay M 2013 Respiratory-induced errors in tumor quantification and delineation in CT attenuation-corrected PET images: effects of tumor size, tumor location, and respiratory trace: a simulation study using the 4D XCAT phantom *Mol. Imaging Biol.* **15** 655–65
Germano G, Chua T, Kavanagh P B, Kiat H and Berman D S 1993 Detection and correction of patient motion in dynamic and static myocardial SPECT using a multi-detector camera *J. Nucl. Med.* **34** 1349–55
Germino M, Gallezot J D, Yan J H and Carson R E 2017 Direct reconstruction of parametric images for brain PET with event-by-event motion correction: evaluation in two tracers across count levels *Phys. Med. Biol.* **62** 5344–64
Gigengack F, Ruthotto L, Burger M, Wolters C H, Jiang X Y and Schäfers K P 2012 Motion correction in dual gated cardiac PET using mass-preserving image registration *IEEE Trans. Med. Imaging* **31** 698–712
Gilland D R, Mair B A and Parker J G 2008 Motion estimation for cardiac emission tomography by optical flow methods *Phys. Med. Biol.* **53** 2991–3006
Gillman A, Smith J, Thomas P, Rose S and Dowson N 2017 PET motion correction in context of integrated PET/MR: Current techniques, limitations, and future projections *Med. Phys.* **44** e430–45
Giraud P *et al* 2001 Conformal radiotherapy (CRT) planning for lung cancer: analysis of intrathoracic organ motion during extreme phases of breathing *Int. J. Radiat. Oncol. Biol. Phys.* **51** 1081–92
Goddard J, Baba J, Lee S, Weisenberger A, Stolin A, McKisson J and Smith M 2009 Intrinsic feature pose measurement for awake animal SPECT imaging *2009 IEEE Nuclear Science Symp. and Medical Imaging Conf. (Orlando, FL, 4 October–1 November 2009)* (Picastaway, NJ: IEEE) pp 2557–60
Godenschweger F, Kägebein U, Stucht D, Yarach U, Sciarra A, Yakupov R, Lüsebrink F, Schulze P and Speck O 2016 Motion correction in MRI of the brain *Phys. Med. Biol.* **61** R32–56
Goldstein S R, Daube-Witherspoon M E, Green M V and Eidsath A 1997 A head motion measurement system suitable for emission computed tomography *IEEE Trans. Med. Imaging* **16** 17–27
Gravier E, Yang Y Y and Jin M W 2007 Tomographic reconstruction of dynamic cardiac image sequences *IEEE Trans. Image Process.* **16** 932–42

Green M V, Seidel J, Stein S D, Tedder T E, Kempner K M, Kertzman C and Zeffiro T A 1994 Head movement in normal subjects during simulated PET brain imaging with and without head restraint *J. Nucl. Med.* **35** 1538–46
Gu J, Bae W and Ye J C 2017 Translational motion correction algorithm for truncated cone-beam CT using opposite projections *J. X-ray Sci. Technol.* **25** 927–44
Gu S X, McNamara J E, Mitra J, Gifford H C, Johnson K, Gennert M A and King M A 2010 Body deformation correction for SPECT imaging *IEEE Trans. Nucl. Sci.* **57** 214–24
Guerin B, Cho S, Chun S Y, Zhu X, Alpert N M, El Fakhri G, Reese T and Catana C 2011 Nonrigid PET motion compensation in the lower abdomen using simultaneous tagged-MRI and PET imaging *Med. Phys.* **38** 3025–38
Guerra L, Ponti E, Morzenti S, Spadavecchia C and Crivellaro C 2017 Respiratory motion management in PET/CT: applications and clinical usefulness *Curr. Radiopharm.* **10** 85–92
Guerra L *et al* 2012 Respiratory gated PET/CT in a European multicentre retrospective study: added diagnostic value in detection and characterization of lung lesions *Eur. J. Nucl. Med. Mol. Imaging* **39** 1381–90
Guerrero T, Zhang G, Huang T C and Lin K 2004 Intrathoracic tumour motion estimation from CT imaging using the 3D optical flow method *Phys. Med. Biol.* **49** 4147–61
Hansis E, Schafer D, Dossel O and Grass M 2008 Projection-based motion compensation for gated coronary artery reconstruction from rotational X-ray angiograms *Phys. Med. Biol.* **53** 3807
Harada T, Shirato H, Ogura S, Oizumi S, Yamazaki K, Shimizu S, Onimaru R, Miyasaka K, Nishimura M and Dosaka-Akita H 2002 Real-time tumor-tracking radiation therapy for lung carcinoma by the aid of insertion of a gold marker using bronchofiberscopy *Cancer* **95** 1720–7
Hartley R and Zisserman A 2004 *Multiple View Geometry in Computer Vision* (Cambridge: Cambridge University Press) (https://doi.org/10.1017/CBO9780511811685)
Herbst M, MacLaren J, Korvink J and Zaitsev M 2011 A practical tracking system to avoid motion artifacts *Proc. Intl. Soc. Mag. Reson. Med.* 19, 2683
Herzog H, Tellman L, Fulton R and Pietrzyk U 2005a Motion correction in PET brain studies *4th Int. Workshop on Multidimensional Systems—NDS 2005* pp 178–81
Herzog H, Tellmann L, Fulton R, Stangier I, Kops E R, Bente K, Boy C, Hurlemann R and Pietrzyk U 2005b Motion artifact reduction on parametric PET images of neuroreceptor binding *J. Nucl. Med.* **46** 1059–65
Hess M, Büther F, Gigengack F, Dawood M and Schäfers K 2016 A dual-Kinect approach to determine torso surface motion for respiratory motion correction in PET *Med. Phys.* **42** 2276–86
Hinkle J, Szegedi M, Wang B, Salter B and Joshi S 2012 4D CT image reconstruction with diffeomorphic motion model *Med. Image Anal.* **16** 1307–16
Horn B K P 1987 Closed-form solution of absolute orientation using unit quaternions *J. Opt. Soc. Am.* A **4** 629–42
Hu D, Hayden C, Casey M and Burbar Z 2004 Stereo computer vision system for measuring movement of patient's head in PET scanning *Nuclear Science Symp. and Medical Imaging Conf. Record* vol 5, pp 2864–7
Huang T C, Chou K T, Wang Y C and Zhang G 2014a Motion freeze for respiration motion correction in PET/CT: a preliminary investigation with lung cancer patient data *BioMed Res. Int.* **2014** 1–7
Huang C, Ackerman J L, Petibon Y, Normandin M D, Brady T J, El Fakhri G and Ouyang J 2014b Motion compensation for brain PET imaging using wireless MR active markers in simultaneous PET-MR: Phantom and non-human primate studies *Neuroimage* **91** 129–37
Huang P, Hu Q, Jin F and Chiang F 1999 Color encoded digital fringe projection projection technique for high-speed three-dimensional surface contouring *Opt. Eng.* **38** 1065–71
Huang X K, Zhang Y, Chen L Y and Wang J 2020 U-net-based deformation vector field estimation for motion-compensated 4D-CBCT reconstruction *Med. Phys.* **47** 3000–12
Hummel J B, Figl M L, Kollman C and Bergmann H 2002 Evaluation of a miniature electromagnetic position tracker *Med. Phys.* **29** 2205–12
Hunter C R R N, Klein R, Beanlands R S and Dekemp R A 2016 Patient motion effects on the quantification of regional myocardial blood flow with dynamic PET imaging *Med. Phys.* **43** 1829–40
Hutton B, Skerrett D and Fulton R 2000 Data-based correction for patient motion during SPECT acquisition *J. Nucl. Med.* **41** 61(abstract)
Hutton B F, Kyme A Z, Lau Y H, Skerrett D W and Fulton R R 2002 A hybrid 3D reconstruction/registration algorithm for correction of head motion in emission tomography *IEEE Trans. Nucl. Sci.* **49** 188–94
Isola A A, Metz C T, Schaap M, Klein S, Grass M and Niessen W J 2012 Cardiac motion-corrected iterative cone-beam CT reconstruction using a semi-automatic minimum cost path-based coronary centerline extraction *Comput. Med. Imaging Graph.* **36** 215–26
Ivanovic M, Pellot-Barakat C, Weber D A, Loncaric S and Shelton D K 2000 Effects of patient motion in coincidence studies on hybrid PET/SPECT system *2000 IEEE Nuclear Science Symp. Conf. Record* vol 3, pp 16/49–16/53
Jacobson M W and Fessler J A 2004 Joint estimation of image and deformation parameters in motion-corrected PET *2003 IEEE Nuclear Science Symp., Conf. Record* vol 1–5 ed S D Metzler pp 3290–4
Jacobson M W and Stayman J W 2008 Compensating for head motion in slowly-rotating cone beam CT systems with optimization transfer based motion estimation *2008 IEEE Nuclear Science Symp. and Medical Imaging Conf. Record* pp 4506–11
Jafari Tadi M, Koivisto T, Pänkäälä M and Paasio A 2014 Accelerometer-based method for extracting respiratory and cardiac gating information for dual gating during nuclear medicine imaging *Int. J. Biomed. Imaging* **2014** 690124
Jafari Tadi M, Teuho J, Lehtonen E, Saraste A, Pänkäälä M, Koivisto T and Teräs M 2017 A novel dual gating approach using joint inertial sensors: Implications for cardiac PET imaging *Phys. Med. Biol.* **62** 8080–101
Jang S, Kim S, Kim M and Ra J B 2018 Head motion correction based on filtered backprojection for x-ray CT imaging *Med. Phys.* **45** 589–604
Jiang C H, Zhang Q Y, Ge Y S, Liang D, Yang Y F, Liu X, Zheng H R and Hu Z L 2019 Wasserstein generative adversarial networks for motion artifact removal in dental CT imaging *Proc. SPIE* **10948** 1094836
Jiao J Q, Salinas C A, Searle G E, Gunn R N and Schnabel J A 2012 Joint estimation of subject motion and tracer kinetic parameters of dynamic PET data in an EM framework *Proc. SPIE* **8314** 83140A
Jiao J Q *et al* 2017 Direct parametric reconstruction with joint motion estimation/correction for dynamic brain PET data *IEEE Trans. Med. Imaging* **36** 203–13
Jin X, Mulnix T, Sandiego C M and Carson R E 2014 Evaluation of frame-based and event-by-event motion-correction methods for awake monkey brain PET imaging *J. Nucl. Med.* **55** 287–93
Jin X, Sandiego C, Mulnix T and Carson R 2010 Multiple acquisition frame-based motion correction for awake monkey PET imaging *IEEE Nuclear Science Symp. and Medical Imaging Conf. (Knoxville, TN, 30 October–6 November 2010)* (Picastaway, NJ: IEEE) pp 2915–20

Jin X A, Mulnix T, Planeta-Wilson B, Gallezot J D and Carson R E 2009 Accuracy of head motion compensation for the HRRT: comparison of methods *IEEE Nuclear Science Symp. Conf. Record (Orlando, FL, 24 October–1 November 2009)* (Picastaway, NJ: IEEE) pp 3199–202
Johnson C A, Thada S, Rodriguez M, Zhao Y S, Iano-Fletcher A R, Liow J S, Barker W C, Martino R L and Carson R E 2004 Software architecture of the MOLAR-HRRT reconstruction engine *IEEE Nuclear Science Symp. Conf. Record* vol 6 *(Rome, Italy , 16–22 October 2004)* (Picastaway, NJ: IEEE) pp 3956–60
Jones W F 2002 Real-time event stream correction for patient motion in clinical 3D PET *IEEE Nuclear Science Symp., Conf. Record* vol 4 *(San Diego, CA, 4–10 November 2001)* (Picastaway, NJ: IEEE) pp 2062–4
Kachelriess M and Kalender W A 1998 Electrocardiogram-correlated image reconstruction from subsecond spiral computed tomography scans of the heart *Med. Phys.* **25** 2417–31
Kachelriess M, Ulzheimer S and Kalender W A 2000 ECG-correlated imaging of the heart with subsecond multislice spiral CT *IEEE Trans. Med. Imaging* **19** 888–901
Kalantari F, Li T F, Jin M W and Wang J 2016 Respiratory motion correction in 4D-PET by simultaneous motion estimation and image reconstruction (SMEIR) *Phys. Med. Biol.* **61** 5639–61
Kangasmaa T S and Sohlberg A O 2014 Optimisation of reconstruction-reprojection-based motion correction for cardiac SPECT *Ann. Nucl. Med.* **28** 580–5
Kaste S 2004 Issues specific to implementing PET/CT for pediatric oncology: What we have learned along the way *Pediatric Radiol.* **34** 205–13
Katsevich A, Silver M and Zamyatin A 2011 Local tomography and the motion estimation problem *SIAM J. Imaging Sci.* **4** 200–19
Keller S H, Sibomana M, Olesen O V, Svarer C, Holm S, Andersen F L and Hojgaard L 2012 Methods for motion correction evaluation using F-18-FDG human brain scans on a high-resolution PET scanner *J. Nucl. Med.* **53** 495–504
Kerekes R A, Goddard J S, Gleason S S, Paulus M J, Weisenberger A G, Smith M F and Welch B 2003 Two methods for tracking small animals in SPECT imaging *Proc. SPIE* **5132** pp 129–39
Kesner A L, Schleyer P J, Büther F, Walter M A, Schäfers K P and Koo P J 2014 On transcending the impasse of respiratory motion correction applications in routine clinical imaging—a consideration of a fully automated data driven motion control framework *EJNMMI Phys.* **1** 1–11
Khurshid K, Wu L Y, Berger K and McGough R J 2006 Automated PET/CT cardiac registration for accurate attenuation correction *Proc. 2006 IEEE Int. Conf. on Electro/Information Technology* (IEEE) pp 409–14
Kim J H, Nuyts J, Kuncic Z and Fulton R 2013 The feasibility of head motion tracking in helical CT: a step toward motion correction *Med. Phys.* **40** 41903
Kim S, Chang Y and Ra J B 2015a Cardiac motion correction based on partial angle reconstructed images in x-ray CT *Med. Phys.* **42** 2560–71
Kim J H, Nuyts J, Kyme A, Kuncic Z and Fulton R 2015b A rigid motion correction method for helical computed tomography (CT) *Phys. Med. Biol.* **60** 2047–73
Kim J H, Sun T, Alcheikh A, Kuncic Z, Nuyts J and Fulton R 2016 Correction for human head motion in helical x-ray CT *Phys. Med. Biol.* **61** 1416–38
Kim S, Chang Y and Ra J B 2018 Cardiac motion correction for helical CT scan with an ordinary pitch *IEEE Trans. Med. Imaging* **37** 1587–96
Klein G, Reutter B and Huesman R 1997 Non-rigid summing of gated PET via optical flow *IEEE Trans. Nucl. Sci.* **44** 1509–12
Klein G J 1999 Forward deformation of PET volumes using non-uniform elastic material constraints *Information Processing in Medical Imaging* (*Lecture Notes in Computer Science* vol. 1613) ed A Kuba *et al* (Berlin: Springer) pp 358–63
Klein G J, Reutter B W, Botvinick E H, Budinger T F and Huesman R H 2001b Fine-scale motion detection using intrinsic list mode PET information *IEEE Workshop on Mathematical Methods in Biomedical Image Analysis, MMBIA 2001 (Kauai, HI, 9–10 December 2001)* (Picastaway, NJ: IEEE) pp 71–8
Klein G J, Reutter B W and Huesman R H 2001a Four-dimensional affine registration models for respiratory-gated PET *IEEE Trans. Nucl. Sci.* **48** 756–60
Klen R, Noponen T, Koikkalainen J, Lotjonen J, Thielemans K, Hoppela E, Sipila H, Teras M and Knuuti J 2016 Evaluation of motion-correction methods for dual-gated cardiac positron emission tomography/computed tomography imaging *Nucl. Med. Commun.* **37** 956–68
Klugmann A, Bier B, Müller K, Maier A and Unberath M 2018 Deformable respiratory motion correction for hepatic rotational angiography *Comput. Med. Imaging Graph.* **66** 82–9
Ko C L, Wu Y W, Cheng M F, Yen R F, Wu W C and Tzen K Y 2015 Data-driven respiratory motion tracking and compensation in CZT cameras: a comprehensive analysis of phantom and human images *J. Nucl. Cardiol.* **22** 308–18
Kochunov P, Lancaster J L, Glahn D C, Purdy D, Laird A R, Gao F and Fox P 2006 Retrospective motion correction protocol for high-resolution anatomical MRI *Hum. Brain Mapp.* **27** 957–62
Kolbitsch C, Neji R, Fenchel M, Schuh A, Mallia A, Marsden P and Schaeffter T 2019 Joint cardiac and respiratory motion estimation for motion-corrected cardiac PET-MR *Phys. Med. Biol.* **64** 15007
Koshino K, Watabe H, Hasegawa S, Hayashi T, Hatazawa J and Iida H 2010 Development of motion correction technique for cardiac O-15-water PET study using an optical motion tracking system *Ann. Nucl. Med.* **24** 1–11
Kovalski G, Israel O, Keidar Z, Frenkel A, Sachs J and Azhari H 2007 Correction of heart motion due to respiration in clinical myocardial perfusion SPECT scans using respiratory gating *J. Nucl. Med.* **48** 630–6
Kovalski G, Keidar Z, Frenkel A, Sachs J, Attia S and Azhari H 2009 Dual 'motion-frozen heart' combining respiration and contraction compensation in clinical myocardial perfusion SPECT imaging *J. Nucl. Cardiol.* **16** 396–404
Küstner T *et al* 2017 MR-based respiratory and cardiac motion correction for PET imaging *Med. Image Anal.* **42** 129–44
Kyme A, Aksoy M, Henry D, Bammer R and Maclaren J 2020 Marker-free optical stereo motion tracking for in-bore MRI and PET-MRI application *Med. Phys.* **47** 3321–31
Kyme A, Meikle S, Baldock C and Fulton R 2012 Tracking and characterizing the head motion of unanaesthetized rats in positron emission tomography *J. R. Soc. Interface* **9** 3094–107
Kyme A, Se S, Meikle S, Angelis G, Ryder W, Popovic K, Yatigammana D and Fulton R 2014 Markerless motion tracking of awake animals in positron emission tomography *IEEE Trans. Med. Imaging* **33** 2180–90
Kyme A, Se S, Meikle S and Fulton R 2018 Markerless motion estimation for motion-compensated clinical brain imaging *Phys. Med. Biol.* **63** 105018
Kyme A Z 2012 Optimised motion tracking in small animal positron emission tomography *PhD Thesis* University of Sydney
Kyme A Z, Hutton B F, Hatton R L, Skerrett D W and Barnden L R 2003 Practical aspects of a data-driven motion correction approach for brain SPECT *IEEE Trans. Med. Imaging* **22** 722–9

Kyme A Z, Zhou V W, Meikle S R, Baldock C and Fulton R R 2011 Optimised motion tracking for positron emission tomography studies of brain function in awake rats *PLoS One* **6** e21727
Kyme A Z, Zhou V W, Meikle S R and Fulton R R 2008 Real-time 3D motion tracking for small animal brain PET *Phys. Med. Biol.* **53** 2651–66
Kyme A Z *et al* 2019 Open-field PET: Simultaneous brain functional imaging and behavioural response measurements in freely moving small animals *NeuroImage* **188** 92–101
Kyriakou Y, Lapp R M, Hillebrand L, Ertel D and Kalender W A 2008 Simultaneous misalignment correction for approximate circular cone-beam computed tomography *Phys. Med. Biol.* **53** 6267–89
Laading J K, McCulloch C, Johnson V E, Gilland D R and Jaszczak R J 1999 A hierarchical feature based deformation model applied to 4D cardiac SPECT data *Information Processing in Medical Imaging* (*Lecture Notes in Computer Science* 1613) *(Visegrad, Hungary, 28 June- 2 July 1999)* ed A Kuba *et al* (Berlin: Springer) pp 266–79
Lamare F, Le Maitre A, Dawood M, Schäfers K P, Fernandez P, Rimoldi O E and Visvikis D 2014 Evaluation of respiratory and cardiac motion correction schemes in dual gated PET/CT cardiac imaging *Med. Phys.* **41** 72504
Lassen M L, Kwiecinski J, Cadet S, Dey D, Wang C, Dweck M R, Berman D S, Germano G, Newby D E and Slomka P J 2019 Data-driven gross patient motion detection and compensation: Implications for coronary 18F-NaF PET imaging *J. Nucl. Med.* **60** 830–6
Le Meunier L, Maass-Moreno R, Carrasquillo J A, Dieckmann W and Bacharach S L 2006 PET/CT imaging: effect of respiratory motion on apparent myocardial uptake *J. Nucl. Cardiol.* **13** 821–30
Lee K J and Barber D C 1998 Use of forward projection to correct patient motion during SPECT imaging *Phys. Med. Biol.* **43** 171–87
Lei Y, Fu Y, Harms J, Wang T, Curran W J, Liu T, Higgins K and Yang X 2019 4D-CT deformable image registration using an unsupervised deep convolutional neural network *Artificial Intelligence in Radiation Therapy* (Cham: Springer International Publishing) pp 26–33
Leng S, Nett B, Speidel M and Chen G 2007 Motion artifact reduction in fan-beam and cone-beam computed tomography via the fan-beam data consistency condition (FDCC) *Proc. SPIE* **6510** 65101W
Li J Y, Jaszczak R J, Wang H L and Coleman R E 1995a A filtered-backprojection algorithm for fan-beam SPECT which corrects for patient motion *Phys. Med. Biol.* **40** 283–94
Li J Y, Jaszczak R J and Coleman R E 1995b A filtered backprojection algorithm for axial head motion correction in fan-beam SPECT *Phys. Med. Biol.* **40** 2053–63
Li M, Castillo E, Zheng X L, Luo H Y, Castillo R, Wu Y and Guerrero T 2013 Modeling lung deformation: a combined deformable image registration method with spatially varying Young's modulus estimates *Med. Phys.* **40** 81902
Li T, Xing L, Munro P, McGuinness C, Chao M, Yang Y, Loo B and Koong A 2006 Four-dimensional cone-beam computed tomography using an on-board imager *Med. Phys.* **33** 3825–33
Li T, Zhang M, Qi W, Asma E and Qi J 2020 Motion correction of respiratory-gated PET images using deep learning based image registration framework *Phys. Med. Biol.* **65** 155003
Lindsay C, Mukherjee J M, Johnson K, Olivier P, Song X, Shao L, King M A, Gimi B and Molthen R C 2015 Marker-less multi-frame motion tracking and compensation in PET-brain imaging *Proc. SPIE* **9417** 94170J
Liu C, Alessio A M and Kinahan P E 2011 Respiratory motion correction for quantitative PET/CT using all detected events with internal-external motion correlation *Med. Phys.* **38** 2715–23
Livieratos L, Rajappan K, Stegger L, Schäfers K, Bailey D L and Camici P G 2006 Respiratory gating of cardiac PET data in list-mode acquisition *Eur. J. Nucl. Med. Mol. Imaging* **33** 584–8
Lopresti B J, Russo A, Jones W F, Fisher T, Crouch D G, Altenburger D E and Townsend D W 1999 Implementation and performance of an optical motion tracking system for high resolution brain PET imaging *IEEE Trans. Nucl. Sci.* **46** 2059–67
Lossau T, Nickisch H, Wissel T, Bippus R, Schmitt H, Morlock M and Grass M 2019a Motion artifact recognition and quantification in coronary CT angiography using convolutional neural networks *Med. Image Anal.* **52** 68–79
Lossau T, Nickisch H, Wissel T, Bippus R, Schmitt H, Morlock M and Grass M 2019b Motion estimation and correction in cardiac CT angiography images using convolutional neural networks *Comput. Med. Imaging Graph.* **76** 101640
Lu W G and Mackie T R 2002 Tomographic motion detection and correction directly in sinogram space *Phys. Med. Biol.* **47** 1267–84
Lu Y, Naganawa M, Toyonaga T, Gallezot J D, Fontaine K, Ren S, Revilla E M, Mulnix T and Carson R E 2020 Data-driven motion detection and event-by-event correction for brain PET: comparison with Vicra *J. Nucl. Med.* **61** 1397–403
Lu Y *et al* 2019 Data-driven voluntary body motion detection and non-rigid event-by-event correction for static and dynamic PET *Phys. Med. Biol.* **64** 65002
Ma L, Gu S X, Nadella S, Bruyant P P, King M A and Gennert M A 2005 A practical rebinning-based method for patient motion compensation in SPECT imaging *International Conference on Computer Graphics, Imaging and Visualisation (Beijing, China, 26-29 July 2005)* pp 209–14
Ma W 2009 Motion estimation for functional medical imaging studies using a stereo video head pose tracking system *PhD Thesis* Simon Fraser University
Maclaren J, Herbst M, Speck O and Zaitsev M 2013 Prospective motion correction in brain imaging: a review *Magn. Reson. Med.* **69** 621–36
Maclaren J *et al* 2012 Measurement and correction of microscopic head motion during magnetic resonance imaging of the brain *PLoS One* **7** 1–9
Maier J, Aichert A, Mehringer W, Bier B, Eskofier B, Levenston M, Gold G, Fahrig R, Bonaretti S and Maier A 2018 Feasibility of motion compensation using inertial measurement in C-arm CT *IEEE Nucl. Science Symp. and Medical Imaging Conf. (Sydney, Australia, 10–17 November 2018)* (Picastaway, NJ: IEEE) pp 1–3
Manber R, Thielemans K, Hutton B F, Wan S, McClelland J, Barnes A, Arridge S, Ourselin S and Atkinson D 2016 Joint PET-MR respiratory motion models for clinical PET motion correction *Phys. Med. Biol.* **61** 6515–30
Marin T, Wernick M N, Yang Y and Brankov J G 2010 Motion-compensated reconstruction of gated cardiac SPECT images using a deformable mesh model *7th IEEE Int. Symp. on Biomedical Imaging: From Nano to Macro (Rotterdam, Netherlands , 14–17 April 2010)* (Picastaway, NJ: IEEE) pp 520–3
Martin C, Berwick J, Johnston D, Zheng Y, Martindale J, Port M, Redgrave P and Mayhew J 2002 Optical imaging spectroscopy in the unanaesthetised rat *J. Neurosci. Methods* **120** 25–34
Martin C, Martindale J, Berwick J and Mayhew J 2006 Investigating neural-hemodynamic coupling and the hemodynamic response function in the awake rat *Neuroimage* **32** 33–48
Matsumoto N, Berman D S, Kavanagh P B, Gerlach J, Hayes S W, Lewin H C, Friedman J D and Germano G 2001 Quantitative assessment of motion artifacts and validation of a new motion-correction program for myocardial perfusion SPECT *J. Nucl. Med.* **42** 687–94
Mawlawi O, Martinez D, Slifstein M, Broft A, Chatterjee R, Hwang D, Huang Y, Simpson N and Ngo K 2001 Imaging human mesolimbic dopamine transmission with positron emission tomography: I. Accuracy and precision of D(2) receptor parameter measurements in ventral striatum *J. Cereb. Blood Flow Metab.* **21** 1034–57

Mawlawi O, Weiss R, Shinn A K, Pidcock J, Slifstein M and Laruelle M 1999 Performance characteristics of a head immobilization device for PET imaging *J. Nucl. Med* **40** 281
McCall K, Barbee D, Kissick M and Jeraj R 2010 PET imaging for the quantification of biologically heterogeneous tumours: measuring the effect of relative position on image-based quantification of dose-painting targets *Phys. Med. Biol.* **55** 2789–806
McCollough C, Bruesewitz M, Daly T and Zink F 2000 Motion artifacts in subsecond conventional CT and electron-beam CT: pictorial demonstration of temporal resolution *Radiographics* **20** 1675–81
McLeish K, Hill D and Atkinson D 2002 A study of the motion and deformation of the heart due to respiration *IEEE Trans. Med. Imaging* **21** 1142–50
McNamara J E, Bruyant P, Johnson K, Feng B, Lehovich A, Gu S X, Gennert M A and King M A 2008 An assessment of a low-cost visual tracking system (VTS) to detect and compensate for patient motion during SPECT *IEEE Trans. Nucl. Sci.* **55** 992–8
McNamara J E, Pretorius P H, Johnson K, Mukherjee J M, Dey J, Gennert M A and King M A 2009 A flexible multicamera visual-tracking system for detecting and correcting motion-induced artifacts in cardiac SPECT slices *Med. Phys.* **36** 1913–23
McQuaid S J and Hutton B F 2008 Sources of attenuation-correction artefacts in cardiac PET/CT and SPECT/CT *Eur. J. Nucl. Med. Mol. Imaging* **35** 1117–23
Meikle S R *et al* 2021 Quantitative PET in the 2020s: a roadmap *Phys. Med. Biol.* **66** 06RM01
Menke M, Atkins M S and Buckley K R 1996 Compensation methods for head motion detected during PET imaging *IEEE Trans. Nucl. Sci.* **43** 310–7
Mester J, Weller R, Clausen M, Bitter F, Henze E, Lietzenmayer R and Adam W E 1991 Upward creep of the heart in exercise Tl-201 single photon-emission tomography—clinical relevance and a simple correction method *Eur. J. Nucl. Med.* **18** 184–90
Metz C, Klein S, Schaap M, van Walsum T and Niessen W 2011 Nonrigid registration of dynamic medical imaging data using nD + t B-splines and a groupwise optimization approach *Med. Image Anal.* **15** 238–49
Migliaccio A A, MacDougall H G, Minor L B and Della Santina C C 2005 Inexpensive system for real-time 3-dimensional video-oculography using a fluorescent marker array *J. Neurosci. Methods* **143** 141–50
Miranda A, Glorie D, Bertoglio D, Vleugels J, De Bruyne G, Stroobants S, Staelens S and Verhaeghe J 2019a Awake 18F-FDG PET imaging of memantine-induced brain activation and test-retest in freely running mice *J. Nucl. Med.* **60** 844–50
Miranda A, Staelens S, Stroobants S and Verhaeghe J 2017 Fast and accurate rat head motion tracking with point sources for awake brain PET *IEEE Trans. Med. Imaging* **36** 1573–82
Miranda A, Verhaeghe J, Parthoens J, Stroobants S and Staelens S 2014 Motion uncertainty deblurring in motion corrected reconstruction for μPET brain imaging of awake rats *IEEE Nuclear Science Symp. and Medical Imaging Conf. (NSS/MIC) (Seattle, WA, 8–15 November 2014)* (Picastaway, NJ: IEEE) pp 1–4
Miranda A *et al* 2019b PET imaging of freely moving interacting rats *NeuroImage* **191** 560–7
Mitra D, Eiland D, Abdallah M, Bouthcko R, Gullberg G T and Schechtmann N 2012 SinoCor: Motion correction in SPECT *Proc. SPIE* **8314** 831452
Mitra D, Eiland D, Walsh T, Bouthcko R, Gullberg G T and Schechtmann N 2011 SinoCor: a clinical tool for sinogram-level patient motion correction in SPECT *Proc. SPIE* **7962** 79624V-79624-5
Mitra J, McNamara J E, Johnson K L, Dey J and King M A 2007 Estimation of rigid-body and respiratory motion of the heart for SPECT motion correction *2007 IEEE Nuclear Science Symp. Conf. Record* vol 5, pp 3570–6
Momosaki S, Hatano K, Kawasumi Y, Kato T, Hosoi R, Kobayashi K, Inoue O and Ito K 2004 Rat-PET study without anesthesia: anesthetics modify the dopamine D1 receptor binding in rat brain *Synapse* **54** 207–13
Montagnat J and Delingette H 2005 4D deformable models with temporal constraints: application to 4D cardiac image segmentation *Med. Image Anal.* **9** 87–100
Montgomery A J, Thielmans K, Mehta M A, Turkheimer F, Mustafovic S and Grasby P M 2006 Correction of head movement on PET studies: comparison of methods *J. Nucl. Med.* **47** 1936–44
Moorrees J and Bezak E 2012 Four dimensional CT imaging: a review of current technologies and modalities *Australas. Phys. Eng. Sci. Med.* **35** 9–23
Mooser R, Forsberg F, Hack E, Székely G and Sennhauser U 2013 Estimation of affine transformations directly from tomographic projections in two and three dimensions *Mach. Vis. Appl.* **24** 419–34
Mukherjee J M, Hutton B F, Johnson K L, Pretorius P H and King M A 2013 An evaluation of data-driven motion estimation in comparison to the usage of external-surrogates in cardiac SPECT imaging *Phys. Med. Biol.* **58** 7625–46
Muraishi H, Hasegawa T, Yoda K, Takeuchi A, Shiba Y, Maruyama K, Kitamura K, Yamaya T, Yoshida E and Murayama H 2004 Head motion correction for jPET-D4 *2004 IEEE Nuclear Science Symp. Conf. Record* vol 4, pp 2352–5
Naum A, Laaksonen M S, Tuunanen H, Oikonen V, Teras M, Kemppainen J, Jarvisalo M J, Nuutila P and Knuuti J 2005 Motion detection and correction for dynamic 15O-water myocardial perfusion PET studies *Eur. J. Nucl. Med. Mol. Imaging* **32** 1378–83
Nazarparvar B, Shamsaei M and Rajabi H 2012 Correction of head movements in positron emission tomography using point source tracking system: a simulation study *Ann. Nucl. Med.* **26** 7–15
Nehmeh S, Erdi Y, Ling C, Rosenzweig K, Squire O, Braban L, Ford E, Sidhu K, Mageras G, Larson S and Humm L 2002 Effect of respiratory gating on reducing lung motion artifacts in PET imaging of lung cancer *Med. Phys.* **29** 366–71
Nehmeh S A, Haj-Ali A A, Qing C, Stearns C, Kalaigian H, Kohlmyer S, Schoder H, Ho A Y, Larson S M and Humm J L 2011 A novel respiratory tracking system for smart-gated PET acquisition *Med. Phys.* **38** 531–8
Nehmeh S A *et al* 2004 Four-dimensional (4D) PET/CT imaging of the thorax *Med. Phys.* **31** 3179–86
Nichols K, Kamran M, Cooke C D, Faber T L, Garcia E V, Bergmann S R and DePuey E G 2002 Feasibility of detecting cardiac torsion in myocardial perfusion gated SPECT data *J. Nucl. Cardiol.* **9** 500–7
Nixon M A, McCallum B C, Fright W R and Price N B 1998 The effects of metals and interfering fields on electromagnetic trackers *Presence* **7** 204–18
Noo F, Clackdoyle R, Mennessier C, White T and Roney T 2000 Analytic method based on identification of ellipse parameters for scanner calibration in cone-beam tomography *Phys. Med. Biol.* **45** 3489–508
Noonan P J, Howard J, Hallett W A and Gunn R N 2015 Repurposing the Microsoft Kinect for Windows v2 for external head motion tracking for brain PET *Phys. Med. Biol.* **60** 8753–66
Noumeir R, Mailloux G E and Lemieux R 1996 Detection of motion during tomographic acquisition by an optical flow algorithm *Comput. Biomed. Res.* **29** 1–15
Nuyts J and Fulton R 2020 Iterative FDK reconstruction for helical CT of the head with rigid motion compensation *Proc. 6th Int. Conf. on Image Formation in X-Ray Computed Tomography (Regensburg, Germany, 3–7 August, 2020)*

O'Connor M K, Kanal K M, Gebhard M W and Rossman P J 1998 Comparison of four motion correction techniques in SPECT imaging of the heart: a cardiac phantom study *J. Nucl. Med.* **39** 2027–34
Ohata M, Fredericks W R, Sundaram U and Rapoport S I 1981 Effects of immobilization stress on regional cerebral blood flow in the conscious rat *J. Cereb. Blood Flow Metab.* **1** 187–94
Olesen O, Andersen F and Holm S 2009 A new tool fixation for external 3D head tracking using the Polaris Vicra system with the HRRT PET scanner *J. Nucl. Med.* **50** 1528
Olesen O, Paulsen R, Hojgaard L, Roed B and Larsen R 2011 Motion tracking for medical imaging: A non-visible structured light tracking approach *IEEE Trans. Med. Imaging* **31** 79–87
Olesen O V, Sullivan J M, Mulnix T, Paulsen R R, Hojgaard L, Roed B, Carson R E, Morris E D and Larsen R 2013 List-mode PET motion correction using markerless head tracking: proof-of-concept with scans of human subject *IEEE Trans. Med. Imaging* **32** 200–9
Ooi M, Aksoy M, Maclaren J, Watkins R and Bammer R 2013 Prospective motion correction using inductively coupled wireless RF coils *Magn. Reson. Med.* **70** 639–47
Orlov S S 1975 Theory of three dimensional reconstruction: I. Conditions for a complete set of projections *Sov. Phys. Crystallogr.* **20** 312–4
Osman M M, Cohade C, Nakamoto Y, Marshall L T, Leal J P and Wahl R L 2003 Clinically significant inaccurate localization of lesions with PET/CT: Frequency in 300 patients *J. Nucl. Med.* **44** 240–3
Ouadah S, Stayman J, Gang G, Ehtiati T and Siewerdsen J 2016 Self-calibration of cone-beam CT geometry using 3D-2D image registration *Phys. Med. Biol.* **61** 26130–32
Ouyang J S, Li Q Z and El Fakhri G 2013 Magnetic resonance-based motion correction for positron emission tomography imaging *Semin. Nucl. Med.* **43** 60–7
Ouyang J S, Petibon Y, Huang C, Reese T G, Kolnick A L and El Fakhri G 2014 Quantitative simultaneous PET-MR imaging *Micro- and Nanotechnology Sensors, Systems, and Applications VI SPIE Defense + Security* (*Proc. SPIE* 9083) *(Baltimore, 5 June 2014)* (https://doi.org/10.1117/12.2051578)
Ozturk C, Derbyshire J A and McVeigh E R 2003 Estimating motion from MRI data *Proc. IEEE* **91** 1627–48
Ozyesil O, Voroninski V, Basri R and Singer A 2017 A survey of structure from motion *Acta Numerica* **26** 305–64
Pauchard Y, Ayres F and Boyd S 2011 Automated quantification of three-dimensional subject motion to monitor image quality in high-resolution peripheral quantitative computed tomography *Phys. Med. Biol.* **56** 6523–43
Pauchard Y and Boyd S K 2008 Landmark based compensation of patient motion artifacts in computed tomography *Medical Imaging 2008: Physics of Medical Imaging* (*Proc. SPIE* 6913) pp C9133–9133
Peeters R R, Tindemans I, De Schutter E and Van der Linden A 2001 Comparing BOLD fMRI signal changes in the awake and anesthetized rat during electrical forepaw stimulation *Magn. Reson. Imaging* **19** 821–6
Pellot-Barakat C, Ivanovic M, Weber D, Herment A and Shelton D 1998 Motion detection in triple scan SPECT imaging *IEEE Trans. Nucl. Sci.* **45** 2238–44
Pepin A, Daouk J, Bailly P, Hapdey S and Meyer M E 2014 Management of respiratory motion in PET/computed tomography: the state of the art *Nucl. Med. Commun.* **35** 113–22
Petibon Y, Ouyang J, Zhu X, Huang C, Reese T G, Chun S Y, Li Q and El Fakhri G 2013 Cardiac motion compensation and resolution modeling in simultaneous PET-MR: a cardiac lesion detection study *Phys. Med. Biol.* **58** 2085–102
Pevsner A, Nehmeh S A, Humm J L, Mageras G S and Erdi Y E 2005 Effect of motion on tracer activity determination in CT attenuation corrected PET images: a lung phantom study *Med. Phys.* **32** 2358–62
Pfanner F, Maier J, Allmendinger T, Flohr T and Kachelrieß M 2013 Monitoring internal organ motion with continuous wave radar in CT *Med. Phys.* **40** 091915
Picard Y and Thompson C 1997 Motion correction of PET images using multiple acquisition frames *IEEE Trans. Med. Imaging* **16** 137–44
Picard Y and Thompson C J 1995 Digitized video subject positioning and surveillance system for PET *IEEE Trans. Nucl. Sci.* **42** 1024–9
Ponisch F, Richter C, Just U and Enghardt W 2008 Attenuation correction of four dimensional (4D) PET using phase-correlated 4D-computed tomography *Phys. Med. Biol.* **53** N259–68
Pretorius H and King M 2008 Spillover compensation in the presence of respiratory motion embedded in SPECT perfusion data *IEEE Trans. Nucl. Sci.* **55** 537–42
Pretorius P H, Johnson K L and King M A 2016 Evaluation of rigid-body motion compensation in cardiac perfusion SPECT employing polar-map quantification *IEEE Trans. Nucl. Sci.* **63** 1419–25
Price G, Sharrock P, Marchant T, Parkhurst J, Burton D, Jain P, Price P and Moore C 2009 An analysis of breast motion using high-frequency, dense surface points catpured by an optical sensor during radiotherapy treatment delivery *Phys. Med. Biol.* **54** 6515–33
Prigent F M, Hyun M, Berman D S and Rozanski A 1993 Effect of motion on thallium-201 SPECT studies: a simulation and clinical study *J. Nucl. Med.* **34** 1845–50
Qi J Y and Huesman R H 2002 List mode reconstruction for PET with motion compensation: a simulation study *Proc. IEEE Int. Symp. on Biomedical Imaging* pp 413–6
Qi W Y, Yang Y Y, Song C, Wernick M N, Pretorius P H and King M A 2017 4-D reconstruction with respiratory correction for gated myocardial perfusion SPECT *IEEE Trans. Med. Imaging* **36** 1626–35
Qiao F, Pan T, Clark J W and Mawlawi O R 2006 A motion-incorporated reconstruction method for gated PET studies *Phys. Med. Biol.* **51** 3769–83
Qin L, van Gelderen P, Derbyshire J, Jin F, Lee J, A de Zwart J, Tao Y and Duyn J 2009 Prospective head-movement correction for high-resolution MRI using an in-bore optical tracking system *Magn. Reson. Med.* **62** 924–34
Raghunath N, Faber T L, Suryanarayanan S and Votaw J R 2009 Motion correction of PET brain images through deconvolution: II. Practical implementation and algorithm optimization *Phys. Med. Biol.* **54** 813–29
Rahmim A, Bloomfield P, Houle S, Lenox M, Michel C, Buckley K R, Ruth T J and Sossi V 2004 Motion compensation in histogram-mode and list-mode EM reconstructions: beyond the event-driven approach *IEEE Trans. Nucl. Sci.* **51** 2588–96
Rahmim A, Rousset O and Zaidi H 2007 Strategies for motion tracking and correction in PET *PET Clin.* **2** 251–66
Rahmim A *et al* 2008 Accurate event-driven motion compensation in high-resolution PET incorporating scattered and random events *IEEE Trans. Med. Imaging* **27** 1018–33
Reader A J, Ally S, Bakatselos F, Manavaki R, Walledge R J, Jeavons A P, Julyan P J, Zhao S, Hastings D L and Zweit J 2002 One-pass list-mode EM algorithm for high-resolution 3D PET image reconstruction into large arrays *IEEE Trans. Nucl. Sci.* **49** 693–9
Redgate S, Barber D C, Fenner J W, Al-Mohammad A, Taylor J C, Hanney M B and Tindale W B 2016 A study to quantify the effect of patient motion and develop methods to detect and correct for motion during myocardial perfusion imaging on a CZT solid-state dedicated cardiac camera *J. Nucl. Cardiol.* **23** 514–26

Reilhac A, Merida I, Irace Z, Stephenson M C, Weekes A A, Chen C, Totman J J, Townsend D W, Fayad H and Costes N 2018 Development of a dedicated rebinner with rigid motion correction for the mMR PET/MR scanner, and validation in a large cohort of 11C-PIB scans *J. Nucl. Med.* **59** 1761–7

Remmell R 2006 Use of an electromagnetic eye movement monitor for easy measurement of arm movements *IEEE Trans. Biomed. Eng.* **53** 2356–61

Ren S, Jin X, Chan C, Jian Y, Mulnix T, Liu C and Carson R E 2017 Data-driven event-by-event respiratory motion correction using TOF PET list-mode centroid of distribution *Phys. Med. Biol.* **62** 4741–55

Ren S L, Lu Y H, Bertolli O, Thielemans K and Carson R E 2019 Event-by-event non-rigid data-driven PET respiratory motion correction methods: comparison of principal component analysis and centroid of distribution *Phys. Med. Biol.* **64** 165014

Reyes M, Malandain G, Koulibaly P, Gonzalez-Ballester M and Darcourt J 2007 Model-based respiratory motion compensation for emission tomography image reconstruction *Phys. Med. Biol.* **52** 3579–600

Ribeiro C, Ferworn A, Denko M and Tran J 2009 Canine pose estimation: a computing for public safety solution *2009 Canadian Conf. on Computer and Robot Vision* (IEEE) pp 37–44

Rit S, Wolthaus J W H, van Herk M and Sonke J J 2009a On-the-fly motion-compensated cone-beam CT using an a priori model of the respiratory motion *Med. Phys.* **36** 2283–96

Rit S, Sarrut D and Desbat L 2009b Comparison of analytic and algebraic methods for motion-compensated cone-beam CT reconstruction of the thorax *IEEE Trans. Med. Imaging* **28** 1513–25

Ritchie C J, Crawford C R, Goodwin J D, King K and Kim Y 1996 Correction of computed tomography motion artifacts using pixel-specific back projection *IEEE Trans. Med. Imaging* **15** 333–42

Ritchie C J, Godwin J D, Crawford C R, Stanford W, Anno H and Kim Y 1992 Minimum scan speeds for suppression of motion artifacts in ct *Radiology* **185** 37–42

Robson P M, Trivieri M, Karakatsanis N A, Padilla M, Abgral R, Dweck M R, Kovacic J C and Fayad Z A 2018 Correction of respiratory and cardiac motion in cardiac PET/MR using MR-based motion modeling *Phys. Med. Biol.* **63** 225011

Roetenberg D, Slycke P J and Veltink P H 2007 Ambulatory position and orientation tracking fusing magnetic and inertial sensing *IEEE Trans. BioMed. Eng.* **54** 883–90

Rohkohl C, Bruder H, Stierstorfer K and Flohr T 2013 Improving best-phase image quality in cardiac CT by motion correction with MAM optimization *Med. Phys.* **40** 031901

Rousseau F, Glenn O A, Iordanova B, Rodriguez-Carranza C, Vigneron D B, Barkovich J A and Studholme C 2006 Registration-based approach for reconstruction of high-resolution in utero fetal MR brain images *Acad. Radiol.* **13** 1072–81

Ruttimann U E, Andreason P J and Rio D 1995 Head motion during positron emission tomography: is it significant? *Psychiatry Res.: Neuroimaging* **61** 43–51

Salvi J, Fernandez S, Pribanic T and Llado X 2010 A state of the art in structured light patterns for surface profilometry *Pattern Recognit.* **43** 2666–80

Schäfer D, Bertram M, Conrads N, Wiegert J, Rose G and Rasche V 2004 Motion compensation for cone-beam CT based on 4D motion field of sinogram tracked markers *Cars 2004: Computer Assisted Radiology and Surgery* (*International Congress Series* 1268) ed H U Lemke *et al* pp 189–94

Schäfer D, Lin M, Rao P P, Loffroy R, Liapi E, Noordhoek N, Eshuis P, Radaelli A, Grass M and Geschwind J F H 2012 Breathing motion compensated reconstruction for C-arm cone beam CT imaging: initial experience based on animal data *SPIE Medical Imaging Medical Imaging 2012: Physics of Medical Imaging* (*Proc. SPIE* 8313) *(San Diego, 3 March 2012)* 83131D

Schechner Y and Kiryati N 2000 Depth from defocus vs. stereo: how different really are they? *Int. J. Comput. Vis.* **39** 141–62

Schicho K, Figl M L, Donat M, Birkefellner W W, Seemann R, Wagner A, Bergmann H and Ewers R 2005 Stability of miniature electromagnetic systems *Phys. Med. Biol.* **50** 2089–98

Schirra C O, Bontus C, van Stevendaal U, Dossel O and Grass M 2009 Improvement of cardiac CT reconstruction using local motion vector fields *Comput. Med. Imaging Graph.* **33** 122–30

Schleyer P J, Dunn J T, Reeves S, Brownings S, Marsden P K and Thielemans K 2015 Detecting and estimating head motion in brain PET acquisitions using raw time-of-flight PET data *Phys. Med. Biol.* **60** 6441–58

Schmidt J, Berg D and Ploeg H L 2009 Precision, repeatability and accuracy of Optotrak optical motion tracking systems *Int. J. Exp. Comput. Biomech.* **1** 114–27

Schretter C, Rose G and Bertram M 2009 Image-based iterative compensation of motion artifacts in computed tomography *Med. Phys.* **36** 5323–30

Schulz J, Siegert T, Reimer E, Zaitsev M, MacLaren J, Herbst M and Turner R 2011 First embedded in-bore system for fast optical prospective head motion-correction in MRI *28th Annual Scientific Meeting of the ESMRMB* p 369

Schumacher H, Modersitzki J and Fischer B 2009 Combined reconstruction and motion correction in SPECT imaging *IEEE Trans. Nucl. Sci.* **56** 73–80

Schwaab J, Kurz C, Sarti C, Bongers A, Schoenahl F, Bert C, Debus J, Parodi K and Jenne J W 2015 First steps toward ultrasound-based motion compensation for imaging and therapy: Calibration with an optical system and 4D PET imaging *Frontiers Oncol.* **5** 258

Segars W P and Tsui B M W 2002 Study of the efficacy of respiratory gating in myocardial SPECT using the new 4-D NCAT phantom *IEEE Trans. Nucl. Sci.* **49** 675–9

Shaeffer D 2013 MEMS inertial sensors: A tutorial overview *IEEE Commun. Mag.* **51** 100–9

Shiri I, Ghafarian P, Geramifar P, Leung K, Ghelichoghli M, Oveisi M, Rhahmim A and Ay M 2019 Direct attenuation correction of brain PET images using only emission data via a deep convolutional encoder-decoder (deep-DAC) *Eur. Radiol.* **29** 6867–79

Silverstein E and Snyder M 2018 Comparative analysis of respiratory motion tracking using Microsoft Kinect v2 sensor *J. Appl. Clin. Med. Phys.* **19** 193–204

Slipsager J M *et al* 2019 Markerless motion tracking and correction for PET, MRI, and simultaneous PET/MRI *PLoS One* **14** e0215524

Sonke J J, Zijp L, Remeijer P and van Herk M 2005 Respiratory correlated cone beam CT *Med. Phys.* **32** 1176–86

Spangler-Bickell M, Lin Z, Kyme A, De Laat B, Fulton R and Nuyts J 2016 Optimising rigid motion compensation for small animal brain PET imaging *Phys. Med. Biol.* **61** 7074–91

Spangler-Bickell M G, Deller T, Bettinardi V and Jansen F 2021 Ultra-fast list-mode reconstruction of short PET frames and example applications *J. Nucl. Med.* **62** 287–92

Spangler-Bickell M G *et al* 2019 Rigid motion correction for brain PET/MR imaging using optical tracking *IEEE Trans. Radiat. Plasma Med. Sci.* **3** 498–503

Sprem J, De Vos B D, De Jong P A, Viergever M A and Isgum I 2017 Classification of coronary artery calcifications according to motion artifacts in chest CT using a convolutional neural network *SPIE Medical Imaging Medical Imaging 2017: Image Processing* (*Proc. SPIE* 10133) *(Orlando)* (https://doi.org/10.1117/12.2253669)
Straw A D, Branson K, Neumann T R and Dickinson M H 2011 Multi-camera real-time three-dimensional tracking of multiple flying animals *J. R. Soc. Interface* **8** 395–409
Su Y 2011 Inter-frame motion correction for small animal PET imaging *4th Int. Conf. on Biomedical Engineering and Informatics (BMEI)* vol 1, pp 338–42
Sun L, Lacy J L, Martin C S, Nayak N and Clark J W 2001 Implementation and performance of a motion tracking system for treadmill MWGC imaging studies *IEEE Nuclear Science Symp. Conf. Record* vol 3 *(San Diego, CA, 4–10 November 2001)* (Picastaway, NJ: IEEE) pp 1700–3
Sun T, Clackdoyle R, Fulton R and Nuyts J 2014 Quantification of local reconstruction accuracy for helical CT with motion correction *2014 IEEE Nuclear Science Symp. and Medical Imaging Conf. (NSS/MIC) (Seattle, WA, 8–15 November 2014)* (Picastaway, NJ: IEEE) pp 1–4
Sun T, Kim J, Fulton R and Nuyts J 2015 Data-driven rigid motion correction for helical CT *Proc. 13th Int. Meeting on Fully Three-Dimensional Image Reconstruction in Radiology and Nuclear Medicine (Newport, RI, 31 May–4 June)*
Sun T, Kim J, Fulton R and Nuyts J 2016 An iterative projection-based motion estimation and compensation scheme for head x-ray CT *Med. Phys.* **43** 5705–16
Tang Q L, Cammin J, Srivastava S and Taguchi K 2012 A fully four-dimensional, iterative motion estimation and compensation method for cardiac CT *Med. Phys.* **39** 4291–305
Tellmann L, Fulton R R, Bente K, Stangier I, Winz O, Just U, Herzog H and Pietrzyk U K 2004 Motion correction of head movements in PET: Realisation for routine usage *2003 IEEE Nuclear Science Symp., Conf. Record* vol 5 *(Portland, OR, 19–25 October 2003)* (Picastaway, NJ: IEEE) pp 3105–7
Thielemans K 2005 Scatter estimation and motion correction in PET *2005 IEEE Nuclear Science Symp. Conf. Record (Fajardo, PR, 23–29 October 2005)* (Picastaway, NJ: IEEE) pp 1745–7
Thielemans K, Morel C, Jacobson M W, Kaempf J H and Mustafovic S 2008 Normalisation of histogrammed list mode data *IEEE Trans. Nucl. Sci.* **55** 543–51
Thielemans K, Mustafovic S and Schnorr L 2004 Image reconstruction of motion corrected sinograms *IEEE Nuclear Science Symp., Conf. Record* vol 4 *(Portland, OR, 19–25 October 2003)* (Picastaway, NJ: IEEE) pp 2401–6
Thomas L, Schultz T, Prokic V, Guckenberger M, Tanadini-Lang S, Hohberg M, Wild M, Drzezga A and Bundschuh R A 2019 4D-CT-based motion correction of PET images using 3D iterative deconvolution *Oncotarget* **10** 2987–95
Thorndyke B, Schreibmann E, Koong A and Xing L 2006 Reducing respiratory motion artifacts in positron emission tomography through retrospective stacking *Med. Phys.* **33** 2632–41
Townsend D W 2008 Combined PET/CT: the historical perspective *Semin. Ultrasound, CT MRI* **29** 232–5
Tsoumpas C, Mackewn J E, Halsted P, King A P, Buerger C, Totman J J, Schaeffter T and Marsden P K 2010 Simultaneous PET-MR acquisition and MR-derived motion fields for correction of non-rigid motion in PET *Ann. Nucl. Med.* **24** 745–50
Turkington T G, DeGrado T R, Hanson M W and Coleman R E 1997 Alignment of dynamic cardiac PET images for correction of motion *IEEE Trans. Nucl. Sci.* **44** 235–42
Tuy H K 1983 An inversion formula for cone-beam reconstruction *SIAM J. Appl. Math.* **43** 546–52
Uchiyama K, Kaminaga T, Waida M, Yasuda M and Chikamatsu T 2005 Performance of the automated motion correction program for the calculation of left ventricular volume and ejection fraction using quantitative gated SPECT software *Ann. Nucl. Med.* **19** 9–15
Ue H, Haneishi H, Iwanaga H and Suga K 2006 Nonlinear motion correction of respiratory-gated lung SPECT images *IEEE Trans. Med. Imaging* **25** 486–95
Ue H, Haneishi H, Iwanaga H and Suga K 2007 Respiratory lung motion analysis using a nonlinear motion correction technique for respiratory-gated lung perfusion SPECT images *Ann. Nucl. Med.* **21** 175–83
Ullisch M, Scheins J, Weirich C, Kops E, Celik A, Tellman L, Stocker T, Herzog H and Shah J 2012 MR-based PET motion correction procedure for simultaneous MR-PET neuroimaging of human brain *PLoS One* **7** e48149
Van Dijk J, Dalen J, Mouden M, Ottervanger J P, Knollema S, Slump C and Jager P 2016 Value of respiratory and patient motion correction in myocardial perfusion imaging using a CZT-based SPECT camera *J. Nucl. Med.* **57**
Van Dijk J D, van Dalen J A, Mouden M, Ottervanger J P, Knollema S, Slump C H and Jager P L 2018 Value of automatic patient motion detection and correction in myocardial perfusion imaging using a CZT-based SPECT camera *J. Nucl. Cardiol.* **25** 419–28
Vassileva J 2012 IAEA survey of pediatric CT practice in 40 countries in Asia, Europe, Latin America, and Africa: I. Frequency and appropriateness *Am. J. Roentgenol.* **198** 1021–31
Visvikis D, Lamare F, Bruyant P, Boussion N and Cheze Le Rest C 2006 Respiratory motion in positron emission tomography for oncology applications: problems and solutions *Nucl. Instrum. Methods Phys. Res.* A **569** 453–7
Wachtel R, Dexter F and Dow A 2009 Growth rates in pediatric diagnostic imaging and sedation *Anesthesia Analgesia* **108** 1616–21
Wade O 1954 Movements of the thoracic cage and diaphragm in respiration *J. Physiol.* **124** 193–212
Wang G and Vannier M W 1995 Preliminary-study on helical CT algorithms for patient motion estimation and compensation *IEEE Trans. Med. Imaging* **14** 205–11
Wang J and Gu X J 2013 Simultaneous motion estimation and image reconstruction (SMEIR) for 4D cone-beam CT *Med. Phys.* **40** 101912-1–11
Watabe H, Koshino K, Bloomfield P M, Fulton R R and Iida H 2004 Development of motion correction technique for PET study using optical tracking system *Quantitation Biomed. Imaging PET MRI* **1265** 31–8
Watabe H, Sato N, Kondoh Y, Fulton R and Iida H 2002 Correction of head movement using an optical motion tracking system during PET study with rhesus monkey *Brain Imaging Using PET* (New York: Academic) pp 1–7
Weinhandl J T, Armstrong B S R, Kusik T P, Barrows R T and O'Connor K M 2010 Validation of a single camera three-dimensional motion tracking system *J. Biomech.* **43** 1437–40
Weisenberger A G *et al* 2005 A restraint-free small animal SPECT imaging system with motion tracking *IEEE Trans. Nucl. Sci.* **52** 638–44
Wells J R, Segars W P, Kigongo C J N and Dobbins J T 2011 Refinement of motion correction strategies for lower-cost CT for under-resourced regions of the world *Proc. SPIE* **7961** 796133
Wells R G, Ruddy T D, DeKemp R A, DaSilva J N and Beanlands R S 2010 Single-phase CT aligned to gated PET for respiratory motion correction in cardiac PET/CT *J. Nucl. Med.* **51** 1182–90
Westermann B and Hauser R 2000 Online head motion tracking applied to the patient registration problem *Comput. Aided Surg.* **5** 137–47
Wheat J M and Currie G M 2004a Incidence and characterization of patient motion in myocardial perfusion SPECT: I *J. Nucl. Med. Technol.* **32** 60–5

Wheat J M and Currie G M 2004b Impact of patient motion on myocardial perfusion SPECT diagnostic integrity: II *J. Nucl. Med. Technol.* **32** 158–63

Wilm J, Olesen O, Paulsen R, Hoijgaard L, Roed B and Larsen R 2011 Real time surface registration for PET motion tracking *Image Analysis* (*Lecture Notes in Computer Science* 6688) ed A Heyden and F Kahl (Berlin: Springer) pp 166–75

Woo J, Tamarappoo B, Dey D, Nakazato R, Le Meunier L, Ramesh A, Lazewatsky J, Germano G, Berman D S and Slomka P J 2011 Automatic 3D registration of dynamic stress and rest Rb-82 and flurpiridaz F18 myocardial perfusion PET data for patient motion detection and correction *Med. Phys.* **38** 6313–26

Woo S K, Song T Y, Choi J Y, Choi Y, Lee K H and Kim B T 2005 Motion correction of respiratory-gated PET/CT images using polynomial warping *IEEE Nuclear Science Symp. Conf. Record (Fajardo, PR, 23–29 October 2005)* (Picastaway, NJ: IEEE) pp 2592–4

Woo S K, Watabe H, Choi Y, Kim K M, Park C C, Fulton R R, Bloomfield P M and Iida H 2003 Development of event-based motion correction technique for PET study using list-mode acquisition and optical motion tracking system *Proc. SPIE* **5032** 1300–7

Woodman O 2007 *An introduction to inertial navigation UCAM-CL-TR-696* University of Cambridge (https://cl.cam.ac.uk/techreports/UCAM-CL-TR-696.pdf)

Wu J and Liu C 2019 Recent advances in cardiac SPECT instrumentation and imaging methods *Phys. Med. Biol.* **64** 06TR01

Würslin C, Schmidt H, Martirosian P, Brendle C, Boss A, Schwenzer N F and Stegger L 2013 Respiratory motion correction in oncologic PET using T1-weighted MR imaging on a simultaneous whole-body PET/MR system *J. Nucl. Med.* **54** 464–71

Xu Q S, Xie K N, Yuan K H, Yu L J, Wang W Z and Ye D T 2012 A statistical study of the factors influencing the extent of respiratory motion blur in PET imaging *Comput. Biol. Med.* **42** 8–18

Xu Q S, Yuan K H and Ye D T 2011 Respiratory motion blur identification and reduction in ungated thoracic PET imaging *Phys. Med. Biol.* **56** 4481–98

Yamashita H, Yamashita M, Futaguchi M, Takenaka R, Shibata S, Yamamoto K *et al* 2014 Individually wide range of renal motion evaluated by four-dimensional computed tomography *SpringerPlus* **3** 131

Yang D, Lu W, Low D and Deasy J 2008 4D-CT motion estimation using deformable image registration and 5D respiratory motion modeling *Med. Phys.* **35** 4577–90

Yang J, Park D, Gullberg G and Seo Y 2018 Joint correction of attenuation and scatter in image space using deep convolutional neural networks for dedicated brain 18F-FDG PET *Phys. Med. Biol.* **64** 75019

Yang Y Y and Gravier E J 2004 Reconstruction of image sequences using motion compensation *Proc. SPIE* **5299** pp 34–42

Yu H Y and Wang G 2007 Data consistency based rigid motion artifact reduction in fan-beam CT *IEEE Trans. Med. Imaging* **26** 249–60

Yu H Y, Wei Y C, Hsieh J and Wang G 2006 Data consistency based translational motion artifact reduction in fan-beam CT *IEEE Trans. Med. Imaging* **25** 792–803

Zafar S 2011 Post scan correction of step, linear and spiral motion effects in CT scans *Int. J. Comput. Appl.* **35** 13–19

Zafar S, Younis W and Sheikh N M 2007 The compensation of head motion artefacts using an infrared tracking system for CT (computerized tomography) imaging *Int. Conf. on Electrical Engineering (Lahore, Pakistan , 11-12 April 2007)* (Picastaway, NJ: IEEE) pp 360–4

Zeng R, Fessler J and Balter J 2005 Respiratory motion estimation from slowly rotating x-ray projections: theory and simulation *Med. Phys.* **32** 984

Zhang C, Kuhn M, Merkl B, Mahfouz M and Fathy A E 2006 Development of an UWB indoor 3D positioning radar with millimeter accuracy *IEEE MTT-S International Microwave Symp. Digest (San Francisco, CA, 11–16 June 2006)* (Picastaway, NJ: IEEE) pp 106–9

Zhang S, Balamurali M and Kyme A 2018 Deep learning-based motion estimation for uninterrupted tracking of awake rodents in PET *IEEE Nuclear Science Symp. and Medical Imaging Conf. (Sydney, Australia, 10–17 November 2018)* (Picastaway, NJ: IEEE) pp 1–3

Zhou V, Eisenhuth J, Kyme A, Akhtar M, Fulton R and Meikle S 2013 A motion adaptive animal chamber for PET imaging of freely moving animals *IEEE Trans. Nucl. Sci.* **60** 3423–31

Zhou V, Kyme A, Meikle S and Fulton R 2008 An event-driven motion correction method for neurological PET studies of awake laboratory animals *Mol. Imaging Biol.* **10** 315–24

Zhou V W, Kyme A Z, Meikle S R and Fulton R 2009 A scheme for PET data normalization in event-based motion correction *Phys. Med. Biol.* **54** 5321–39